1987

Chemistry And Geochemistry Of The Rare Earth Element Phosphates

Ralph George Jonasson

CHEMISTRY AND GEOCHEMISTRY OF THE RARE EARTH ELEMENT PHOSPHATES

by

Ralph G. Jonasson

Department of Chemistry

Submitted in partial fulfilment
of the requirements for the degree of
Doctor of Philosophy

Faculty of Graduate Studies
The University of Western Ontario
London, Ontario
October, 1986

ISBN 0-315-36100-X

THE UNIVERSITY OF WESTERN ONTARIO

FACULTY OF GRADUATE STUDIES

CERTIFICATE OF EXAMINATION

Chief Advisor	Examining Board
E.R. Cancroft	Wayne Nesbitt
Advisory Committee	Peter Tennant
	M.E. Fleet
C.Riddiford	C.Riddiford

The thesis by

Ralph G. Jonasson

entitled

Chemistry and Geochemistry of

the Rare Earth Element Phosphates

is accepted in partial fulfilment of the

requirements of the degree of

Doctor of Philosophy

Date 27 Oct 1986

John Mungall

Chairman of Examining Board

ABSTRACT

The REE (rare earth element) phosphates are known to be very insoluble, and thus have potential importance in the immobilization of REE in nuclear waste forms and in ocean environments. The hydrous REE phosphates were synthesized with rhabdophane (light REE), and xenotime (heavy REE) structures from dilute nitric acid at or below 100°C, using the acid hydrolysis of the respective REE-pyrophosphate ($P_2O_7^{4-}$), over a period of 4 to 6 weeks. Derivatives for several REE were characterized by scanning electron microscopy (SEM), powder x-ray diffraction (XRD), differential thermal analysis (DTA) and thermogravimetric analysis (TGA). The $DyPO_4 \cdot xH_2O$ derivative was shown to be dimorphic. The behaviour of a specimen of natural rhabdophane (Idaho, U.S.A.), was found to resemble that of synthetic $LaPO_4 \cdot xH_2O$. Secondary ion mass spectrometry (SIMS) showed the natural sample to be enriched in LREE, (e.g. La).

Solubility products of several hydrous REE phosphates were measured using spectrophotometry and instrumental neutron activation analysis (INAA). The pK values (plus or minus 0.2), were found to be La=24.5 (25°C), Pr=26.0 (100°C), Nd=24.7 (25°C), Sm=25.7 (25°C), Ho=24.6 (25°C) and Er=25.2 (25°C). The solubilities were predicted to decrease with increasing temperature. The hydrous REE phosphates dissolve in dilute acid with first order,

reversible kinetics, with equilibrium achieved in 40 days. Seawater REE concentrations were predicted to be on the order of 1-200 pmol/L, which is also the range actually measured by other workers.

Anhydrous REE phosphate single crystals, (L.A. Boatner, ORNL), and natural monazite, (Petaca district, New Mexico), were found to dissolve much more slowly than the hydrous phosphates, so that solubility products could not be determined by this method.

Specimens of apatite, hydrous REE phosphates and anhydrous REE phosphates were reacted with dissolved REE between pH's of 2 and 6. Exchange reactions involving the formation of new phases were shown to occur using XRD, XPS and SIMS. The surface reactions required several months, but the kinetics could not be quantified.

ACKNOWLEDGEMENTS

There are many people whom I should thank: were it not for their patient help, the thesis work would have taken longer, and been less interesting.

First of all I must thank my parents for their moral and financial support. Next I must thank Professor Kramer for providing me with summer work in the lab during several of my undergraduate years, and consequently fostering my interest in research.

I must thank the people associated with Surface Science Western. In particular I thank Ian Muir and Dr. Jim Metson for their help with the SIMS, Margaret Hyland and Darleen Johnston for their help with the ESCA, Gary Mount and Bill Chauvin for their help with the SEM. To all the others I am also grateful for their help and cooperation.

I would like to thank Yuchi Cheng (Dept. of Geology) and J. Snider (AECL, Pinawa) for obtaining the x-ray powder patterns and R.I. Haines (AECL, Pinawa) for the IR spectra. I also thank the reviewers at AECL (Pinawa) in particular, P. Taylor, J.C. Tait and P.J. Hayward.

I thank Professor Fyfe for sponsoring a trip I took to Whiteshell Nuclear Research Establishment (Pinawa), and the people at Whiteshell, especially Dr. Peter Sargent, for their kind welcome.

I thank Dr. L.A. Boatner at Oak Ridge National Laboratory for the many excellent single crystals and interesting reprints.

I thank Dr. E.R. Vance (AECL, Pinawa) for his correspondence and collaboration on a paper.

For many enjoyable conversations I am grateful to Brian James, Dr. Brian Yates, Professor Ron Martin, Dr. John Harder, Dr. Alistair McLennan, Mike Jennings, Dr. Leighton Coatsworth, Jo-Ann (Forrest) Bice, Margaret Hyland, Brenda Addison, Dr. Giles Jean, Ian Muir, John Bozak and Steven Tolman. I could go on, but I hope all the others would not be too offended if I acknowledged them with a general Thank-You.

Finally I must thank my supervisors, Professors Mike Bancroft and Wayne Nesbitt, first for the moral support and freedom they allowed me, and second for their financial support over the years. It was Mike's idea that I should look at the REE phosphates, and Wayne's idea that I should examine their geochemistry.

I have learned a great deal over the past few years, and for that I am truly grateful!

LIST OF FIGURES

LIST OF PHOTOGRAPHIC PLATES

LIST OF TABLES

LIST OF FIGURES

NOMENCLATURE

Symbol	Definition
A	coefficient in Davies equation
A	relative isotopic abundance
A	general term for cation
A	Angstrom unit; 100 picometers
An	actinide
a	activity
ap	apatite
b	ratio of rate constants
C	Celsius or Centigrade.
C,c	concentration of dissolved species
C_{eq}	equilibrium concentration
cm^{-1}	wavenumber
cps	counts per second
d	spacing of crystallographic planes, in A
DTA	differential thermal analysis
DMSO	dimethyl sulfoxide
E	energy
eV	electron volts
EDTA	ethylenediaminetetraacetic acid, disodium salt
EPR	electron paramagnetic resonance
F	final
F^k	Slater integral
G	free energy
H	enthalpy
h	peak height
HREE	heavy rare earth element, Dy-Lu + Y.
I	ionic strength
I	intensity
I_o	initial intensity
INAA	instrumental neutron activation analysis
J	joules, $kg\text{-}m^2s^{-2}$
K	Kelvins, (absolute temperature scale)

Symbol	Definition
K	equilibrium constant
K^{o}	ion activity equilibrium constant
k	rate constant
kg	kilogram
L	liter
l	path length of absorption cell
LREE	light rare earth element, La-Tb.
ln	natural logarithm
log	logarithm, base 10.
M	monazite
M	molarity, moles per liter
m	molality, moles per kilogram solvent
m	medium
m	meter
MW	molecular weight
mL	milliliter
mM	millimolar
nm	nanometer
P	gas pressure
P	total phosphate concentration
p	negative logarithm, base 10
pH	negative log H^{+} concentration, see chapter 4
pmol/kg	picomoles per kilogram, (molality)
ppm	parts per million, weight for weight
ppt	parts per thousand
R	gas constant, 8.31433 $JK^{-1}mole^{-1}$
R	rhabdophane
r	rate of reaction
r	radius of ion
REE	rare earth element, La-Lu + Y
S	entropy
S	number of surface sites
s	second
s	solid

Symbol	Definition
s	strong
SEM	scanning electron microscopy
SIMS	secondar ion mass spectrometry
T	temperature
T_p	temperature of sample preparation
T_1	temperature of endothermic peak
T_2	temperature of exothermic peak
T_3	maximum temperature for isochronal heating
T_c	total calculated elemental intensity, (SIMS)
t	time
TGA	thermogravimetric analysis
UV	ultraviolet
v	volume of gas adsorbed on surface
v_m	maximum volume of gas adsorbed on surface
vw	very weak
w	weak
X	xenotime
X	general symbol for anion, or central atom in an oxy-anion
x	mole fraction
XRD	x-ray diffraction
z	charge on ion
α	solid state phase designation
β	"
γ	"
γ	activity coefficient
$\gamma_\pm$	mean activity coefficient
ϵ	molar extinction coefficient
ζ	spin-orbit coupling constant
θ	surface coverage
θ	angle measurement, degrees
λ	wavelength
μ	micro-

Symbol	Definition
$\tilde{\nu}$	vibration mode in IR
ρ	relative density
σ	cross-section of absorption
( )	activity units
[ ]	concentration units

1 PURPOSE AND INTRODUCTION

1.1 Purpose and Outline

The principal objectives of the thesis work were to investigate the dissolution and adsorption behaviour of rare earth element (REE) phosphates, in view of their potential use as nuclear waste host matrices; to investigate REE geochemistry in view of what was learned about REE phosphate behaviour; and to contribute to the understanding of the dissolution and adsorption behaviour of minerals in general. A secondary objective was to evaluate several surface analytical techniques for their usefulness in studying the surface reactions of REE phosphates.

Crystalline forms of REE phosphates were prepared for a selection of REE. The development of acceptable synthesis techniques required quite some time, and the refinement of the techniques continued up to the end of the laboratory section of the thesis work. The usual products of these syntheses were hydrated REE phosphates. Anhydrous REE phosphate single crystals were prepared by a high temperature flux technique, and kindly donated by L.A. Boatner at Oak Ridge National Laboratory, (Oak Ridge Tennessee). The hydrous forms were characterized by powder x-ray diffraction (XRD), scanning electron microscopy (SEM) and differential thermal analysis (DTA).

The single crystals were analyzed for impurities by secondary ion mass spectrometry (SIMS).

Solubility products were measured for the hydrous REE phosphates. Previous determinations[4] indicated that the REE phosphates are very insoluble, (pK_{sp}= 24). This helped to explain why materials were so difficult to crystallize from aqueous solution. Because the literature contained very few determinations of REE phosphate solubility products, a method was developed for measuring these relatively easily. Advantage was taken of the fact that H_3PO_4 is a moderately weak acid, so that the solubility of the particular REE phosphate rises quickly with a decrease in pH. The colored REE ions were measured by optical spectrophotometry, while lanthanum concentrations were measured by instrumental neutron activation analysis.

The solubility products obtained were used to evaluate the dissolution kinetics data, and surface reaction data, as well as explaining oceanic REE concentrations.

The kinetics of surface reactions such as replacement, were difficult to measure and evaluate because the surface analytical techniques were found to be less sensitive and quantitative than had been hoped originally. The qualitative results obtained were nevertheless useful in the debate about surface reactions (chapter 5), in that they showed the importance of long term immobilization processes in REE geochemistry, as opposed to transient adsorption.

1.2 REE Phosphates as Nuclear Waste Hosts

There are many aspects to the problem of nuclear waste containment[2,3], but it has become apparent that the form of the actual waste is not as important a consideration as the manner and location of the burial[4]. In the last few years, the emphasis has shifted to the modelling of radionuclides in the groundwater and geological environment surrounding the disposal site[5]. The emphasis in the thesis work is therefore on those surface reactions which retard or halt the aqueous transport of radionuclides, in particular the REE and actinides. The REE phosphates are important both as nuclear waste hosts and as possible products of surface reactions of dissolved REE.

There are basically two forms of REE phosphates which have been proposed as nuclear waste hosts, namely glasses and ceramics. In 1978 McCarthy et al.,[6] pointed out that monazite, a phosphate of REE, Ca, Th and U, could be used as a model for studying the long term behaviour of REE-phosphate based waste forms. Monazite accumulates in beach sands[6] which suggests its chemical and mechanical stability under humid, ambient conditions. It is also known to form in hydrothermal systems, which suggests its stability under conditions of elevated temperature and pressure. These are conditions which might conceivably occur in some disposal systems. In addition, monazite is fairly resistant to metamictization, (radiation-induced lattice damage).

Since 1980, Boatner et al.,[7] have examined the synthesis, crystal chemistry and dissolution of pure and doped single crystals and ceramics, with[8] and without[9] nuclear defense and reactor waste. Comparative measurements of corrosion rates of monazite ceramics, borosilicate glass and SYNROC showed that monazite had the lowest corrosion rate of the forms considered,[10]. In another study[11] the leach rates of Cs, Sr and U from synthetic monazite at 90°C were more than 20 times lower than those from borosilicate glass.

Grambow and Lutze[12] studied the behaviour of complex phosphate glasses containing Fe, Al and waste oxides under hydrothermal conditions, (i.e., greater than 100°C and at elevated pressure). The glass crystallized under these conditions, but the leach rate was still considerably less than that of borosilicate glass.

In 1984 Sales and Boatner[13] announced the development of a particular iron/lead phosphate glass which had considerably lower corrosion rates than borosilicate glass for the pH range 3 to 11. The advantage of using glass over ceramic is that a greater variety of chemical elements can be incorporated than into any particular crystal lattice.

With regard to the immobilization of radionuclides after dissolution from the waste host, autoradiography has demonstrated the strong "adsorption" of ^{147}Pm by apatite in granite[14]. The particularly strong adsorption

was interpreted to indicate a reaction between the REE and apatite to form monazite. Further, the behaviour of ^{241}Am was found to parallel that of ^{147}Pm in these systems.

1.3 Geochemistry of the Rare Earth Elements

Geochemistry is concerned with modelling the physical and chemical behaviour of the elements in nature. In building such models it is often convenient to group similar elements together. Such elements often occur together in nature. Good examples are the element pairs Zr and Hf, and Nb and Ta. Such grouping allows a more efficient collection and interpretation of data. The rare earth elements, (lanthanides plus yttrium), also constitute such a group. The two principal factors controlling the distribution of the REE in nature are their absolute or cosmic abundances, and their crystal chemistry. Figure 1.1 shows the relative abundances of REE in carbonaceous chondrites[15], (meteorites which are considered to be very primitive, chemically), and the corresponding ionic radii for the $3+$ ions in 8-fold coordination sites[16]. In the case of REE fluorides, (upon which the radii are based), Y falls between Er and Ho. The change in ionic radius is fairly smooth, suggesting a smooth change in the chemical behaviours of the REE as the atomic number is increased. A good example is provided by the REE/EDTA solution complexes. The free energies of formation presented in figure 1.2, show a smooth change with a change in the atomic number of the REE. Examination of the changes in enthalpy and entropy reveals a more complicated trend, however.

Figure 1.1 Ionic radii of the REE, (CN = 8) and REE cosmic abundances, based on a compilation of chemical analyses of C1-type chondritic meteorites. Data are from Shannon and Prewitt[16] and Anders and Ebihara[15], respectively.

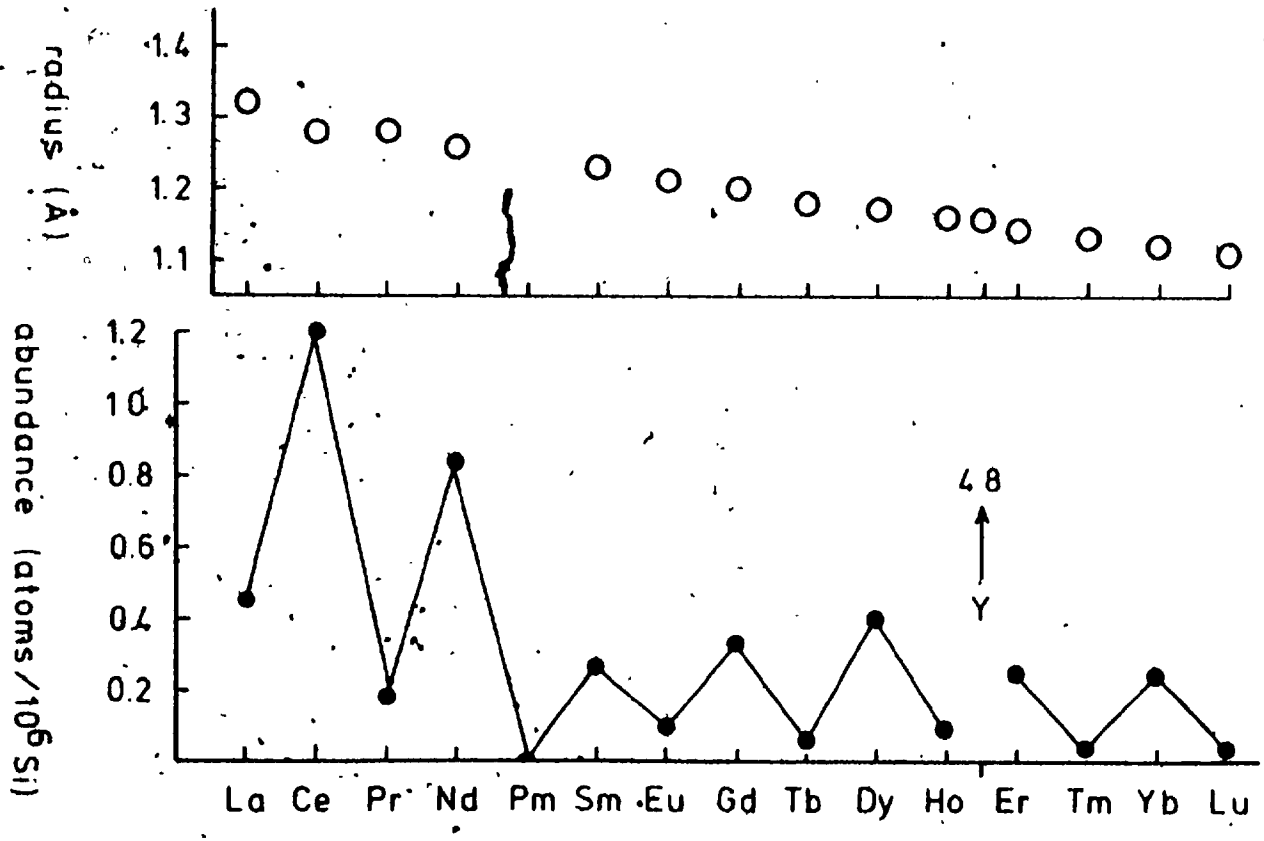

Figure 1.2 Thermochemical data for formation of REE EDTA complexes at 25° C as a function of ionic radius.

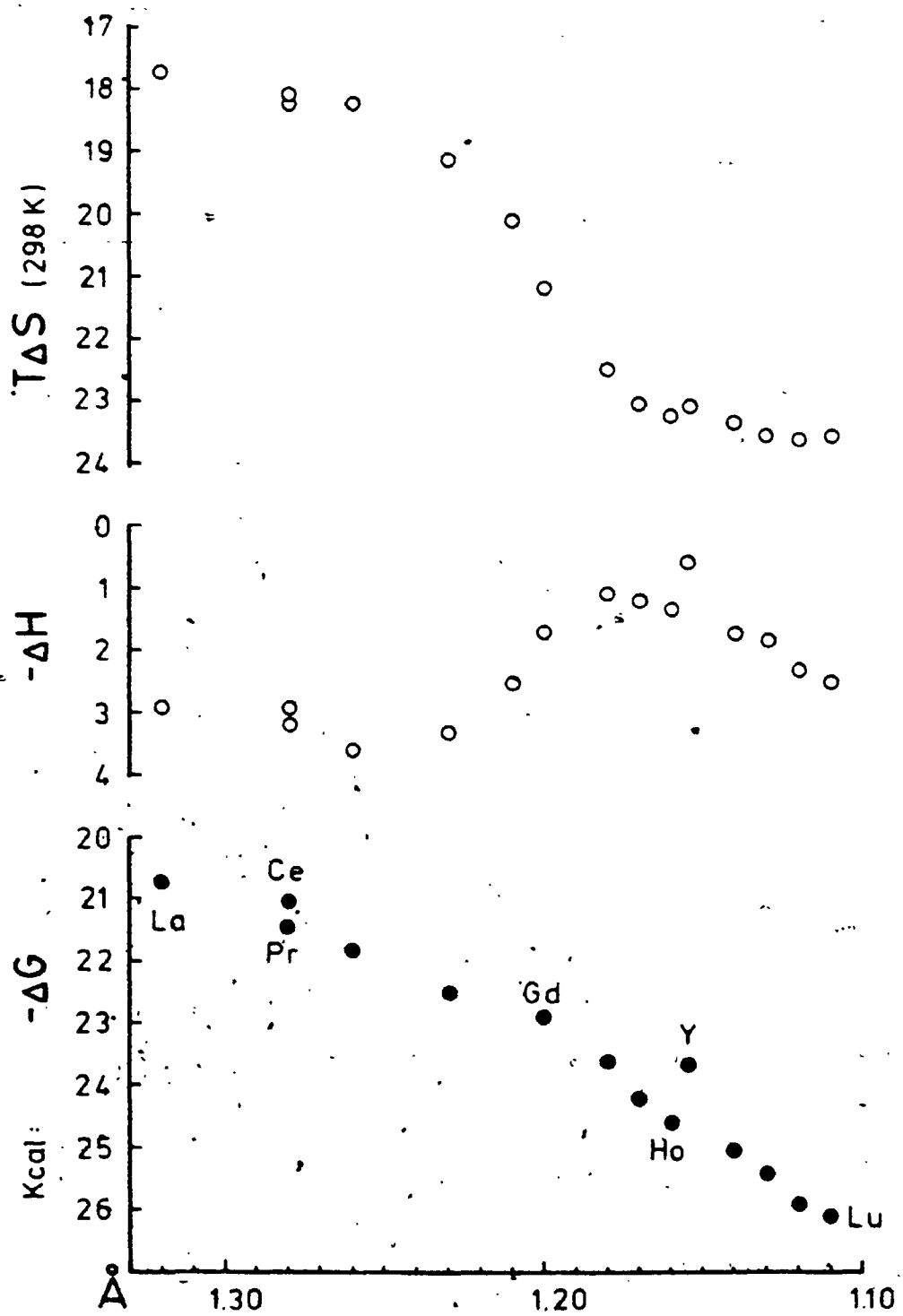

The knowledge of the geochemical behaviour of the REE is not yet sufficient to permit detailed geochemical cycles to be constructed. A good review of the status of REE geochemistry is provided by Fleet[18]. A few points are summarized here which are relevant to the discussion at the end of chapter 4.

1) The REE resemble each other in their chemical properties.

2) Ce and Eu may be separated from the other REE under oxidizing or reducing conditions, respectively.

3) REE tend to fractionate when phase separations occur. The lighter REE tend to form different minerals than the heavy REE, though complete separation never occurs in nature.

4) REE in the earth's crust tend to be enriched in the LREE relative to chondrite values[19].

5) REE tend to form, or be found in insoluble mineral phases at or near the earth's surface. Most of the REE material entering the sea is transported as particulate matter[18].

6) REE are mobilized in the solution phase only under extreme weathering conditions[20]. They tend to be quickly reprecipitated as insoluble phases such as florencite or rhabdophane[21].

7) Because of rules 4 and 5, shales tend to reflect crustal REE abundances, and so also show enrichment in LREE.

8) REE are ubiquitous in nature, though concentrations do vary. Total REE abundances in seashells are about 2 ppm; in chondrites about 5 ppm; in coals about 35 ppm; in North American shales about 230 ppm and in phosphorites 420 ppm[22,23].

9) Seawater patterns of dissolved REE suggest a mixed source for dissolved REE, consisting of continental plus marine volcanic components[19].

In this study, contributions will be made to the study of REE geochemistry by preparing and characterizing REE phosphates. Solubility products for some of these REE phosphates will be obtained and used to enhance the discussion of seawater REE concentrations.

1.4 Surface Reactions

There are many types of surface reaction important in geochemistry. One such type is adsorption, which IUPAC[24] defines as: "...the enrichment (positive adsorption, or briefly, adsorption) or depletion (negative adsorption) of one or more components in an interfacial layer." Processes which tranfer components from one bulk phase to another can be termed absorption. When it is difficult to distinguish experimentally between adsorption and absorption, the term sorption can be used.

All these definitions imply that the substrate is not chemically altered as a result of sorption processes. Further, adsorption is implicitly a 2-dimensional process, as opposed to precipitation, which is a 3-dimensional process[25]. Multilayer adsorption has been treated as a special case of adsorption, however.[26]

For the purposes of the discussions in this work, surface reaction will be defined as any physical or chemical process occurring at the solid/solution interface which results in an experimentally detectable change in the structure or composition of the surface region of the substrate. It will be the purpose of chapter 5 to discuss which surface reactions are important with regard to REE phosphates.

There is no single, universal model of adsorption, partly because there are many different processes which might be called adsorption. However there is one type of adsorption isotherm which is often used to model adsorption data, and constitutes a good example in an introduction to the study of adsorption. This is the Langmuir Adsorption Isotherm. The following derivation was taken from Adamson[27]. Originally, the model was developed for the adsorption of gases on homogeneous solid surfaces. The first step is to assume that the rate of adsorption r_a, is given by

$$r_a = k_2 P S_o = k_2 P(S - S_1) \qquad (1.1)$$

and the rate of desorption r_d, is given by

$$r_d = k_1 S_1 \qquad (1.2)$$

where k_2 and k_1 are rate constants, P is the pressure of the single component gas, S is the number of 'sites', S_o the number of unoccupied sites, and S_1 the number of sites which are occupied. At equilibrium the two rates are equal, so that

$$S_1/S = \theta = bP(1 + bP) \qquad (1.3)$$

where θ is the fractional surface coverage, and $b = k_2/k_1$. Assuming there is one molecule of adsorbed gas per site,

equation 1.3 can be written,

$$v = v_m bP/(1 + bP) \qquad (1.4)$$

where v is the volume of gas adsorbed, and v_m is the maximum volume of gas which can be adsorbed. Equation 1.4 can also be written as

$$P/v = 1/(bv_m) + P/v_m. \qquad (1.5)$$

This model is often applied to adsorption from solution. However, the model does not always work in the case of a single component gas, and is less successful when applied to adsorption from solution.

There are a number of assumptions in the model which might explain the lack of consistent success. The model is an equilibrium model. It assumes that binding energies for all sites are equal and independent of surface coverage. It also assumes that there is no interaction between adsorbate molecules. It assumes that there is no further reaction between substrate and adsorbate; i.e., the substrate is otherwise inert. The model also implies, but does not require, that the number of sites is independent of the nature of the adsorbing gas. This is an assumption which is routinely made in adsorption studies. Finally, the definition of 'site' is unclear. Implicitly, the size of the site is defined by the effective size of the adsorbing molecule. This is not consistent with the assumption of the constancy of the number of sites.

Further, Sposito[25] points out (on page 122), that "The adherence of experimental sorption data to an adsorption isotherm equation provides no evidence as to the actual mechanism of a sorption process,..."

The problem of deciding which of several processes is actually going on in a particular system will be further discussed in chapter 5.

REFERENCES FOR CHAPTER 1

1. Tananaev I.V. and V.P. Vasil'eva (1963) Russ. J. Inorg. Chem. 8, 555-469.
2. Brookins D.G. (1984) Geochemical Aspects of Radioactive Waste Disposal. Springer-Verlag.
3. Gilmore W.R., Ed. (1977) Radioactive Waste Disposal Noyes Data Corporation.
4. Bird G.W. and W.S. Fyfe (1982) Chem. Geol. 36, 1-13.
5. Chapman N.A. and F.P. Sargent (1984) The Geochemistry of High-Level Waste Disposal in Granitic Rocks. Atomic Energy of Canada Limited, #AECL-8361. (This is an unrestricted, unpublished report available from SDDO, CRNL-AECL, KOJ 1JO).
6. McCarthy G.J., W.B. White and D.E. Pfoertsch (1978) Mat. Res. Bull. 13, 1239-1245.
7. Boatner L.A., G.W. Beall, M.M. Abraham, C.B. Finch, P.G. Huray and M. Rappaz (1980) Scientific Basis for Nuclear Waste Management 2, 289-296. C.J.M. Northrup, Jr. Plenum Press.
8. Abraham M.M., L.A. Boatner, T.C. Quinby, D.K. Thomas and M. Rappaz (1980) Radioactive Waste Management 1, 181-191.
9. Petek M., M.M. Abraham and L.A. Boatner (1982) The Scientific Basis for Nuclear Waste Management 5, 181-186. S.V. Topp, Ed. Elsevier.

10. Sales B.C., M. Petek and L.A. Boatner (1983) Mat. Res. Soc. Symp. Proc. 15, 251-258.

11. Sales B.C., C.W. White and L.A. Boatner (1983) Nuclear and Chemical Waste Management 4, 281-289.

12. Grambow B. and W. Lutze (1980) Scientific Basis for Nuclear Waste Management 2, 109-116. C.J.M. Northrup, Jr. Ed. Plenum Press.

13. Sales B.C. and L.A. Boatner (1984) Science 226, 45-48.

14. Kamineni D.C., T.T. Vandergraaf and K.V. Ticknor (1983) Can. Mineral. 21, 625-636.

15. Anders E. and M. Ebihara (1982) Geochim. Cosmochim. Acta 46, 2363-2380.

16. Shannon R.D. and C.T. Prewitt (1969) Acta Cryst. B25, 925-946.

17. Phillips C.S.G. and R.J.P. Williams (1966) Inorganic Chemistry vol.2. Oxford University Press.

18. Fleet A.J. (1984) Rare Earth Element Geochemistry P. Henderson, Ed. Elsevier.

19. Piper D.Z. (1974) Chem. Geol. 14, 285-304.

20. Nesbitt H.W. (1979) Nature 279, 206-210.

21. Sawka W.N., J.F. Banfield and B.W. Chappell (1986) Geochim. Cosmochim. Acta 50, 171-175.

22. Schofield A. and L. Haskin (1966) Geochim. Cosmochim. Acta 28, 437-446.

23. Haskin L.A., T.R. Wildeman, F.A. Frey, K.A. Collins, C.R. Keedy and M.A. Haskin (1966) J. Geophys. Res. 71, 6091-6105.

24. IUPAC, (prepared by D.H. Everett), (1972) Pure and Applied Chem. 31, 579-638.

25. Sposito, G. (1984) The Surface Chemistry of Soils Oxford University Press.

26. Greenland D.J. and M.H.B. Hayes, Eds. (1981) The Chemistry of Soil Processes. John Wiley and Sons.

27. Adamson A.W. (1973) A Textbook of Physical Chemistry. Academic Press.

2. MATERIALS

2.1 Introduction and Review

In discussing the REE phosphates, it would be useful to review isostructural compounds at the same time. One reason for this is that such compounds often undergo similar structural changes with temperature and pressure. Information about a well studied compound can be used to predict or interpret physical properties of less well studied analogs. Further isostructural compounds often have considerable mutual miscibilities. It is this aspect of REE phosphates that makes them attractive nuclear waste hosts.

There are essentially four structure types which are of interest when discussing REE phosphates with stoichiometries AXO_4 or $AXO_4 \cdot xH_2O$: 1) monoclinic MONAZITE ($P2_1/n$); 2) tetragonal XENOTIME or ZIRCON ($I4_1/amd$); 3) hexagonal RHABDOPHANE ($P6_222$ or $C3_121$, there is some controversy here) and 4) "HYDROUS XENOTIME" ($I4_1/amd$). (The convention is adopted in this work that capitalized mineral names refer to structure types and any synthetic compound adopting that structure). In table 2.1 some examples of minerals and synthetic compounds are listed. A number of similar compounds with alternate structures are listed for completeness. Examples of compounds with either SCHEELITE or FERGUSONITE structures are included to demonstrate variations which may take place with

Table.2.1 Compilation of compounds of the AXO_4 or $AXO_4.xH_2O$ stoichiometry, according to structure type.

Mineral or Compound	Composition	Comments	Reference
MONAZITE structure type:		($P2_1/n$)	
monazite	(LREE,HREE)PO_4		1
cheralite	(Th,Ca,LREE)PO_4		2
$LaPO_4$-$GdPO_4$		powder	3,4
		single xl.	5,6,7
$LaVO_4$			3,4
$LaAsO_4$-$NdAsO_4$			3
$PuPO_4$			8,9
$AmPO_4$			9
$PuAsO_4$, $AmAsO_4$			9
$M^{II}Th(PO_4)_2$, M= Cd;Ca;Sr;Pb			10
$M^{II}Th(AsO_4)_2$, M= Ba;Pb;Sr			10
$PbTh(VO_4)_2$		high temp	11
huttonite	$ThSiO_4$	high temp	12
		single xl.	13
$BiPO_4$, $BiAsO_4$			3
$CmPO_4$			14
FERGUSONITE	($YNbO_4$)	($P4_2/n$)	
$LaNbO_4$-$LuNbO_4$; $YNbO_4$			4

Table 2.1 Continued...

SCHEELITE, $CaWO_4$		$(I4_1/a)$	
$PbTh(VO_4)_2$		low temp	11
$SmAsO_4$-$LuAsO_4$		high pressure	15
$PrVO_4$-$LuVO_4$		high pressure	15
XENOTIME, (HREE)PO_4		$(I4_1/amd)$	
$TbPO_4$-$LuPO_4$; $ScPO_4$; YPO_4			3,4
$TbPO_4$-$LuPO_4$		single xl.	16
$CeVO_4$-$LuVO_4$; $ScVO_4$; YVO_4			3,4
$SmAsO_4$-$LuAsO_4$			3
$AmVO_4$			9
zircon	$(Zr,Hf,Th)SiO_4$		1
thorite	$ThSiO_4$	low temp	12
		single xl.	13
$CaTh(AsO_4)_2$; $CdTh(AsO_4)_2$			10
$PbTh(VO_4)_2$		intermediate temp	11
HYDROUS XENOTIME, (HREE)$PO_4 \cdot xH_2O$		$(I4_1/amd)$	
$HoPO_4$-$LuPO_4$, (1.5-2 H_2O)			17
NINGYOITE		(P222)	
ningyoite	$(U,Ca,REE)PO_4 \cdot 1\text{-}2H_2O$		18
$UCa(PO_4)_2$		synthetic	18
$DyPO_4 \cdot 1.5H_2O$; $HoPO_4 \cdot 2H_2O$			19

Table 2.1 Continued...

GYPSUM, $CaSO_4 \cdot 2H_2O$	(C2/c)	
churchite	$(HREE)PO_4 \cdot xH_2O$	20
RHABDOPHANE	($P6_222$ or $C3_121$)	
rhabdophane	$(LREE)PO_4 \cdot 1\text{-}2H_2O$	21,22
tristramite	$(Ca,U,Fe)(PO_4,SO_4,CO_3) \cdot 2H_2O$	22
brockite	$(Ca,Th,REE)(PO_4,CO_3) \cdot 0.9H_2O$	24
$REEPO_4 \cdot xH_2O$, REE= La;Ce;Nd		25,26
$PmPO_4 \cdot \frac{1}{2}H_2O$		27
$AcPO_4 \cdot \frac{1}{2}H_2O$; $AmPO_4 \cdot \frac{1}{2}H_2O$		9
$PuPO_4 \cdot \frac{1}{2}H_2O$		8,9
$BiPO_4 \cdot \frac{1}{2}H_2O$		28

variations in temperature, pressure or composition. Examples of such variations are discussed by Fukunaga and Yamaoka[29] and Stubican and Roy[15]. As might be inferred from table 2.1, the radius ratio r(A):r(X) in AXO_4 is very important in determining the structure adopted by a particular compound. It is, for example, this ratio which determines whether the cation A, exists in a 9-fold site, (MONAZITE) or an 8-fold site (XENOTIME). The ideal geometries of these sites are depicted in figures 2.1 and 2.2. As was seen in figure 1.1, the ionic radii of the lanthanides decrease smoothly from 132 pm for La to 111 pm for Lu. Yttrium has a corresponding radius of 115.5 pm, placing Y between Yb and Er in the series. It is for this reason that Y is always abundant in minerals of the HREE. These radii also help to explain why early or light REE form phosphates with cation sites of higher coordination number than the late or heavy REE. In fact the dividing line separating the heavy from the light REE is not fixed. It depends, for example, on the radius ratio, r(A):r(X). For the phosphates of REE, the dividing line is between Gd and Tb. Some workers have found that $TbPO_4$ is in fact dimorphic[32]. For the arsenates of REE, the dividing line is between Nd and Sm; for the vanadates, between La and Ce.

This observation of a dividing line in the REE series also occurs in the series of hydrous REE phosphates. RHABDOPHANE derivatives tend to transform to the corresponding MONAZITE derivatives at elevated temperature.

Figure 2.1 . Idealized sketch of oxygen coordination about metal center in MONAZITE: pentagonal interpenetrating tetrahedral polyhedron,(6).

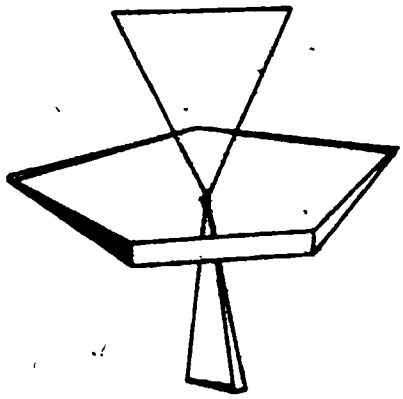

Figure 2.2 Idealized sketch of oxygen coordination about metal center in XENOTIME: two interpenetrating tetrahedra,(30).

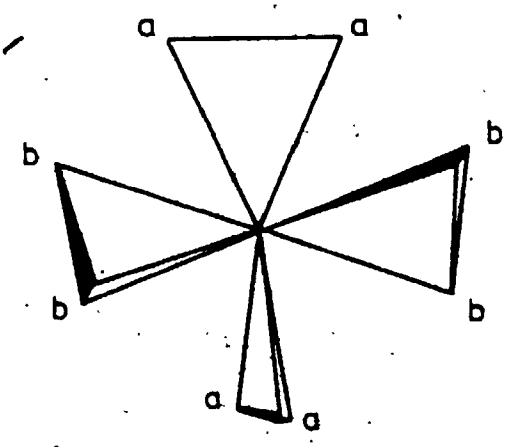

The actual dividing line in the RHABDOPHANE/XENOTIME series of compounds is not so clear. This point will be investigated in chapter 3.

Of course in attempting to relate the crystal chemistry of REE phosphates to the problems of geochemistry and nuclear waste stability, other factors become important. One is the tendency of similar phases to form solid solutions. The other is the ability of several REE and many actinides to have several oxidation states, depending on the redox conditions. As a result of favourable entropies of mixing, many phases tend to form solid solutions at elevated temperatures. Monazite is known to contain all naturally occurring REE, in addition to Th and Ca. In the case of the REE, the entropies of mixing are sufficient to permit some degree of solid solution among the REE at room temperatures. Rhabdophane, which is known to form as an alteration product of REE minerals at ambient temperatures, contains all the REE; though of course the HREE are depleted relative to natural abundance levels, (see chapter 3). It is expected that many actinides, in addition to Th and U will form mixed phosphate phases with the REE. Pu(III)-RHABDOPHANE and Pu(III)-, Am(III)- and Cm(III)- MONAZITE are known compounds, (table 2.1).

The extent of miscibility is limited however, by variations in the oxidation states of many of the elements of interest. For example, Ce can be separated in nature

and in the laboratory from the other REE by its oxidation to the (IV) state. As Ce(IV), it resembles Th in its chemistry. Both are more easily hydrolyzed than the REE(III) ions; both have shorter residence times in the oceans than the 3+ ions.

Uranium resembles Th only when the redox conditions permit the reduction of U(VI) to U(IV). Figure 2.3 shows a redox diagram for U, Np and Pu at a pH of 8. Uranium along with Np, Pu and Am tend to form the species AnO_2^{2+} and AnO_2^{+} under oxidizing conditions, (An = actinide). These oxy-cations are much less soluble in solid REE phosphate phases than are the An(III) and An(IV) ions. The oxy-cations also form phosphate phases of their own, but these tend to be much more soluble in aqueous solutions than phosphates of An(III), REE(III) and An(IV).

Figure 2.3 suggests that of the several oxidation states available to Np, only the (V) and (IV) states are are likely to be important in nature. Important boundaries in figure 2.3 are the potentials for the reduction, (-0.47 V) and oxidation of water (+0.76 V), at a pH of 8, and a temperature of 25° C. These values are convenient markers for bracketing the range of expected redox potentials in nature. It must also be pointed out that such diagrams are only a guide. The redox potentials of reactions are strongly dependent on the pH of the system. Further, the ligand environment of the cation strongly affects the stability of the oxidation states of the ion. The data in

Figure 2.3 Distribution diagrams for hydrolysis products of a) U, b) Np and c) Pu, as functions of the redox potential at a pH of 8. Diagrams were adapted from Allard et al.,[53].

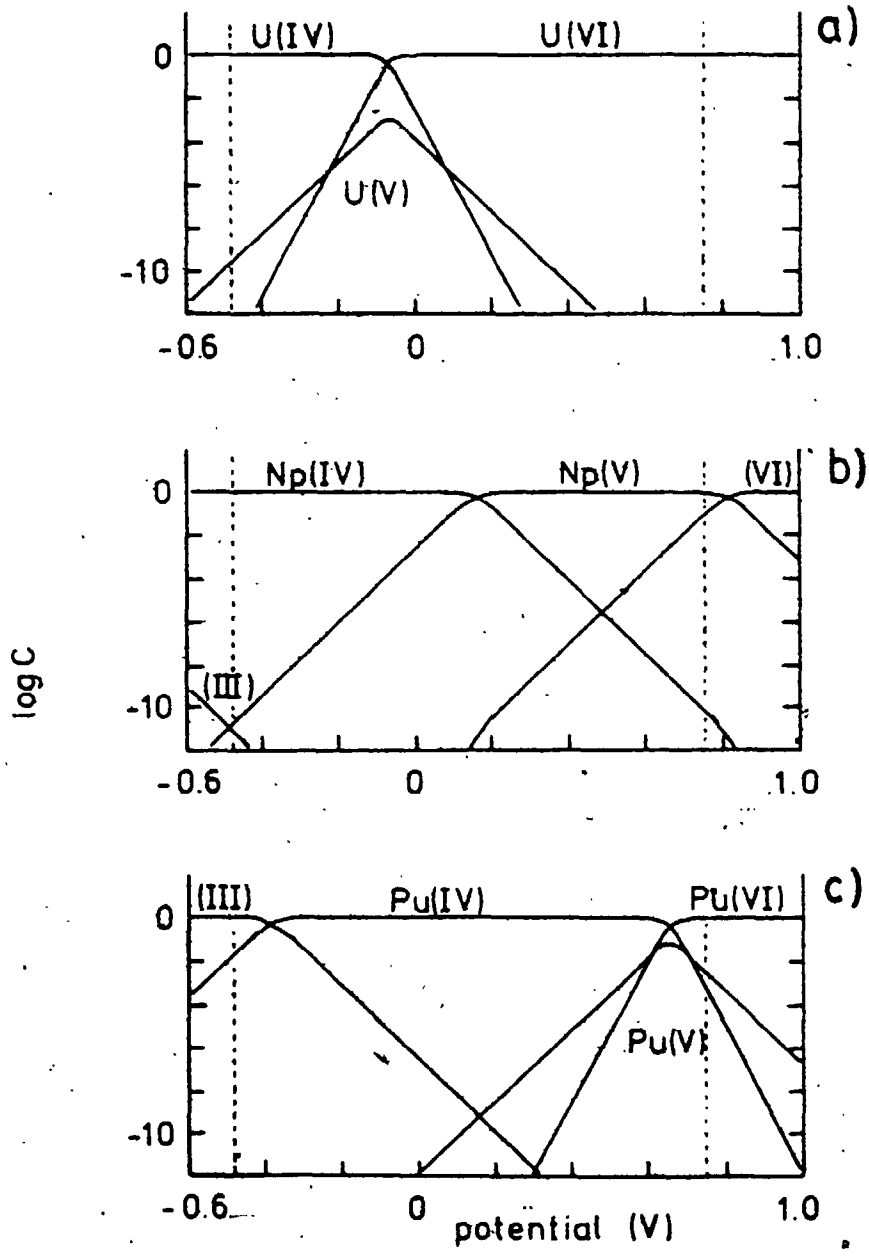

figure 2.3 are from Allard et al.,[53] who considered only the hydroxycomplexes of U, Np and Pu in drawing the figures. Finally, the temperature affects the complexation and redox potentials of reactions. Brookins[37] gives a good presentation of redox diagrams relevant to the geochemistry of actinides.

In the case of Pu, the (VI) and (V) states are important under oxidizing conditions, while the (III) and (IV) states are important under reducing conditions[33,34]. High temperatures tend to favour the lower oxidation states. For example, Pu(IV) phosphates tend to lose O_2 at high temperatures to form $PuPO_4$[35]. Again, only the reduced forms of Pu resemble the REE cations. Both Pu(III) and Pu(IV) are scavenged from acidic solutions by phosphate, though the Pu(IV) forms are more completely precipitated.

Data presented in Brookins[37] suggest that for Am, the important oxidation states are (III) and (IV). The later transplutonium elements are most likely to be found in the (III) state. Thus the actinides are in general expected to resemble the REE in their geochemistry. The significant exceptions are Pa(V), U(VI), Pu(V), Pu(VI) and Np(V). (Further general discussions of the chemistry of the actinides and lanthanides are given in 36 and 38).

2.2 Review of Synthesis Methods From the Literature

Several criteria were used in selecting a method from the literature for the preparation of REE phosphate compounds. The solids must be coarse enough to be easily filtered. The solids must be homogeneous, both chemically as well as crystallographically. The crystals must be large enough that surface energies do not contribute significantly to their solubilities. This requires a minimum grain size of about 1 μm. The method has to be practical and inexpensive. Finally, it would be highly desirable to be able to precipitate these phases from aqueous solutions. This way, solubility data could be obtained from supersaturation as well as from undersaturation.

Methods used to prepare compounds of the sort listed in table 2.1 fall into three categories. Use of high temperatures can result in anhydrous, coarsely crystalline materials. Lower temperature precipitation from aqueous solutions tends to yield materials of a fine-grained or even amorphous nature. These materials will tend to be chemically impure because of occlusion, adsorption, and coprecipitation. Hydrothermal methods produce either hydrous or anhydrous materials of good crystallinity, depending on the temperature.

The first category of synthesis can be further subdivided into flux-growth, and sintering or calcining methods. For example, the lead-pyrophosphate technique

involves preparing a melt of $Pb_2P_2O_7$ from $PbHPO_4$. To this melt is added a particular REE oxide in a platinum crucible, and heated to about 1400° C. The system is cooled at about 1 Celsius degree per hour to about 900°, (39,40,41). The flux surrounding the crystals is removed by boiling the mass in nitric acid. The single crystals so obtained are typically several mm in length. (This was the method used by L.A. Boatner[41] to prepare the crystals used in this study).

In the sintering method[42] the respective REE phosphate is precipitated from dilute acid solutions with $NH_4H_2PO_4$ as a very fine-grained powder. The suspension is filtered and dried, and then heated to 600°C. The powder is then cooled, crushed, re-pelletized and fired at 1200° for 35 hr. The last step is then repeated. The anhydrous REE phosphates obtained in this manner are suitable for powder x-ray diffraction.

In the second major category of synthesis methods, the pH of the solution used for the precipitation reactions was found to be an important parameter determining the nature and quality of the precipitate. Often well crystallized materials could only be obtained at low pH, (8,17,25,26,35). Occasionally, the crystallinity was found to be poor[43]. As the pH is raised, solid phases containing other cations introduced into the solution as counter-ions, were found to form[44]. At even higher pH's

hydrolysis of the REE ions was apparent, and the products consequently consisted of hydroxy-phosphates.[43] In all the latter cases, the precipitates had to be sintered in order for powder diffraction patterns to be obtained.

Hydrothermal methods, involving closed systems and temperatures between 50 and 300° C have been employed to produce hydrous and anhydrous phosphate derivatives of lanthanides[32] and actinides[9]. In the case of LREE, RHABDOPHANE phases were observed to form at temperatures up to 250° C; at 300°, MONAZITE was observed to form. These results do not constitute a determination of the phase diagram, however. It was found that by keeping the REE phosphate at 250° for a year that MONAZITE was the final product.

So far the methods described are concerned with preparing phosphates with only a single REE. Studies have also been carried out with the purpose of examining the extents of substitution of other cations in REE phosphates, and the behaviour of these solid solutions as a function of temperature.

Bamberger et al.,[35] studied the effects of varying the solution Ce(III)/Bi(III) ratios on the nature and composition of phosphates precipitated from dilute nitric acid solutions. The phases involved were α-$CePO_4$, (RHABDOPHANE), β-$CePO_4$ (MONAZITE), α-$BiPO_4$ (RHABDOPHANE), β-$BiPO_4$ (MONAZITE) and δ-$BiPO_4$ (high temperature form).

For all the Ce/Ce+Bi ratios examined, except that equal to one, the product was α-$BiPO_4$. The similarity of the α-Ce and α-Bi phosphates prevented a distinction being made between these two phases by powder XRD. Raman spectroscopy indicated that the product consisted of a mechanical mixture, (i.e., two phases), of Ce and Bi phosphates. When this mixture is heated, separate phases could be indentified by powder XRD, for those mixtures with Ce contents of less than 30%. Above that value, only Ce-MONAZITE could be identified. Raman spectra indicated that for Ce contents greater than 10%, Ce/Bi phosphate solid solutions were obtained. These results are not surprising since, in general, mutual miscibilities increase with increasing temperature.

The same study also looked at the effects of varying Ce(IV)/Bi(III) ratios during the precipitation of the phosphate. It was found that only above a certain Ce/Bi ratio could separate Ce(IV) phosphate phases be detected, which suggests a considerable substitution of Ce(IV) for Bi. The nature of the charge compensation involved was not determined. Ignition of these products between 400 and 600° C resulted in the reduction of Ce(IV) to Ce(III), with the elimination of O_2. Again solid solutions of Ce(III) and Bi(III) phosphates were the result.

Another example of a study involving substitution reactions is provided by Carron et al.,[32] who fractionally precipitated adjacent pairs of REE with phosphoric acid

at temperatures between 50 and 300° C. The total-REE to phosphate ratios varied between 4:1 and 2:1. Separation factors were found to vary in a surprisingly irregular manner with atomic number. Samarium was found to be precipitated preferentially to the other REE. Among the HREE, the Yb phosphate was formed first. The products were all examined via powder XRD. Since the purpose of the study was to evaluate fractional precipitation as a means of separating the REE, the nature of the products in terms of solid solutions versus mechanical mixtures was not examined, however.

Finally, a series of studies should be mentioned involving the ERP measurements of REE phosphates doped with REE and actinide metal ions. In these studies, the single crystals were prepared by the $Pb_2P_2O_7$ technique[41] mentioned earlier.

In an initial study of the oxidation states of actinides in $LaPO_4$ single crystals, optical absorption spectroscopy was used to determine the oxidation states of U, Np, Pu Am and Cm doped in percent quantities into the monazite host[45]. Species found included U(IV), U(III), Pu(IV), Np(IV), Am(III) and probably Cm(III). The ambiguity of the Cm results prompted an EPR experiment using ^{243}Cm and ^{244}Cm doped into $LuPO_4$ host crystals[46]. Electron paramagnetic resonance (EPR), is particularly well suited to the study of paramagnetic impurities, such as paramagnetic actinide and lanthanide ions. The method gives information about

the valence state of a particular element from the number and positions of measured transitions in the EPR spectrum. Multiplets result from the removal of the free-ion energy level degeneracy by the crystalline field. Simulation calculations thus yield information about the site symmetry of the ion in question. Finally, the hyperfine splitting of the EPR signals can be used to help identify the isotopes in the sample, (i.e., those isotopes with odd numbers of protons and/or neutrons in the nucleus). (Further discussion is given by Boatner and Abraham[47] and Rappaz et al.[48]). Such studies have also shown that Gd^{3+} substitutes into normal cation sites in XENOTIME[41] even though pure $GdPO_4$ has the monazite structure. In the $Cm:LaPO_4$ experiment, the Cm was shown to be Cm(III).

2.3 Introduction to Synthesis Methods Used in this Study

Rare earth chloride hydrates were obtained from Aldrich (99.9% purity). Where necessary, the solutions prepared from the REE salts were standardized against EDTA in a 1M buffer solution, (NH_4Cl + NH_4acetate), using Arsenazo I as an indicator. The REE chloride hydrates are hygroscopic, but will lose water of crystallization upon drying in an oven or desiccator. The salts KH_2PO_4, $Na_4P_2O_7.10H_2O$ and $NaH_2PO_2.H_2O$ were all Fisher Certified Reagent Grade. The water used was obtained from an in-lab ion-exchange column.

Initial attempts to prepare crystalline $LaPO_4$ directly from dilute nitric acid solution upon addition of H_3PO_4 or KH_2PO_4 were unsuccessful. Even after refluxing in dilute nitric acid for days or weeks, the precipitates were too fine to filter through 0.45 μm Millipore filters. Attempts were made to optimize the pH such that the precipitation occurred slowly, for example, overnight, (pH = 0.9). Interestingly, other M(III) phosphates could be prepared by carefully raising the pH and digesting the solutions for one or two weeks, (M = Fe, Al, V). XRD showed the respective products to have the crystal structures of 'phosphosiderite' ($FePO_4.2H_2O$) and 'taranakite' ($H_6K_3Al_5(PO_4)_8.18H_2O$). (The V(III) compound was not further characterized). An Fe-arsenate was also prepared, and found to have the structure of 'scorodite' ($FeAsO_4.2H_2O$). It was therefore surprising that this

would not work for the REE.

The next approach involved the slow, drop-wise addition of a $LaCl_3$ solution to a refluxing solution of H_3PO_4. This method also yielded unsatisfactory results.

Various complexing agents were added to the initial $LaCl_3$ solution, in the expectation that the kinetics of complex-hydrolysis would limit the free La^{3+} concentration to such an extent that slow crystal growth would be permitted. A procedure involving the slow acid-hydrolysis of Et_3PO_4 was tried. Unfortunately, the hydrolysis of Et_3PO_4 is quite slow, (several months), and the product is none-the-less of poor quality. Further, it was not known whether various partially hydrolyzed phosphate esters were also presnt in the precipitate.

After many attempts, five potentially useful syntheses were found.

1) Acid-hydrolysis of the respective REE-pyrophosphate.
2) H_2O_2/H^+ oxidation of the respective hypophosphite.
3) Reaction of crystalline $La(ClO_4)_3$ with H_3PO_4 in 1M $HClO_4$.
4) Reaction of crystalline $LaHEDTA.nH_2O$ with H_3PO_4.
5) Direct precipitation of $LaPO_4$ from DMSO solutions of $LaCl_3.6H_2O$ by H_3PO_4. (For some reason, the rate of precipitation from DMSO is much slower than that from water.)

None of these procedures is ideal, in that they all

require at least a month..Only the pyrophosphate method was extensively used, since it was the first useful method developed, since it was the fastest of four slow methods and since it seemed to give the most reproducible results.

In all these procedures the pH was intentionally kept below 7, so that there would be little or no chance of REE-ion hydrolysis or carbonate co-precipitation. Also, calculations indicated that $LaPO_4$ is least soluble at pH's around 7 or 8. Material precipitated in this pH range would most likely be poorly crystallized, because of the extreme supersaturation levels.

Plates 1 and 2 show representative SEM photos of La-RHABDOPHANE and Sm-RHABDOPHANE respectively. The plates will be discussed in greater detail later in this chapter; they are included here to show that even good products of syntheses are fine grained. All the hydrous REE phosphates examined by SEM showed this habit of clusters of very fine prismatic crystals. The properties of these hydrous phosphates will be examined further in chapter 3.

Thus, although the syntheses developed yielded solids which could easily be separated by filtration, the solids were still fine-grained enough that surface free energies are expected to contribute to the free energies of the bulk phase.

Plate 1. SEM photograph of La-RHABDOPHANE crystals prepared by the perchlorate method. The scale bar refers to the left most photo.

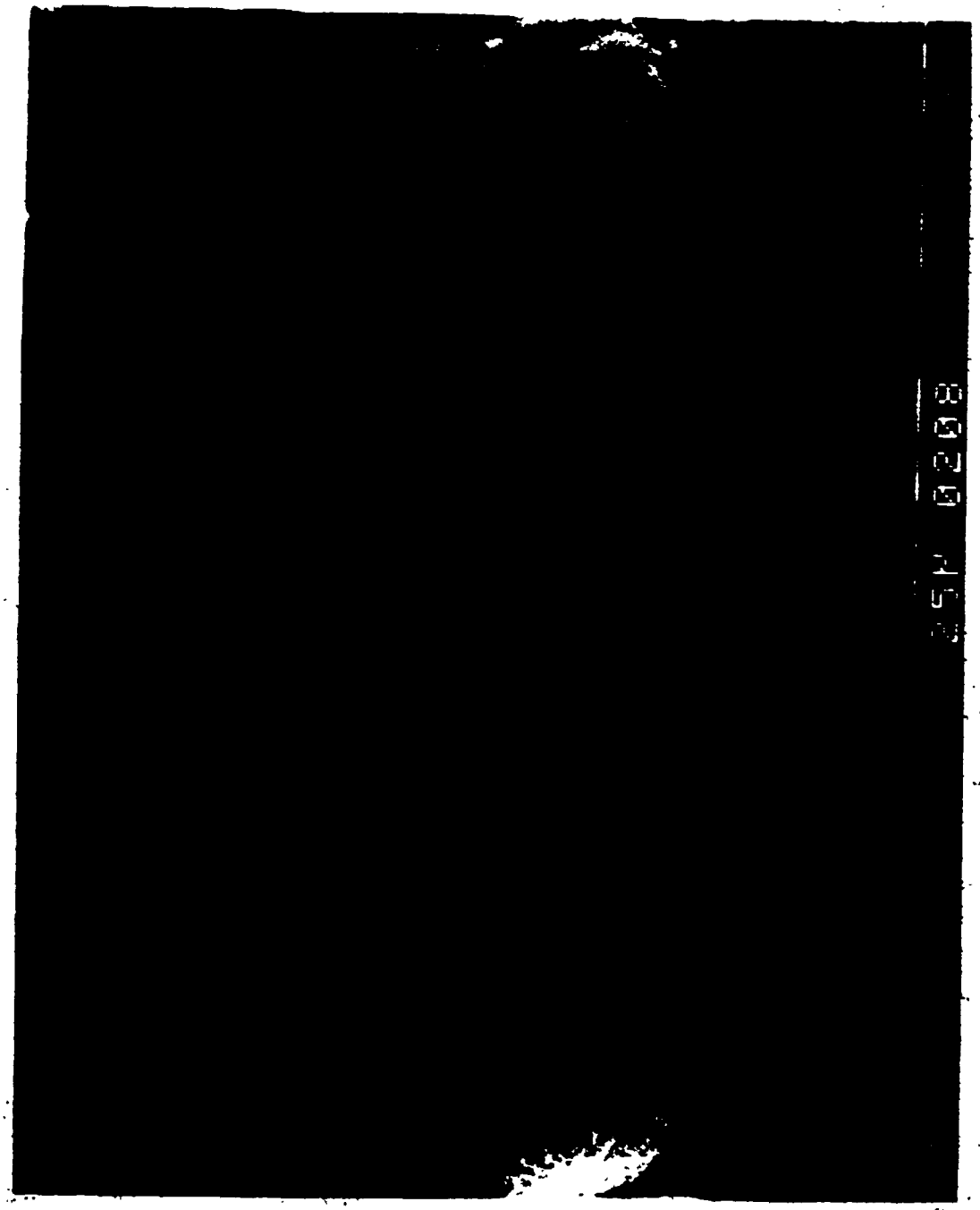

Plate 2. SEM photograph of Sm-RHABDOPHANE crystals prepared by the pyrophosphate method. Though the photos are somewhat fuzzy, the hexagonal cross-section of the prismatic crystals is visible.

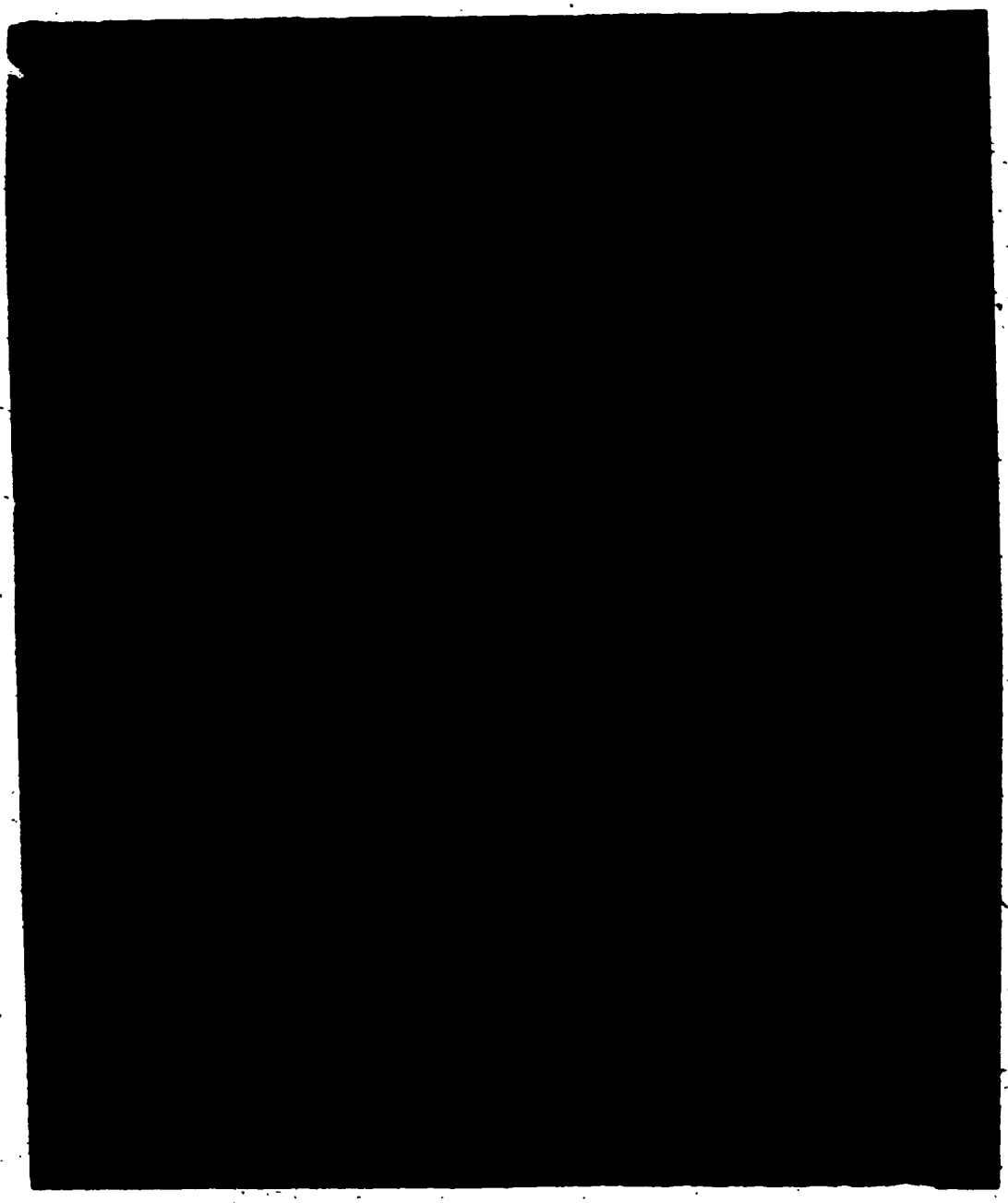

2.4 The Pyrophosphate Method

In general, hydrous REE phosphates can be formed by refluxing 500 mL of 0.1 mol/L HNO_3 containing 0.02 mole $RECl_3$, 0.01 mole $Na_4P_2O_7$ and an additional 0.04 mole HNO_3, (to neutralize $P_2O_7^{4-}$), for ½ to 1½ months. The pH can be varied between syntheses without apparent effect, other than yield, (the lower the pH, the lower the yield).

The pyrophosphate intermediate phase is formed within a period of a few hours, to a few days, again, depending on the pH, (the lower the pH, the slower the crystal growth). The REE pyrophosphate can be identified under optical microscopy by its characteristic crystals. The crystals appear for all the REE examined, to be rectangular, micaceous laths, often clustered in radiating spheroids. Crystals of the LREE are generally smaller than those of the HREE. SEM showed La-pyrophosphate crystals to be on the order of 20 x 5 x 0.1 micrometers. Ho-pyrophosphate crystals have been grown as large as 1-2 mm long. (Further characterization will be given later in the section).

After 1 to 2 weeks the crystals are seen under optical microscopy, to be in the process of corrosion and replacement. The new crystals are very small, and tend to form polycrystalline masses that retain the overall shape of the original pyrophosphate crystal. X-ray powder diffraction showed these new crystals to have powder patterns of rhabdophane, (for Pr, Nd, Sm and Gd) or xenotime, (for Ho, Er, Yb and Y).

When the replacement reaction is complete, as determined by XRD, the mixture is filtered through 0.45 micrometer Millipore filters, washed and dried at 80° C for 2-4 hours. In some cases, the mother liqour was retained and analyzed for REE concentration and pH, in order to calculate solubility products.

Certain REE gave variable results.

$LaPO_4$ and $NdPO_4$: When prepared at 100° C, both La and Nd phosphates were found to consist of a mixture of RHABDOPHANE and MONAZITE. For this reason, the hydrolysis reaction for La- and Nd-pyrophosphate was carried out at reduced temperatures, (i.e., 25° C), and longer times, (several months). In this case, only the RHABDOPHANE derivatives were obtained.

$CePO_4$: When Ce-pyrophosphate is first formed, it is almost colorless. During reflux, however, it was found that the powder becomes increasing colored, so that the final phosphate product was a grey-ish brown. XRD showed the product to be a mixture of MONAZITE and RHABDOPHANE. The darkening of the color is probably due to partial oxidation of the Ce(III) to Ce(IV) by air and/or HNO_3. When the hydrolysis reaction was carried out at 60° C, the product was closer to being colorless, and was found to consist of only RHABDOPHANE.

$DyPO_4$: The Dy derivative was found by XRD to be a mixture of XENOTIME with minor RHABDOPHANE. In this case, it

seems that Dy is on the dividing line between RHABDOPHANE and XENOTIME. Carron et al.,[32] found this dividing line to fall in the region Gd-Tb-Dy. These findings will be further discussed under the DTA section.

2.5 Further Characterization of the REE Pyrophosphates

The REE pyrophosphates were characterized by IR spectroscopy, partial wet chemical analysis and x-ray powder diffraction. Attempts to prepare single crystals for x-ray studies and structure resolution were discouraging. The micaceous crystal habit meant that one was either dealing with several crystals, or one very thin one.

Infrared absorption band positions are listed in table 2.2 , along with values from the literature for similar compounds. Steger and Leukroth[49] obtained IR spectra for cubic $M(IV)P_2O_7$ derivatives, which had been prepared by heating the freshly precipitated M(IV) hydroxide with H_3PO_4 to between 200 and 250° C. Petrov et al.,[50] obtained spectra for hydrous and anhydrous compounds of the type $REE_4(P_2O_7)_3$, prepared by adding $Na_4P_2O_7$ solutions to solutions of the respective REE salt. Kizilyalli[51] repeated these studies with Gd^{3+}. The initial products had similar water contents and similar IR spectra. Both groups of workers found the un-sintered powders to be x-ray amorphous. The similarity of all these IR spectra

Table 2.2 Measured and literature positions of IR-active bands for REE(III) and M(IV) pyrophosphates. (Values in cm^{-1}).

assignment	1	2	3	4	5
δ (PO)	N/S*	540	550	500	566
δ (PO)	610	640	630	548	625
ν sym(POP)	770	750	...	750	750
ν as(POP)	950	930	900	958-983	958-962
ν sym'(PO_3)	1030	1100	925-1150	1058-1125	1062-1092
ν as'(PO_3)	1220	1150	N/S	...	...
. water	1650	N/S		1654	1654

1) This work; lower scan limit = 600 cm^{-1}).

2) Ref. 50; $Pr_4(P_2O_7)_3 \cdot 13H_2O$.

3) Ref. 51; $Gd_4(P_2O_7)_3$; dried at 210° C.

4) Ref. 49; ZrP_2O_7.

5) Ref. 49; TiP_2O_7.

*) N/S = not scanned.

suggests that the materials investigated in this study do contain the pyrophosphate ion.

The $REE_4(P_2O_7)_3$ compounds of Kizilyalli were prepared at pH's around 3. Use of higher pH's resulted in considerable uptake of Na by the products. Such Na/REE pyrophosphate double salts are known and have been described[52]. If the pH used was less than 3, materials of the rough stoichiometry $GdH(P_2O_7)$ were produced[51].

The fact that the REE pyrophosphates studied in this investigation were prepared at pH's less than 3, suggests that they also would have the stoichiometry found by Kizilyalli. Chemical analyses presented in tables 2.3 and 2.4 tend to support this conclusion. Analyses were carried out by drying and weighing the respective REE pyrophosphate and dissolving in a known final volume of dilute HNO_3. The REE concentration was measured against standards on a CARY 118 spectrophotometer. (Section 4.1).

Table 2.3 Analysis of Pr-pyrophosphate: "$PrHP_2O_7 \cdot 1\text{-}2H_2O$"

Possible Comp.	Weight % Pr	Trial #	Measured Pr
$Pr_4(P_2O_7)_3$	51.9	1	43.6 ± 1
$PrHP_2O_7$	44.6	2	39.2 ± 1
$PrHP_2O_7 \cdot H_2O$	42.2	mean	41.4 ± 1

Table 2.4 Analysis of Ho-pyrophosphate: "$HoHP_2O_7 \cdot 3\text{-}5H_2O$"

Possible Comp.	Weight % Ho	Trial#	Measured Ho
$Ho_4(P_2O_7)_3$	55.8	1	41.1 ± 1
$HoHP_2O_7$	48.5	2	39.1 ± 1
$HoHP_2O_7 \cdot 4H_2O$	40.04	mean	40.1 ± 1

The error limits indicated in the tables refer to errors in measuring peaks in the optical absorption spectrum.

In order to help decide whether these REE pyrophosphates had been previously described, powder x-ray diffraction patterns were obtained for a selection of REE derivatives. The corresponding "d-spacings" and intensity values are listed in Appendix 1. Pyrophosphates of Pr, Ho and Y were found to be quite different from each other. Further, none of the powder patterns resembled those obtained for $Gd_4(P_2O_7)_3$ by Kizilyalli[51], (700° C form was tetragonal; 900° form was cubic). In obtaining powder patterns for these compounds, Kizilyalli found additional diffraction lines corresponding to those of Gd-MONAZITE.

2.6 The Hypophosphite Method

In this experiment, a wide range of REE were tested under the same conditions. (REE = La, Nd, Sm, Eu, Gd, Ho, Er, Yb and Y.) Into 30 mL test tubes the following reagents were introduced: 1 mmole $NaH_2PO_2 \cdot H_2O$, 1 mmole $REECl_3 \cdot nH_2O$, 1 mL 30% H_2O_2, 0.6 mmoles HCl and water to make a final volume of 20 mL.

The progress of the reaction was monitored for close to two years. When necessary, water was added to replace any lost by evaporation, (the test tubes were sealed with Parafilm). The qualitative results are given in table 2.5. The method is slow, but can yield well formed crystals, as shown in plate 3.

Since the REE hypophosphites are only slightly soluble, there is a danger that crystals of this material are mistaken for the final product. Again, optical microscopy and powder x-ray diffraction are useful in this regard.

Not unexpectedly, the light REE show different crystallization behaviour from the heavy REE. The LREE tend to form thin, polycrystalline coatings on the sides of the test tubes, whereas the HREE tend to form larger crystals, or clusters of larger crystals.

Table 2.5 Observations made during the hypophosphite synthesis experiment.

REE	15 days	22 days	27 days	189 days	669 days
La	clear sol'n	clear sol'n	fine coat	no major	fine coat
Nd	fine coat		fine coat	changes	fine coat
Sm	clear sol'n		coat + xls		fine ppt
Eu	clear sol'n		coat + xls		fine ppt
Gd	fine ppt		fine xls		fine coat
Ho	clear sol'n		fine coat		fine coat + xls
Er	clear sol'n		large xls		fine coat + xls
Yb	clear sol'n	settled xls	large xls		fine coat + xls
Y	clear sol'n		few xls		fine coat + xls

fine coat refers to a coating on the walls of the container;

xls = crystals; ppt = precipitate.

Plate 3. SEM photograph of Dy-RHABDOPHANE, (hexagonal prisms), and Dy-XENOTIME, (bladed crystals in the background). These crystals were grown by the hypophosphite method.

2.? The Perchlorate Method

In this method 1 mmole of $LaCl_3$ was dissolved in 20 mL 1.1 M $HClO_4$. Single macroscopic crystals of lanthanum perchlorate were seen to form. To this mixture 1 mmole of KH_2PO_4 was added. For several months nothing was observed to happen. Optical microscopy showed the presence of a poorly adhering polycrystalline coat on the surface of the rounded $La(ClO_4)_3$ crystals. An electron micrograph of the coat is shown in plate 1. The coat consists of roughly flat clusters of spheroid clusters of apparently randomly oriented vermiform crystals. Note the similarity of the crystals in plate 1 and plate 2. (showing Sm-RHABDOPHANE). This habit of forming clusters of clusters of colloid sized crystals seems to be common for LREE-RHABDOPHANE derivatives. It is this property that allows these very fine crystals to be filtered through 0.45 μm filters.

2.8 The EDTA Method

In this method 10 mL of 0.10 M $NdCl_3$ and 25 mL of 0.05 M disodium dihydrogen ethylenediaminetetraacetate (EDTA) were mixed at room temperature. After 12 hours some single crystals of $NdHEDTA \cdot nH_2O$ were seen to form. At this point 10 mL of 0.10 M KH_2PO_4 were added. After an hour, a faint precipitate was observed. After 5 days, the original crystals were still present, and a fine coat of material was observed on the walls of the container. After one year, all the NdHEDTA crystals had dissolved, and the coat of Nd-RHABDOPHANE had sloughed off the walls of the container.

In a subsequent series of experiments, the REE/EDTA crystals were separated from the mother liqour before adding the KH_2PO_4 solution, (REE = La, Sm and Y). After 4½ months, only the SmHEDTA crystals were observed to have reacted. Even here, optical microscopy only indicated small amounts of tiny new crystals growing on the surfaces of the original crystals.

The conclusion drawn from these experiments was that solution complexes of EDTA and a REE react too quickly with phosphoric acid, while the crystals react too slowly to allow the method to be used routinely.

2.9 The Dimethylsulfoxide Method

In this method 1 mmole of $NdCl_3 \cdot 6H_2O$ was dissolved in 20 mL of dimethylsulfoxide to give a clear, purple solution. Then 1 mmole of 99% H_3PO_4 was added to form a single, clear phase. After a year, a fine purple precipitate was seen to form.

A few additional solvents were substituted, including Et_3PO_4 and triphenyl phosphite, with similar results. Because the common REE salts are readily soluble in polar organic solvents, a considerable variety of solvent systems might be examined in order to improve the method. No further studies have been undertaken, though.

References for Chapter 2

1. Deer W.A., R.A. Howie and J. Zussman (1966) An Introduction to the Rock Forming Minerals, Longman Group, Limited: London. (8th Impression, 1975).

2. Finney J.J. and N.N. Rao (1967) Amer. Mineral. 52, 13-19.

3. Schwarz H. (1963) Z. anorg. allgem. Chem. 323 44-56.

4. Aldred A.T. (1984) Acta. Cryst. B40, 569-574.

5. Beall, G.W., L.A. Boatner, D.F. Mullica and W.O. Milligan (1981) J. Inorg. Nucl. Chem. 43, 101-105.

6. Mullica D.F., D.A. Grossie and L.A. Boatner (1985) J. Solid State Chem. 58, 71-77.

7. Mullica D.F., D.A. Grossie and L.A. Boatner (1985) Inorg. Chim. Acta 69, 105-110.

8. Bjorklund C.W. (1957) J. Amer. Chem. Soc. 79, 6347-6350.

9. Keller C. and K.H. Walter (1969) J. Inorg. Nucl. Chem. 27, 1253-1260.

10. Schwartz H. (1964) Z. anorg. allgem. Chem. 334, 175-185.

11. Calestani G. and C.D. Andreeti (1984) Z. Kristallogr. 168, 41-51.

12. Finch C.B., L.A. Harris and G.W. Clark (1964) Amer. Mineral. 49, 782-785.

13. Taylor M. and R.C. Ewing (1978) Acta Cryst. B34, 1074-1079.

14. Weigel F. and Haug H. (1965) Radiochim. Acta 4, 227-228.

15. Stubican V.S. and R. Roy (1963) Z. Kristallogr. 119, 90-97.

16. Milligan W.O., D.F. Mullica, H.O. Perkins, G.W. Beall and L.A. Boatner (1983) Inorg. Chim. Acta 77, L23-L25.

17. Hezel A. and S.D. Ross (1967) J. Inorg. Nucl. Chem. 29, 2085-2089.

18. Muto T., R. Meyrowitz, A.M. Pommer and T. Murano (1959) Amer. Mineral. 44, 633-650.

19. Donalson J.D., A. Hezel and S.D. Ross (1967) J. Inorg. Nucl. Chem. 29, 1239-1242.

20. Claringbull G.F. and M.H. Hey (1953) Amer. Mineral. 30, 211-217.

21. Bowles J.F.W. and D.J. Morgan (1984) Mineral. Mag. 48, 146-148.

22. Mitchell R.S. (1965) Amer. Mineral. 50, 231-235.

23. Atkin D., I.R. Basham and J.F.W. Bowles (1983) Mineral. Mag. 47, 393-396.

24. Fisher F.G. and R. Meyrowitz (1962) Amer. Mineral. 47, 1346-1355.

25. Mooney R.C.L. (1948) J. Chem. Phys. 16, 1003.

26. Mooney R.C.L. (1950) Acta Cryst. 3, 337-340.

27. Weigel F., V. Scherer and H. Henschel (1965) Radiochim. Acta 4, 18-23.

28. Mooney-Slater R.C.L. (1962) Z. Kristallogr. 117, 371-385.

29. Fukunaga O. and S. Yamaoka (1979) Phys. Chem. Minerals 5, 167-177.

30. Milligan W.O., D.F. Mullica, G.W. Beall and L.A. Boatner (1982) Inorg. Chim. Acta 60, 39-43.

31. Shannon R.D. and C.T. Prewitt (1969) Acta Cryst. B25, 925-946.

32. Carron M.K., C.R. Naeser, H.J. Rose, Jr. and F.A. Hildebrand (1965) Geol. Survey Bull. 1036-N.

33. Allard B. and J. Rydberg (1983) Chap. 19 IN Plutonium Chemistry, ACS Symposium Series; M. Joan Comstock, Series Editor.

34. Watters R.L. (1983) Chap. 20 IN Plutonium Chemistry ACS Symposium Series; M. Joan Comstock, Series Editor.

35. Bamberger C.E., G.M. Begun, J. Brynestad and J.F. Land (1982) Radiochim. Acta 31, 57-64.

36. Cotton F.A. and G. Wilkinson (1980) Advanced Inorganic Chemistry, A Comprehensive Text. John Wiley and Sons. 4th Ed.

37. Brookins D.G. (1984) Geochemical Aspects of Radioactive Waste Disposal. Springer-Verlag.

38. Choppin G.R. and J. Rydberg (1980) Nuclear Chemistry Theory and Applications. Pergamon Press.

39. Wickham D.G. (1962) J. Appl. Phys. 33, 3597-3598.

40. Feigelson R.S. (1964) J. Amer. Ceram. Soc. 47, 257-258.

41. Rappaz M., L.A. Boatner and M.M. Abraham (1980) J. Chem. Phys. 73, 1095-1103.

42. Pepin J.G. and E.R. Vance (1981) J. Inorg. Nucl. Chem. 43, 2807-2809.

43. Tananaev I.V. and V.P. Vasil'eva (1963) Russ. J. Inorg. Chem. 8 555-558.

44. Tananaev I.V. and S.M. Petushkova (1967) Russ. J. Inorg. Chem. 12, 39-42.

45. Kelly K.L., G.W. Beall, J.P.Young and L.A. Boatner (1981) IN Scientific Basis for Nuclear Waste Management, 3, 189-195. Plenum Publishing Corporation.

46. Abraham M.M. and L.A. Boatner (1982) Phys. Rev. B 26, 1434-1437.

47. Boatner L.A. and M.M. Abraham (1978) Reports on Progress in Physics 41, 87-155.

48. Rappaz M., M.M. Abraham, J.O Ramey and L.A. Boatner (1981) Phys. Rev. B 23, 1012-1030.

49. Steger E. and G. Leukroth (1960) Z. anorg. allgem. Chem. 303, 169-176.

50. Petrov K.I., Yu.B. Kirillov and S.M. Petushkova (1970) Russ. J. Inorg. Chem. 15, 1648-1649.

51. Kizilyalli M. (1976) J. Inorg. Nucl. Chem. 38, 483-486.

52. Petrov K.I., E.V. Zharavova, A.K. Mustaev and R.T. Yakovenko (1976) Russ. J. Inorg. Chem. 21, 952-955.

53. Allard B., H. Kipatsi and J.O. Liljenzen (1980) J. Inorg. Nucl. Chem. 42, 1015-1027.

3. CHARACTERIZATION OF REE PHOSPHATES

3.1 Analysis by Secondary Ion Mass Spectrometry (SIMS)

Two aspects of the SIMS technique were examined in this study. The use of SIMS for the detection and order-of-magnitude measurement of elements in inorganic solids will be the topic of this section. The use of SIMS for depth profiling through the surfaces of inorganic solids will be the topic covered in chapter 5.

In terms of its ability to do bulk chemical analysis SIMS has some attractive aspects. For homogeneous samples little or no sample preparation is required. Samples which are not homogeneous can either be sampled across the surface by the 40-50 μm wide primary beam, or be fused into a homogeneous glass prior to analysis. A bar graph showing semi-quantitative abundances of isotopes over 4 to 6 orders of magnitude can be obtained in about 10 minutes. A detailed mass spectrum over 10 mass numbers can be obtained in a matter of hours. Two aspects of SIMS limit its use as a quantitative tool, however. First is the problem of interferences, the second is the difficult problem of obtaining reproducible ion-yields.

In the SIMS technique, a primary ion beam consisting of such species as O^-, Cs^+ or Xe^+ is accelerated at the surface of a sample, resulting in the local formation of a plasma, as the surface is etched away. Ions in the plasma, either +ve or -ve, are sampled by a mass

spectrometer. In the case of the Cameca IMS-3F instrument, the secondary ions are sampled and focused by an immersion lens followed by a transfer lens. The kinetic energies of the secondary ions are analyzed by an electrostatic analyzer. Mass analysis is done by a sector magnet. The filtered ions are then focused onto a channeltron plate. Further details on the operation of the instrument used in this study can be found in Lau et al.[1].

The problem of variable ion-yields and some of the interferences can be related to the fact that it is a plasma which is being sampled by the mass spectrometer. In the plasma, only a fraction of the mixture is in a form desired for analysis. Much of the material is in the form of neutral atoms, which are not sampled. Another fraction is in the form of molecular ions, yet another in the form of multiply charged atoms. There exists as yet no way of controlling the proportions of the various chemical species in the plasma. Ion-yields will vary from one sort of sample to the next, (matrix effects) and even from one analysis to the next (instrumental effects). To make matters worse, the plasma tends to condense in the sample chamber, only to be re-volatilized during a subsequent run, (memory effects).

To some degree, a selection can be made as to what portions of the plasma are being admitted to the mass analyzer. In the Specimen-Isolation mode[1,2,3], advantage is taken of the fact that insulating specimens develop

a considerable electrical charge under bombardment by the primary beam. The result of this is that the energy distribution of molecular ions and atomic ions is quite different. Unfortunately, this means sampling in an energy region where the yields of atomic ions are not maximum. The mass spectra obtained via this mode are remarkably 'cleaner', however. Most of the mass spectra obtained in this report were obtained by operating the instrument in this mode.

Multiply charged ions are not removed by this method, but they can be identified bylooking at the intensities of the corresponding singly charged ions, which are normally one or more orders-of-magnitude greater.

Memory effects can often be recognized by the presence of totally unexpected peaks in the spectrum. Further, spectra can be re-run, in order to monitor ion-intensities for consistency: memory effects tend to diminish with time.

A simple and valuable procedure adopted in this study is to examine the isotopic ratios for those elements which possess multiple isotopes. Although the SIMS technique causes a certain amount of isotopic fractionation, this effect is usually small. Normally, isotopic ratios in the SIMS spectrum should agree to within 10% of literature values.

Although the "bar-graph" mode of data presentation is convenient and rapid, there are a few points to keep

in mind. The instrumental parameters are not normally set to ensure that the mass range sampled in the bar-graph mode,corresponds to the maximum intensity for each isotope. Deuterium is not normally seen in bar graphs for this reason. In the case of heavier elements, mass spectral peaks are often broad enough to overlap two sampling regions, particularly when the intensity is large. When there is doubt, a mass spectrum should be run, (as opposed to a bar-graph).

Finally a point should be raised about chemical mixing during bombardment. This point will become very important in the discussion in chapter 5, but can be important for bulk analyses as well. Because the primary beam is energetic, it results in a certain amount of damage in the sampled area. Specifically, atoms from near the surface are 'knocked-on' into the sample, which can then be sampled at a later point in the analysis. Also, as a crevice is produced and deepens during bombardment, the walls of the crevice become more likely, unintended targets of the primary beam. Material ejected from the crevice also tends to condense on the surface of the sample around the crevice, contaminating the surface. These effects can to some degree be eliminated by rastering the beam over a larger area.

The problem of ion-yields is the greatest problem as far as chemical analysis is concerned, however. In this study, the data will not be corrected for ion-yields

with the result that the data are only semi-quantitative. For the REE, this procedure is not a serious handicap anyway, since the ion-yields of the REE are similar. For the other elements, other analytical tools will have to be used where more accurate results are required.

In subsequent sections of this chapter, the SIMS technique will be used to characterise natural and synthetic samples of REE phosphates.

3.2 SIMS of Natural Rhabdophane

Since it was deemed necessary to carry out differential thermal analyses (DTA) on the hydrous REE phosphates, it was thought useful to include a sample of natural rhabdophane for comparison. Since the natural material was not characterized, a SIMS bar graph was run on the powder to examine the relative REE abundances and check for impurities. The powder diffraction data is presented in the next section.

3.2.1 Experimental

The sample of rhabdophane from Idaho, U.S.A. was obtained as a fine, light brown powder from the Smithsonian Institution, Washington, D.C., (sample number 121789).

The SIMS spectrum was run on the powder after it had been studied by DTA, (i.e., after it had been heated to 900°C). The powder was mounted on adhesive copper tape and analyzed by a Cameca IMS-3f ion microscope. A portion of the bar graph showing the ion intensities of REE isotopes is shown in figure 3.1. The copper tape itself was also run as a blank.

The primary ion beam consisted of O^- ions, and positive secondary ions were detected.

Figure 3.1 SIMS bar graph of REE in rhabdophane. Note the strong Ce-anomaly.

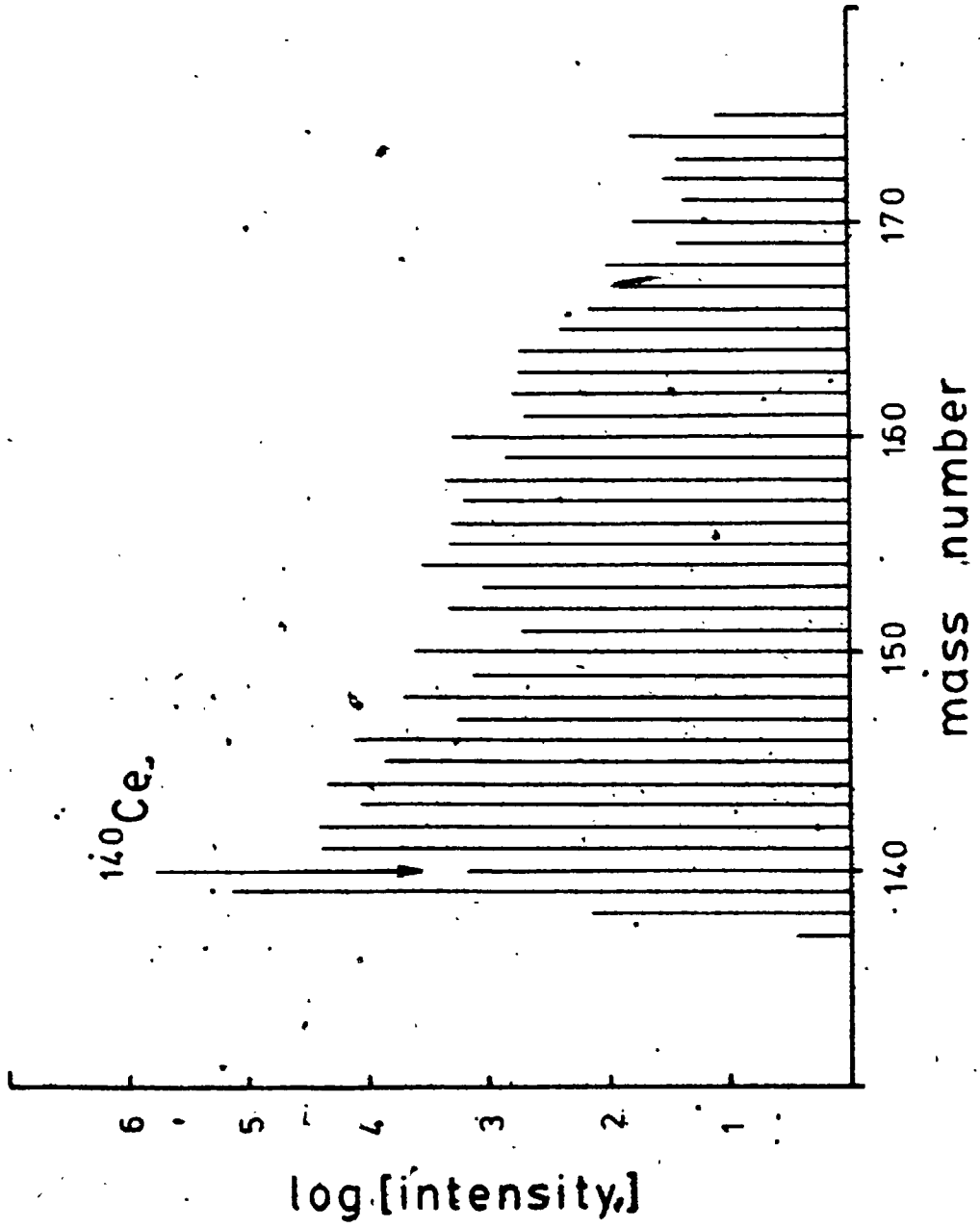

Figure 3.2 Simulated SIMS bar graph of REE in chondrites, (from Anders and Ebihara, et. Mass numbers with no elemental overlaps are indicated.

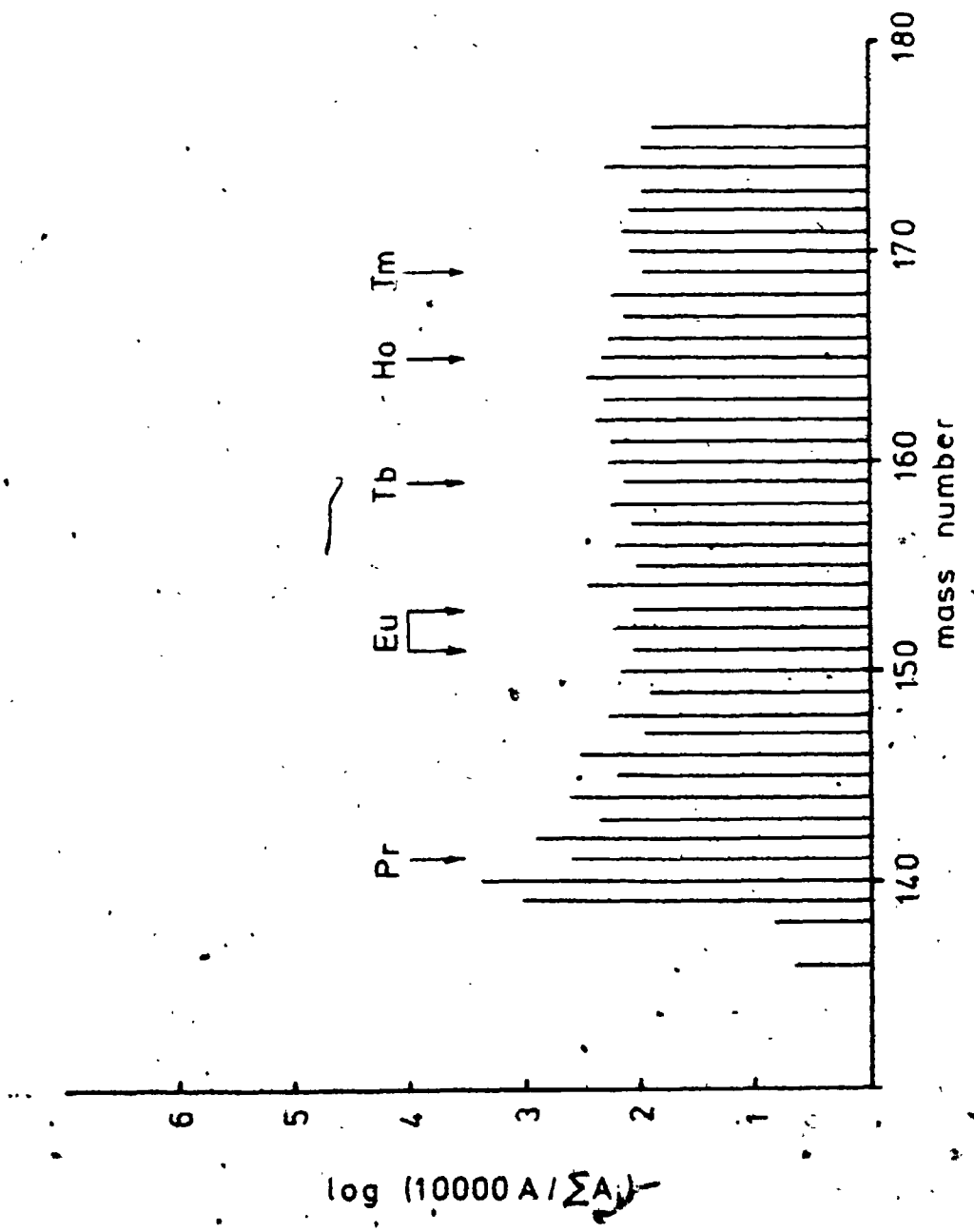

3.2.2 Results and Discussion

In figure 3.2 a simulated bar graph of REE in chondrites is shown to allow quick visual comparison with the REE pattern in rhabdophane. In the rhabdophane sample, the HREE are depleted as expected.[5] There also exists a strong, negative Ce anomaly. Normally, Ce is the most abundant REE in minerals of LREE. It is possible that conditions of formation of the rhabdophane were oxidizing, and that the Ce was separated as Ce^{4+} in another phase.

A detailed analysis of the SIMS data is given in table 3.1. The ion-intensities of each mass number were assigned elemental identities. Each ion-intensity was then multiplied by the inverse of the isotopic abundance of the corresponding element. If the total elemental ion-intensities all agree for a particular element, then no interferences were considered likely.

Next, evaluations of the data are presented on the basis of what was expected from the known composition of other rhabdophane samples. It seems that the rhabdophane sample contains additional phases rich in Al, Si, Fe and Mg. Since rhabdophane is known to be a secondary mineral, it is likely that the contamination comes from one or more clay minerals, though not enough was present to show up in the powder diffraction pattern, (next section). The SIMS results suggest an approximate formula for rhabdophane of $(La,Nd,Y,Gd,Sm,Ca)PO_4 \cdot xH_2O$.

Table 3.1 Detailed interpretation of SIMS analysis of natural rhabdophane, (heated powder).

isotope	I(cps)	A^{-1}	T_c	comments	T_c/I(La)
1 H^+	1.3 E4	1	1.3 E4	ec	
7 N^{2+}	10				
8 O^{2+}	1.1 E2				
9 Be^+	2.6 E3	1	2.6 E3	uc	1.9 E-2 m
10 B	4	5.05	20		
11 B	12	1.25	15	uc	1.1 E-4 tr
12 C	7.8 E3	1.01	7.9 E3	ec/s	
13 C	88	90.1	7.9 E3		
14 N	2.5 E2	1.00	2.5 E2	ec/s	
15 N	4	273.	1.1 E3		
16 O	2.8 E4	1.00	2.8 E4	e	7.9 E-2 M
17 O	33	2632	8.7 E4		
18 O	23	490.	1.1 E4		
19 F	2.4 E2	1	2.4 E2	ec	1.7 E-3 m
20 Ca^{2+}	1.6 E3	1.03	1.6 E3	e	
21 Ca	9	154.	1.4 E3		
22 Ca	31	48.0	1.5 E3		
23 Na	5.4 E2	1	5.4 E2	uc	3.9 E-3 m
24 Mg	5.6 E3	1.27	7.1 E3	uc	4.6 E-2 m
25 Mg	7.1 E2	10.0	7.1 E3		
26 Mg	7.2 E2	9.08	6.5 E3		
27 Al	1.2 E5	.1	1.2 E5	uc	8.6 E-1 M

A= fractional isotopic abundance; Anders and Ebihara[4].

T_c= total calculated element intensity (cps).

e= expected; ec= expected contaminant; un= unexpected contaminant; s= sample chamber; i= interference.

M= major; m= minor; tr= trace.

Table 3.1 (continued)

isotope	I(cps)	A^{-1}	T_c	comments	$T_c/I(La)$	
28 Si	4.4 E4	1.08	1.0 E5	uc	7.1 E-1	M
29 Si	4.9 E3	21.4	1.0 E5			
30 Si	3.2 E3	32.3	1.0 E5			
31 P	5.3 E4	1	5.3 E4	e	3.8	M
32 S	74	1.05	78	uc		tr
34 S	0	23.8	0			
35 Cl	29	1.32	38			
37 Cl	7	4.13	29	uc	2.1 E-4	tr
39 K	7.6 E2	1.07	8.1 E2	uc	5.8 E-3	m
41 K	4.7 E2	14.9	7.0 E3	i Ca- peak overlap		
40 Ca	7.8 E4	1.03	8.0 E4	e	5.7 E-1	M
42 Ca	6.1 E2	155.	9.5 E4			
43 Ca	1.3 E2	741.	9.6 E4			
44 Ca	1.7 E3	47.8	8.1 E4			
48 Ca	3.5 E3	535.	1.9 E6	i Ti		
45 Sc	45	1	45	e	3.2 E-4	tr
46 Ti	3.7 E2	12.2	4.5 E3			
47 Ti	3.6 E2	13.5	4.9 E3			
48 Ti	3.5 E3	1.36	4.8 E3			
49 Ti	2.2 E2	18.5	4.1 E3	uc	2.9 E-2	m
50 Ti	2.7 E2	19.2	5.2 E3	i V,Cr		
50 V	2.7 E2	400.	1.1 E5	i Ti,Cr		
51 V	36	1.00	36	ec	2.6 E-4	tr
50 Cr	2.7 E2	23.0	6.21 E3	i Ti,V		
52 Cr	36	1.19	43	uc	3.1 E-4	tr
53 Cr	7	10.5	74			
54 Cr	2.2 E3	42.4	9.3 E4	i Fe		
55 Mn	5.4 E2	1	5.4 E2	uc	3.9 E-3	tr
54 Fe	2.2 E3	17.2	3.8 E4	i Cr		
56 Fe	3.0 E4	1.09	3.3 E4	uc/s?		
57 Fe	7.0 E2	46.9	3.3 E4			
58 Fe	88	344.	3.0 E4		2.1 E-1	M
63 Cu	17	1.45	25	ec/s		
65 Cu	11	3.25	36			

Table 3.1 (continued)

isotope	I(cps)	A^{-1}	T_c	comments	T_c/I(La)
64 Zn^+	6.3 E2	2.06	1.3 E3		
66 Zn	2.7 E2	3.58	9.7 E2		
67 Zn	34	24.4	8.3 E2		
68 Zn	1.4 E2	5.32	7.4 E2	uc	5.3 E-3 m
70 Zn	45	161.	7.2 E3	i Ce^{2+}	
70 Ce^{2+}	45	1.13	51	e	
71 Ce	4.3 E2	9.01	3.9 E3	i Nd^{2+}	
71 Nd^{2+}	4.3 E2	3.68	1.6 E3	e	
72 Nd	3.4 E2	8.20	2.8 E3	i Sm^{2+}	
73 Nd	2.3 E2	4.20	9.7 E2		
74 Nd	86	17.5	1.5 E3	i Sm	
75 Nd	8.2 E2	17.9	1.5 E4	i Sm	
72 Sm^{2+}	3.4 E2	32.3	1.1 E4	i Nd^{2+}	
74 Sm	86	8.85	7.6 E2	i Nd	
75 Sm	8.2 E2	13.5	1.1 E4	i Nd	
76 Sm	73	3.76	2.7 E2		
77 Sm	44	4.42	1.9 E2	i Gd^{2+}	
77 Gd^{2+}	44	47.6	2.1 E3	i Sm^{2+}	
78 Gd	34	4.85	1.6 E2		
79 Gd	38	4.03	1.5 E2		
80 Gd	38	4.59	1.7 E2	i Dy^{2+}	
80 Dy^{2+}	38	43.5	1.6 E3	i Gd^{2+}	
81 Dy	23	3.92	90		
82 Dy	9	3.55	32		
84 Sr^+	0	179.	0		
86 Sr	36	10.2	3.7 E2	e	2.6 E-3 m
87 Sr	32	13.5	4.3 E2		
88 Sr	3.1 E2	1.22	3.7 E2		
89 Y	1.6 E4	1	1.6 E4	e	1.1 E-1 M
105 ?					
127 I	23	1	23	uc/s	1.6 E-4 tr
138 La	1.5 E2	1124	1.7 E5	i Ce^+	
139 La	1.4 E5	1.00	1.4 E5	e	1.00 M
136 Ce	0	526.	0		
138 Ce	1.5 E2	394.	5.9 E4	i La	
140 Ce	1.3 E3	1.13	1.7 E3	e	1.2 E-2 m
142 Ce	2.8 E4	9.01	2.5 E5	i Nd	

Table 3.1 (continued)

isotope	I(cps)	A^{-1}	T_c	comments	$T_c/I(La)$
141 Pr	2.7 E4	1	2.7 E4	e	1.9 E-1 M
142 Nd	2.8 E4	3.68	1.0 E5	i Ce	
143 Nd	1.3 E4	8.20	1.1 E5		
144 Nd	2.2 E4	4.20	9.2 E4	i Sm	
145 Nd	7.7 E3	12.0	9.2 E4		
146 Nd	1.4 E4	5.81	8.1 E4	e	5.8 E-1 M
148 Nd	5.4 E3	17.5	9.5 E4	i Sm	
150 Nd	4.2 E3	17.9	8.3 E4	i Sm	
144 Sm	2.2 E4	32.3	7.1 E5	i Nd	
147 Sm	2.0 E3	6.62	1.3 E4		
148 Sm	5.4 E3	8.85	4.8 E4	i Nd	
149 Sm	1.4 E3	7.19	1.0 E4	e	7.1 E-2 M
150 Sm	4.2 E3	13.5	5.7 E4	i Nd	
152 Sm	2.3 E3	3.76	8.6 E3	i Gd	
154 Sm	3.7 E3	4.42	1.6 E4	i Gd	
151 Eu	5.6 E2	2.09	1.2 E3	e	8.6 E-3 m
153 Eu	1.1 E3	1.92	2.1 E3		
152 Gd	2.3 E3	500.	1.2 E6	i Sm	
154 Gd	3.7 E3	47.6	1.7 E5	i Sm	
155 Gd	2.1 E3	6.76	1.4 E4		
156 Gd	2.0 E3	4.85	9.7 E3	e	6.9 E-2 m
157 Gd	1.7 E3	6.37	1.1 E4		
158 Gd	2.3 E3	4.03	9.3 E3	i Dy	
160 Gd	2.1 E3	4.59	9.6 E3	i Dy	
159 Tb	7.6 E2	1	7.6 E2	e	5.4 E-3 m
158 Dy	2.3 E3	1000	2.3 E6	i Gd	
160 Dy	2.1 E3	43.5	9.1 E4	i Gd	
161 Dy	5.4 E2	5.26	2.8 E3		
162 Dy	6.6 E2	3.92	2.6 E3	i Er	
163 Dy	5.9 E2	4.02	2.4 E3	e	1.7 E-2 m
164 Dy	5.9 E2	3.55	2.1 E3	i Er	
165 Ho	2.5 E2	1	2.5 E2	e	1.8 E-3 m
162 Er	6.6 E2	714.	4.7 E5	i Dy	
164 Er	5.9 E2	64.1	3.8 E4	i Dy	
166 Er	1.5 E2	2.99	5.0 E2		
167 Er	80	4.37	3.5 E2	e	2.5 E-3 m
168 Er	1.1 E2	3.69	4.1 E2	i Yb	
170 Er	65.	6.71	4.3 E2	i Yb	

Table 3.1 (continued)

isotope	I(cps)	A^{-1}	T_c	comments	T_c/I(La)
169 Tm^+	28	1	28	e	2.0 E-4 tr
168 Yb	1.1 E2	741.	8.1 E4	i Er	
170 Yb	65	32.2	2.1 E3	i Er	
171 Yb	25	6.94	1.7 E2		
172 Yb	36	4.57	1.6 E2	e	1.2 E-3 m
173 Yb	28	6.17	1.7 E2		
174 Yb	67	3.16	2.1 E2		
176 Yb	19	7.94	1.5 E2	i Lu	
175 Lu	13	1.03	13	e	9.3 E-5 tr
176 Lu	19	38.0	7.3 E2	i Yb	
239 (^{238}U)	20	1.01	20	e	1.4 E-4 tr

A= fractional isotopic abundance: Anders and Ebihara[4]

T_c = total calculated element intensity, (cps).

e= expected; ec= expected contamination; uc= unexpected contamination; s= sample chamber, (memory effects); i= interference. M= major; m= minor; tr= trace.

T_c/I(La)= total elemental intensity normalized to the La measured intensity.

3.3 Powder Diffraction Patterns of Some Rhabdophanes.

In order to check the identities and purities of the various synthetic and natural rhabdophane samples, powder x-ray diffraction patterns were run on one of two diffractometers fitted with a graphite monochromator using Cu K_α radiation.

The derived unit cell parameters are presented and compared with literature values in table 3.2. Note that the unit cell parameters of the natural rhabdophane fall between those of the La and Nd derivatives, as would be expected from the composition of the rhabdophane.

Note also that heating which would drive off the water of crystallization (next section), did not affect the unit cell parameters within experimental error. This, and the variable water contents support the conclusion that the water in rhabdophane is "zeolitic".[6]

The powder diffraction pattern of natural rhabdophane was fairly 'clean', except for peaks which could be assigned to monazite. The latter was estimated to constitute about 5% of the total sample.

3.3.1. The Space Group of Rhabdophane

Two space groups have previously been assigned to rhabdophane, namely $P6_222$[6] and $O3_121$[7,9]. The problem is that the two space groups are very similar. High and low quartz have the same respective space groups, for

Table 3.2 Unit cell parameters of rhabdophane and RHABDOPHANE derivatives, (La, Pr, Nd, Sm and Gd).

REE	a	c	comments	references
La	7.05(4)	6.51(4)	unheated	1
	7.081(5)	6.468(8)		Mooney, 6
Pr	7.01(1)	6.45(4)	unheated	1
	6.98(2)	6.40(2)	"	1
	7.00(?)	6.43(?)		Hezel & Ross, 7
Nd	7.00(1)	6.38(1)	unheated	1
	6.99(3)	6.40(2)	"	1
	7.02(3)	6.40(2)	635°C	1
	6.98(1)	6.34(2)		Mooney, 6
Sm	6.93(7)	6.41(8)	750°C	1
Gd	6.87(2)	6.31(1)	unheated	1
	6.88(2)	6.29(1)	750°C	1
	6.90(?)	6.32(?)		Hezel & Ross, 7
nat.	7.07(7)	6.38(9)		Idaho, #121789
	7.06(?)	6.39(?)		Virginia, Mitchell, 8

1. This work, using Cu K_α radiation.

example. The transition between the two forms in quartz is rapid at the transition temperature, since it involves no bond breaking or major rearrangement of atoms. Powder x-ray diffraction alone would be unable to distinguish two such similar structures.

The $C3_121$ assignment for rhabdophane is based on infrared spectroscopy[9], in particular on the point symmetry of the phosphate group which the IR spectra imply.

The powder diffraction results relating directly to the interpretation of the DTA results will be discussed in the section dealing with DTA, namely section 3.4.

3.4 Differential Thermal Analyses of Some Hydrous REE Phosphates including Natural Rhabdophane

A representative selection of REE phosphates were studied by DTA in order to help define the relationship between the hydrous and anhydrous forms as a function of the position of the respective REE in the periodic table.

3.4.1 Experimental

Simultaneous differential thermal analysis and thermogravimetric determinations were made up to 1300°C with a Stanton-Redcroft STA-781 instrument using a heating rate of 10°C/min, 50-100 mg of sample, α-Al_2O_3 as an inert reference and an atmosphere of flowing air or argon. X-ray powder diffraction patterns were also obtained for samples heated to various temperatures, (see section 3.3). The DTA studies were supplemented by isochronal heating experiments.

Powder infrared (IR) spectra were obtained of the starting materials on a Nicolet MX-1 instrument over the wavenumber range 400-4000 cm^{-1}. Pellets were prepared from 0.5-3 mg of sample mixed with 300 mg KBr.

The DTA, IR and most of the XRD measurements were done at Whiteshell Nuclear Research Establishment, through E.R. Vance. The remaining XRD results were obtained on a Rigaku x-ray diffractometer in the department of Geology at the University of Western Ontario.

3.4.2. Results and Discussion

The differential thermal analysis and thermogravimetric results are listed in table 3.3 for the RHABDOPHANE, rhabdophane and XENOTIME samples. A representative set of DTA and TGA curves are presented in figure 3.3. The endothermic peaks can be seen to correspond to the loss of water. The exothermic peaks were shown by x-ray powder diffraction to correspond to the transition RHABDOPHANE to MONAZITE. The exothermic peaks vary in intensity from absent (La-derivative) to strong and sharp (Gd-derivative). The transition temperatures are seen to increase from the La-derivative to the Dy-derivative. This is depicted graphically in figure 3.4. As expected, no transitions were observed in the xenotime derivatives up to a temperature of 1300° C.

Although the dehydrated form of RHABDOPHANE was observed to be stable over a considerable temperature range, (i.e., several hundred degrees centigrade), the transition back to RHABDOPHANE from MONAZITE was not observed. Perhaps if the partial pressure of water were high enough, the reaction could be reversed for a low enough temperature. Evidence from hydrothermal studies (10) suggests that Ce-RHABDOPHANE may be stable up to 250° C when the partial pressure of water is high enough. Hydrothermal experiments actually starting with MONAZITE were not performed, however.

Figure 3.5 Infrared absorption spectrum of Pr-RHABDOPHANE; KBr pressed pellet.

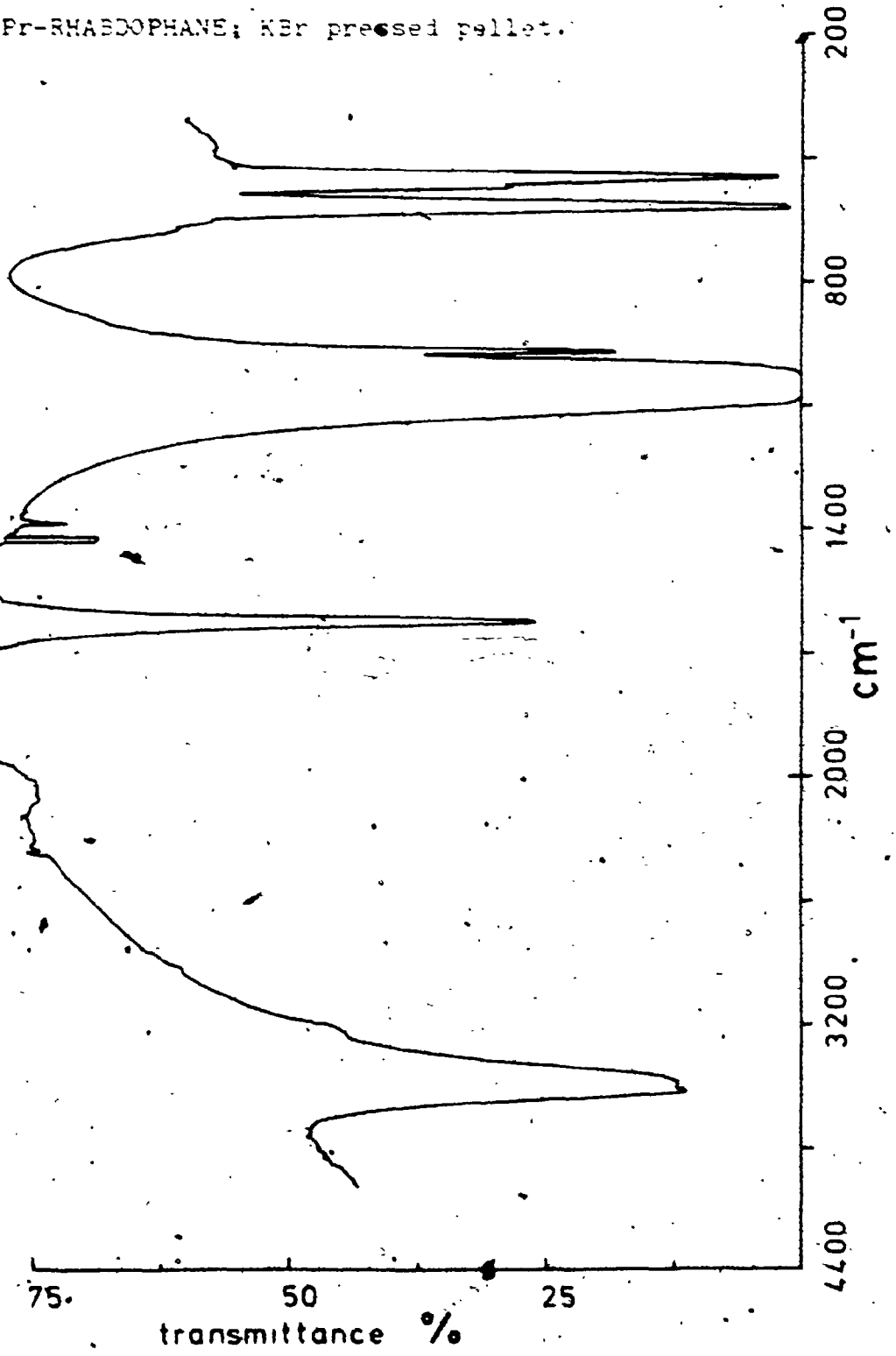

Table 3.3 Results of DTA/TGA (100° min) and isochronal (1hr) heating for hydrated phosphates, $REEPO_4 \cdot xH_2O$.

REE	T_p(°C)	I	T_1	x	T_2	T_3	F
La	100	M	100,230	0.7	(a)	---	M
	25	R	100,230	1.6	(a)	500	M
Ce	100	M+R	80,200	0.6	700w	600	M
	60	R	100,250	1.0	715vw	600	M
Pr	100	R	120.250	0.7	(a)	700	M
Nd	100	R	100,230	0.7	790vw	700	M
	100	R	110,230	0.7	680vw	700	M
Sm	100	R	80,220	1.0	800m	700	M
Gd	100	R	210	0.8	815s	800	M
Dy	60	X+R	80,180	1.0	950w	900	X*
Ho	100	X	110	1.4	---	---	X
Er	100	X	110	0.8	---	---	X
Yb	100	X	65	1.1	---	---	X
Nat.	?	R+M	120,230	1.7	(a)	(b)	M

T_p = preparation temperature.
I = initial phase, (by powder XRD).
T_1 = endothermic peak temperature, ± 5°C.
T_2 = exothermic peak temperature, ± 50°C.
T_3 = isochronal heating experiments, ± 50°C.
F = final phase.
M = monazite; R = rhabdophane; X = xenotime
(a) = absent; (b) = not determined; vw = very weak;
w = weak; m = medium; s = strong.
X* = unique transformation: R to M to X at temperatures above 900°C.

Figure 3.3 Representative DTA (a) and TGA (b) curves for La-RHABDOPHANE and Gd-RHABDOPHANE; the dashed line is for La. Heating rate 10° C/min. The curves were normalized to the heating curve of the inert reference.

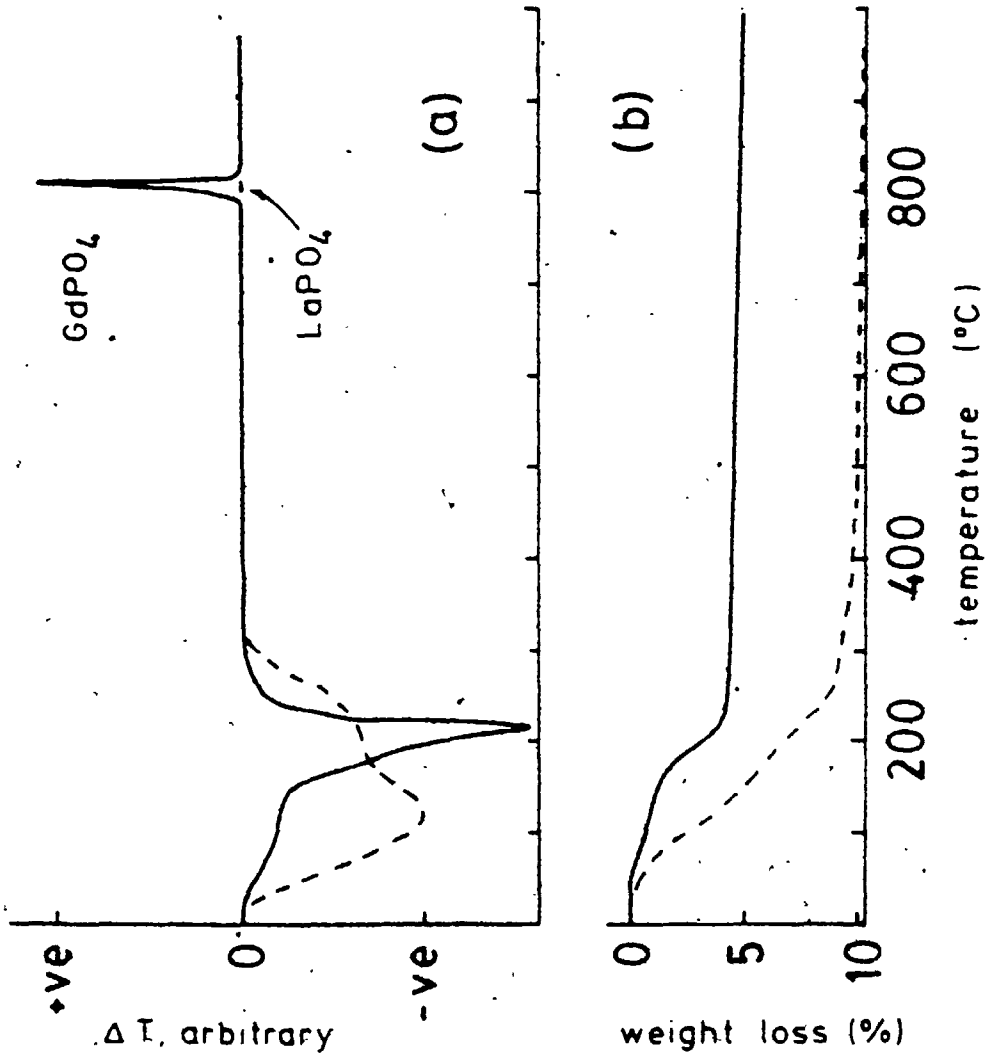

Figure 3.4 RHABDOPHANE to MONAZITE transformation temperatures for various REE. The x's refer to isochronal heating experiments. (1hr.). Dots refer to DTA data. (positions of peaks).

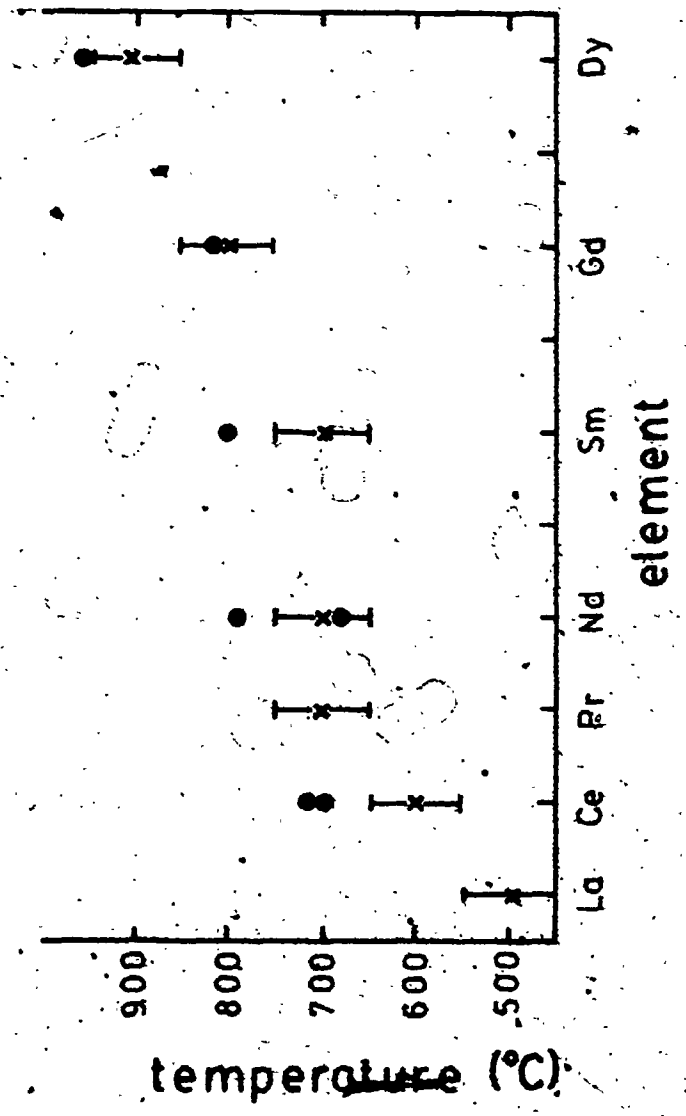

In section 3.3 it was shown that the x-ray powder diffraction patterns for the hydrous REE phosphates synthesized by the pyrophosphate method were identical within error with synthetic RHABDOPHANES obtained by other workers. It was also shown that loss of water did not significantly affect the unit cell parameters. Infrared spectra obtained for the RHABDOPHANES were also found to be similar to those obtained by Hezel and Ross[9] for analogous compounds. The IR spectrum obtained for the natural rhabdophane agreed well with those obtained for La- and Nd-RHABDOPHANE, except that several, weak extra absorption bands were found at 1400, 1460, 3625 and 3700 cm^{-1}. These bands were assigned to absorption by OH^-. A representative IR spectrum for Pr-RHABDOPHANE is shown in figure 3.5. IR spectra obtained for the XENOTIME derivatives also agreed with literature results[9].

Considering that the composition of the rhabdophane is dominated by La and Nd, and that the XRD and IR results resemble those of the La- and Nd- derivatives, it is not surprising that the DTA/TGA results for rhabdophane should resemble those obtained for the La- and Nd-derivatives. Specifically, the DTA curve shows a broad endotherm between 100 and 250° C corresponding to the loss of water. The exothermic peak is completely absent, even though XRD showed a transition to monazite.

Figure 3.5 Infrared absorption spectrum of Pr-RHABDOPHANE; KBr pressed pellet.

3.4.3 The Special Case of $DyPO_4 \cdot xH_2O$

The hydrous phosphate of Dy is exceptional in that it falls into the transition zone between those REE which form RHABDOPHANE exclusively, and those which form XENOTIME. Powder x-ray diffraction results obtained by Donaldson, et al.[11] for the hydrous phosphates of Dy and Ho lead these workers to conclude that these compounds had neither the XENOTIME nor the RHABDOPHANE structure, but rather a structure with space group P222. The alternative interpretation is that the product is a mixture of phases. There is a precedent for this interpretation. Carron et al[10] found in their hydrothermal studies that anhydrous $TbPO_4$ is dimorphic. $TbPO_4$ crystallized from glass ampules had the MONAZITE structure, while that crystallized from silver ampules had the XENOTIME structure.

The powder diffraction data of Donalson et al[11] for the Dy-derivative agrees with the data obtained in this study, so that both can be discussed at the same time. Among the diffraction peaks found in the pattern are several at 2θ values of 14.9, 20.6, 25.8, 29.7 and 30.2, which can be assigned to the pattern of rhabdophane, and indeed represent the stronger lines in that pattern. The line at 29.7 can also be assigned to the strongest line in the monazite pattern. When these lines are subtracted from the diffraction pattern, only lines remain which belong to the xenotime diffraction pattern.

3.6 SIMS Analysis of Flux-grown Single Crystals

In this section SIMS bar graph analyses of flux-grown single crystals of anhydrous REE phosphates including MONAZITE and XENOTIME will be presented. As indicated in section 2.2, these crystals were grown by L.A. Boatner at Oak Ridge National Laboratory, from a lead pyrophosphate melt, by slow cooling from 1400° C to about 900° at a rate of about 1 Celsius degree per hour[12].

The XENOTIME crystals were typically square or rectangular prisms about 5 to 15 mm long. The MONAZITE crystals were flat discs with less well developed crystal faces. The crystals were also more often than not clear and transparent. The colored crystals had the color characteristic for that REE ion. The YPO_4 crystals were slightly yellow.

The Cameca SIMS instrument was operated in the Specimen Isolation mode, using O^- primary ions; positive secondary ions were detected by the mass spectrometer. The primary beam was not rastered in this case. The results are given in abbreviated form in table 3.5. Known intereferences such as carbon are not included. The total calculated elemental ion-intensities of the element in question were normalized to that of the principal REE. Where an element had multiple isotopes, the isotope of lowest ion-intensity was used. Negative interferences are less common than positive interferences in SIMS.

3.5 SIMS of Natural Monazite

In order to characterize the specimen of monazite, and at the same time evaluate the use of SIMS for characterization purposes, a number of SIMS analyses were obtained, and compared with results obtained by instrumental neutron activation analysis, (INAA).

3.5.1 Experimental

Monazite from the Petaca district, New Mexico, was obtained as large, (1-3 cm), homogeneous light-orange-brown lumps from Ward's Natural Science Establishment, Inc. Thin sections of the monazite showed it to be transparent and homogeneous. The material is somewhat friable, but 0.5x1x1.5 cm sections could be cut with a diamond saw. These sections were polished on one side in preparation for surface studies.

SIMS spectra were obtained as before on a Cameca instrument using O^- primary ions. The monazite is non-conducting, and so could be analyzed in the Specimen-Isolation mode, (section 3.1).

A small amount (51.7 mg), was analyzed by Nuclear Activation Services Limited, of Hamilton, Ontario by instrumental neutron activation. The complete results are listed in Appendix II.

3.5.2. Results

An abbreviated list of results is given in table 3.4. The elements Si, As and V are expected to substitute for P in monazite, (see chapter 2). The elements Ca, Pb, Th and U are expected to substitute for the REE.

The SIMS and INAA results are compared as a log-log plot in figure 3.6. Note that the agreement of REE concentrations is quite good, considering that the SIMS data were not corrected for ion-yields. The SIMS data for Th and U are about an order of magnitude less than the INAA results, suggesting that the ion-yields for Th and U are about an order of magnitude less than those for the REE.

The results suggest an approximate formula for this specimen of monazite of $(Th,Ce,Nd,La,Gd,Sm,Ca)(PO_4,SiO_4)$. The sample should more properly be called cheralite, (see table 2.1).

Table 3.5 Interpretation of SIMS Analyses of Flux-Grown Single Crystals of Anhydrous REE Phosphates.

$LaPO_4$

isotope	I	A^{-1}	T_c	comments	T_c/T_c(REE)
27 Al	1.3 E2	1	1.3 E2		1.1 E-3
28 Si	2.0 E2	1.08	2.2 E2		1.8 E-3
29 Si	18	21.4	3.9 E2		
30 Si	8	32.3	2.6 E2		
31 P	6.3 E4	1	6.3 E4		5.3 E-1
40 Ca	8.6 E2	1.03	8.9 E2		
44 Ca	15	47.8	7.2 E2		6.0 E-3
46 Ti	15	12.2	1.8 E2		
47 Ti	20	13.5	2.7 E2		
48 Ti	55	1.36	75		6.3 E-4
49 Ti	10	18.5	1.9 E2		
50 Ti	4	19.2	77		
138 La	1.2 E2	1124.	1.3 E5		
139 La	1.2 E5	1.00	1.2 E5		1
140 Ce	16	1.13	18	i LaH	1.5 E-4

YPO_4

27 Al	4	1	4		1.1 E-5
28 Si	31	1.08	33		9.4 E-5
29 Si	2	21.4	43		
30 Si	2	32.3	65		
31 P	9.5 E4	1	9.5 E4		2.7 E-1
40 Ca	1.5 E2	1.03	1.5 E2		4.3 E-4
44 Ca	8	47.8	3.7 E2		
89 Y	3.5 E5	1	3.5 E5		
171 ?	1.8 E2			not Yb	

Table 3.4 (continued)

isotope	I(cps)	A^{-1}	T_c	comments	C(ppm)
155 Gd	1.1 E3	6.76	7.4 E3		34000
156 Gd	1.8 E3	4.85	8.7 E3		
157 Gd	1.4 E3	6.37	8.9 E3		
159 Tb	1.1 E3	1	1.1 E3		8000
161 Dy	8.6 E2	5.26	4.5 E3		
162 Dy	1.2 E3	3.92	4.7 E3		
163 Dy	1.0 E3	4.02	4.0 E3		20000
165 Ho	3.3 E2	1	3.3 E2		1400
166 Er	1.5 E2	2.99	4.5 E2		
167 Er	98	4.37	4.3 E2		1800
168 Er	1.3 E2	3.69	4.9 E2		
169 Tm	29	1	29		150
171 Yb	28	6.94	1.9 E2		
172 Yb	40	4.57	1.8 E2		
173 Yb	13	6.17	80		600
174 Yb	44	3.16	1.4 E2		
175 Lu	9	1.03	9		60
176 Lu	21	46.3	9.7 E2		
204 Pb	0	51.5	0		
206 Pb	0	5.23	0		
207 Pb	3	4.85	15		
208 Pb	22	1.71	38	Th-decay	
232 Th	3.5 E3	1	3.5 E3		150000
235 U	0	139			
238 U	37	1.01	37		2000
248 ThO	30	1	30		

Species present in SIMS bar graph, but not included:

H^+, O, N, C, B, Be, Na, Mg, Al, Ti, Fe, S, Cl, REE^{2+}, interfering REE.

Table 3. 5 (continued)

$NdPO_4$

isotope	I	A^{-1}	T_c	comments	T_c/T_c(REE)
27 Al	8.0 E2	1	8.0 E2		2.5 E-3
28 Si	1.9 E3	1.08	2.1 E3		
29 Si	76	21.4	1.6 E3		1.3 E-3
30 Si	49	32.3	1.6 E3		
31 P	2.4 E5	1	2.4 E5		7.5 E-1
40 Ca	1.7 E2	1.03	1.8 E2		
44 Ca	3	47.8	1.4 E2		4.4 E-4
54 Fe	5	17.2	86		
56 Fe	17	1.09	19	i ^{40}CaO	
57 Fe	0	46.5	0		
89 Y	11	1	11		3.4 E-5
139 La	48	1.00	48		1.5 E-4
140 Ce	60	1.13	68		2.1 E-4
141 Pr	3.2 E2	1	3.2 E2		1.0 E-3
143 Nd	6.8 E4	8.20	5.6 E5		
145 Nd	3.1 E4	12.0	3.7 E5		
146 Nd	5.6 E4	5.81	3.2 E5		1
147 Sm	6.8 E3	6.62	4.5 E4	i NdH	
149 Sm	2.5 E3	7.19	1.8 E4	i NdH	
152 Sm	0	3.76	0		
154 Sm	0	4.42	0		
206 Pb	33	6.23	1.7 E2		
207 Pb	39	4.85	1.9 E2		
208 Pb	58	1.71	1.0 E2		3.1 E-4

Table 3. 5 (continued)

$NdPO_4$

isotope	I	A^{-1}	T_c	comments	T_c/T_c(REE)
27 Al	8.0 E2	1	8.0 E2		2.5 E-3
28 Si	1.9 E3	1.08	2.1 E3		
29 Si	76	21.4	1.6 E3		1.3 E-3
30 Si	49	32.3	1.6 E3		
31 P	2.4 E5	1	2.4 E5		7.5 E-1
40 Ca	1.7 E2	1.03	1.8 E2		
44 Ca	3	47.8	1.4 E2		4.4 E-4
54 Fe	5	17.2	86		
56 Fe	17	1.09	19	i ^{40}CaO	
57 Fe	0	46.5	0		
89 Y	11	1	11		3.4 E-5
139 La	48	1.00	48		1.5 E-4
140 Ce	60	1.13	68		2.1 E-4
141 Pr	3.2 E2	1	3.2 E2		1.0 E-3
143 Nd	6.8 E4	8.20	5.6 E5		
145 Nd	3.1 E4	12.0	3.7 E5		
146 Nd	5.6 E4	5.81	3.2 E5		1
147 Sm	6.8 E3	6.62	4.5 E4	i NdH	
149 Sm	2.5 E3	7.19	1.8 E4	i NdH	
152 Sm	0	3.76	0		
154 Sm	0	4.42	0		
206 Pb	33	6.23	1.7 E2		
207 Pb	39	4.85	1.9 E2		
208 Pb	58	1.71	1.0 E2		3.1 E-4

Table 3.5 Interpretation of SIMS Analyses of Flux-Grown Single Crystals of Anhydrous REE Phosphates.

$LaPO_4$

isotope	I	A^{-1}	T_c	comments	T_c/T_c(REE)
27 Al	1.3 E2	1	1.3 E2		1.1 E-3
28 Si	2.0 E2	1.08	2.2 E2		1.8 E-3
29 Si	18	21.4	3.9 E2		
30 Si	8	32.3	2.6 E2		
31 P	6.3 E4	1	6.3 E4		5.3 E-1
40 Ca	8.6 E2	1.03	8.9 E2		
44 Ca	15	47.8	7.2 E2		6.0 E-3
46 Ti	15	12.2	1.8 E2		
47 Ti	20	13.5	2.7 E2		
48 Ti	55	1.36	75		6.3 E-4
49 Ti	10	18.5	1.9 E2		
50 Ti	4	19.2	77		
138 La	1.2 E2	1124.	1.3 E5		
139 La	1.2 E5	1.00	1.2 E5		1
140 Ce	16	1.13	18	i LaH	1.5 E-4

YPO_4

27 Al	4	1	4		1.1 E-5
28 Si	31	1.08	33		9.4 E-5
29 Si	2	21.4	43		
30 Si	2	32.3	65		
31 P	9.5 E4	1	9.5 E4		2.7 E-1
40 Ca	1.5 E2	1.03	1.5 E2		4.3 E-4
44 Ca	8	47.8	3.7 E2		
89 Y	3.5 E5	1	3.5 E5		
171 ?	1.8 E2			not Yb	

Table 3. 5 (continued)

$NdPO_4$

isotope	I	A^{-1}	T_c	comments	T_c/T_c(REE)
27 Al	8.0 E2	1	8.0 E2		2.5 E-3
28 Si	1.9 E3	1.08	2.1 E3		
29 Si	76	21.4	1.6 E3		1.3 E-3
30 Si	49	32.3	1.6 E3		
31 P	2.4 E5	1	2.4 E5		7.5 E-1
40 Ca	1.7 E2	1.03	1.8 E2		
44 Ca	3	47.8	1.4 E2		4.4 E-4
54 Fe	5	17.2	86		
56 Fe	17	1.09	19	i ^{40}CaO	
57 Fe	0	46.5	0		
89 Y	11	1	11		3.4 E-5
139 La	48	1.00	48		1.5 E-4
140 Ce	60	1.13	68		2.1 E-4
141 Pr	3.2 E2	1	3.2 E2		1.0 E-3
143 Nd	6.8 E4	8.20	5.6 E5		
145 Nd	3.1 E4	12.0	3.7 E5		
146 Nd	5.6 E4	5.81	3.2 E5		1
147 Sm	6.8 E3	6.62	4.5 E4	i NdH	
149 Sm	2.5 E3	7.19	1.8 E4	i NdH	
152 Sm	0	3.76	0		
154 Sm	0	4.42	0		
206 Pb	33	6.23	1.7 E2		
207 Pb	39	4.85	1.9 E2		
208 Pb	58	1.71	1.0 E2		3.1 E-4

Table 3.5 (continued)

$SmPO_4$

isotope	I	A^{-1}	T_c	comments	T_c/T_c(REE)
27 Al	3.4 E2	1	3.4 E2		2.8 E-3
28 Si	1.2 E3	1.08	1.3 E3		
29 Si	37	21.4	7.9 E2		6.6 E-3
30 Si	27	32.3	8.7 E2		
31 P	2.3 E5	1	2.3 E5		1.9 E0
89 Y	53	1	53		4.4 E-4
139 La	3	1.00	3		2.5 E-5
140 Ce	25	1.13	28		2.3 E-4
141 Pr	70	1	70		5.8 E-4
143 Nd	0				
144 Sm	1.6 E4	32.3	5.2 E5		
147 Sm	4.8 E4	6.62	3.2 E5		
148 Sm	4.0 E4	8.85	3.5 E5		
149 Sm	3.5 E4	7.19	2.5 E5		
150 Sm	2.1 E4	13.5	2.8 E5		
152 Sm	3.2 E4	3.76	1.2 E5		1
154 Sm	1.4 E5	4.42	6.2 E5	i Gd	
155 Gd	9.6 E3	6.76	6.5 E4	i SmH	
156 Gd	23	4.85	1.1 E2		
157 Gd	5	6.37	32		2.7 E-4
158 Gd	21	4.03	85		
160 Gd	48	4.59	2.2 E2	i ^{144}SmO	
159 Tm	7	1	7	i ^{158}SmH	
206 Pb	15	5.23	78		
207 Pb	27	4.85	1.3 E2		
208 Pb	39	1.71	69		5.8 E-4

Table 3.5 (continued)

$HoPO_4$

isotope	I	A^{-1}	T_c	comments	T_c/T_c(REE)
27 Al	4.4 E2	1	4.4 E2		2.4 E-3
28 Si	4.6 E5	1.08	5.0 E5	(!)	2.8 E0
29 Si	2.4 E4	21.4	5.1 E5		
30 Si	1.7 E4	32.3	5.5 E5		
31 P	2.1 E5	1	2.1 E5		1.2 E0
40 Ca	7.9 E2	1.03	8.1 E2		4.5 E-3
44 Ca	73	47.8	3.5 E3	i ^{28}SiO	
46 Ti	3.5 E2	12.2	4.3 E3		
47 Ti	3.0 E2	13.5	4.1 E3		
48 Ti	2.3 E3	1.36	3.1 E3		1.7 E-2
49 Ti	1.9 E2	18.5	3.5 E3		
50 Ti	1.8 E2	19.2	3.5 E3		
89 Y	17	1	17		9.4 E-5
90 Zr	2.5 E2	1.94	4.9 E2		
91 Zr	76	8.93	6.9 E2		
92 Zr	67	5.85	3.9 E2		2.2 E-3
94 Zr	1.3 E2	5.75	7.5 E2		
96 Zr	17	35.7	6.1 E2		
116 Sn	28	6.76	1.9 E2		
117 Sn	15	12.9	1.9 E2		
118 Sn	43	4.12	1.8 E2		1.0 E-3
119 Sn	30	1.16	3.5 E2		
120 Sn	90	3.09	2.8 E2		
122 Sn	15	21.9	3.3 E2		
124 Sn	22	17.7	3.9 E2		
165 Ho	1.8 E5	1	1.8 E5		
164 Er	3	64.1	1.9 E2		
167 Er	34	4.37	1.5 E2		
168 Er	23	3.69	85		
170 Er	11	6.71	74		4.1 E-4

Table 3.5 (continued).

$ErPO_4$

isotope	I	A^{-1}	T_c	comments	T_c/T_c(REE)
27 Al	1.3 E2	-1	1.3 E2		8.7 E-4
28 Si	4.5 E2	1.08	4.9 E2		3.3 E-3
29 Si	23	21.4	4.9 E2		
30 Si	19	32.3	6.1 E2		
31 P	3.2 E5	1	3.2 E5		2.1 E0
40 Ca	2.2 E2	1.03	2.2 E2		1.5 E-3
44 Ca	5	47.5	2.4 E2		
89 Y	5.6 E2	1	5.6 E2		3.7 E-3
140 Ce	15	1.13	17		1.1 E-4
159 Tb	39	1	39		2.6 E-4
158 Dy	3	1000	3.0 E3		
160 Dy	17	43.5	7.4 E2		
161 Dy	13	5.26	68		4.5 E-4
162 Dy	3.6 E2	3.92	1.4 E3	i Er	
163 Dy	92	4.02	3.7 E2		
165 Ho	6.4 E2	1	6.4 E2	i ^{164}Er	
166 Er	6.5 E4	2.99	1.9 E5		
167 Er	5.4 E4	4.37	2.4 E5		
168 Er	5.4 E4	3.69	2.0 E5		
170 Er	2.3 E4	6.71	1.5 E5		1
169 Tm	9.9 E3	1	9.9 E3	i ^{168}ErH	
171 Yb	5.6 E3	6.94	3.9 E4	i ^{170}ErH	
172 Yb	13	4.57	59		
173 Yb	7	6.17	43		2.9 E-4
174 Yb	19	3.16	60		
175 Lu	15	1.03	15		1.0 E-4

Table 3.5 (continued)

$LuPO_4$

Isotope	I	A^{-1}	T_c	comments	T_c/T_c(REE)
27 Al	90	1	90'		1.2 E-3
28 Si	1.3 E3	1.08	1.4 E3		1.8 E-2
29 Si	73	21.4	1.6 E3		
30 Si	53	32.3	1.7 E3		
31 R	1.3 E5	1	1.3 E5		1.7 E0
40 Ca	1.0 E3	1.03	1.0 E3		1.3 E-2
44 Ca	38	47.8	1.8 E3		
46 Ti	17	12.2	2.1 E2	^{30}SiO	
47 Ti	22	13.5	3.0 E2		
48 Ti	1.5 E2	1.36	2.0 E2		2.6 E-3
49 Ti	13	18.5	2.4 E2		
50 Ti	15	19.2	2.9 E2		
88 ?	2.8 E2			$^{176}Lu^{2+}$	
89 Y	31	1	31		4.1 E-4
140 Ce	5.7 E2	1.13	6.4 E2		
142 Ce	65	9.01	5.9 E2		7.8 E-3
175 Lu	7.4 E4	1.03	7.6 E4		1
176 Lu	3.1 E3	38.3	1.2 E5		

3.6.1 Comments on the Purity of the Single Crystals

The SIMS results indicate that the crystals are quite pure, particularly in regard to contamination by other REE. Usually only REE neighbouring the REE in question are present at levels detectable by the SIMS bar graph analysis mode. This is understandable considering the separation techniques used by chemical firms to separate the REE, namely solvent extraction and ion-exchange.

The analyses indicate that the elements Al, Si, Ca and Ti are always present in the parts per thousand (ppt) level, (atom for atom). These elements are common in dust in the laboratory and are expected to enter the synthesis mixtures at various stages during sample preparation. Also, these elements are common contaminants in the SIMS sample chamber itself, if geological samples are often analyzed.

The presence of lead in a couple of samples is not surprising, since the crystals were grown from a lead-based flux. Lead has been detected in crystals prepared by the same flux technique by electron paramagnetic resonance[13]. Interestingly, the lead found in samples of YPO_4 and $LuPO_4$ was shown to be present as the Pb^{3+} ion.

The case of the $HoPO_4$ sample is also noteworthy because the SIMS bar graph shows the presence of Si in levels comparable to that of phosphorus. This is a significant level of contamination, even allowing for a difference in ion yields of Si and P of one or two

orders of magnitude. In such a situation, the Si is expected to interfere with the surface exchange experiments. as well as the surface analytical techniques used to study the surfaces. The presence of Ti, Zr and Sn is also anomalous, and may reflect a contaminated crucible.

The $HoPO_4$ example is also useful for demonstrating the value of SIMS as a rapid, semi-quantitative tool for testing the purities of compounds. The fact that the problem of ion yields is not yet solved should not detract from the usefulness of SIMS in this regard.

Table 4-1 Extinction coefficients of major absorption peaks of some REE^{3+} ions in solutions of given composition.

ion	solution composition	λ (nm)		ϵ ($M^{-1}cm^{-1}$)	
Nd^{3+}	$NdCl_3$= 0.05 M	790	±2	6.0	±0.1
	HNO_3= 0.32 M	735		6.0	
	KH_2PO_4= 0.05 M	727		3.6	
		571*		6.3	
		518		3.5	
		508		1.5	
		352		3.1	
		346		2.0	
Nd^{3+} †	$NdCl_3$= 0.10 M	790		5.8	
	NH_4Cl= 1.0 M	735		6.3	
		727		3.4	
		572*		6.4	
		520		3.7	
		510		1.5	
		354		3.2	
		346		2.1	
Sm^{3+}	$SmCl_3$= 0.0945 M	401*		3.12	
Ho^{3+}	$HoCl_3$= 0.050 M	650		2.0	
		637		3.3	
		534*		4.9	
		484		1.8	
		449		4.2	
		415		2.6	
Er^{3+}	$ErCl_3$= 0.0432 M	647		1.85	
	HNO_3= 1.6 M	519		2.89	
	KH_2PO_4= 0.0450 M	484		1.62	
		376*		5.00	
		362		1.27	

* Principal peaks used in routine chemical analysis.
† Nd^{3+} peak intensities for chloride-dominated media are listed for comparison.

12. Rappaz M., L.A. Boatner and M.M. Abraham (1980) J. Chem. Phys. 73, 1095-1103.

13. Abraham M.M., L.A. Boatner and M. Rappaz (1980) Phys. Rev. Lett. 45, 839-842.

4. SOLUBILITIES AND GEOCHEMISTRY

4.1 Optical Absorption Spectroscopy of 3+ REE Ions

The solution concentrations of the REE ions can be conveniently measured by spectrophotometry, if the REE concentration is greater than about 0.1 mM. As long as no more than two or three colored REE ions are in solution the spectra over wavelengths 200 to 800 nm can be used to obtain concentrations[1]. Some ions such as NO_3^- interfere in the UV spectra of Ce^{3+}. Assignment of peaks is straightforward. Spectra between 200 and 5000 nm of all 3+ REE ions in aqueous solution have been obtained[2]. Free-ion electronic states of 3+ ions have been labled and tabulated[3].

For the purposes of analytical chemistry, the important spectroscopic parameters are the wavelength of the transition band maximum and the corresponding extinction coefficient, ϵ (also called the molar absorptivity), given by the Beer-Lambert law:

$$\epsilon = 1/(cl) \times \log(I_o/I) \qquad M^{-1}cm^{-1} \qquad (4.1)$$

where c is the concentration of the absorbing species in moles per liter, l is the path length of the sample cell, in centimeters, and $\log(I_o/I)$ is the absorption measured at the wavelength of interest. The spectra of the individual REE are easily recognized, as the f-f transitions are less sensitive to the ligand field than are

say the d-d transitions of the first-row transition metal ions. However, differences do occur. In recent years, it has become apparent that such small differences are important and interesting. The importance of certain REE in laser technology is an obvious case. The identification of several Eu^{3+}/NO_3^- complexes in dilute nitric acid solutions[4] by high resolution spectroscopy is another, more relevant example.

Also, it has been known for some time that certain REE, namely Nd, Eu, Ho and Er have in their spectra certain "hypersensitive" transitions that depend rather more strongly on changes in the ion's chemical environment. These transitions involve electric quadrupole selection rules[2], whereas most transitions in REE spectra are of either induced electric dipole nature or, less commonly, of magnetic dipole nature[5,6]. Since f-f transitions are orbitally forbidden, the extinction coefficients are of modest values, namely 1 to 10 $M^{-1}cm^{-1}$. Spectra of Ce^{3+} are exceptional in this regard, involving f-d transitions. As a result, extiction coefficients are larger: the band at 252 nm has an ϵ value of 630 $M^{-1}cm^{-1}$.

Introductions to the theory of REE spectra are available (2,7). Hufner's text[8] is recent and comprehensive, while that of Wybourne[9] is somewhat older and mathematically more detailed.

Carnall[2] gives the electronic state energies as

$$E = \sum_{k=2}^{6} F^k(nf,nf) f_k + \zeta A_{SO} + E_{CI} + E_{CF} \qquad (4.2)$$

where k are even, f_k and A_{SO} represent the angular parts of the electrostatic and spin-orbit interactions, respectively. The F^k are Slater integrals for purely electrostatic interactions among f-electrons, ζ is the spin-orbit coupling constant, E_{CI} corrects for the effects of configuration interaction and E_{CF} corrects for the effects of the crystal field. Normally, states are labelled according to the Russell-Saunders coupling scheme, even though the use of intermediate coupling in calculations removes L and S as good quantum numbers. The splitting of levels due to the crystal field is usually small; no more than 340 cm^{-1} in Pr^{3+} spectra, for example. By comparison, spin-orbit effects can cause splitting up to 4300 cm^{-1} for Pr^{3+}. The result of this is that spectrometers such as that used in this study cannot resolve crystal field splittings. Only the envelope over the multiplets is observed to change its shape as the chemical environment of the ion is changed. The use of low temperatures (4.2 K), and high resolution spectroscopy by other workers[7,10,11] allowed the resolution of crystal field, as well as vibrational components. An optical absorption spectrum for Nd^{3+} which is representative of the sort of spectra obtained in this study is presented in figure 4.1. The solution consisted

Figure 4.1 Representative spectrum of Nd^{3+} with term symbols assigned. Ground state is $^4I_{9/2}$.

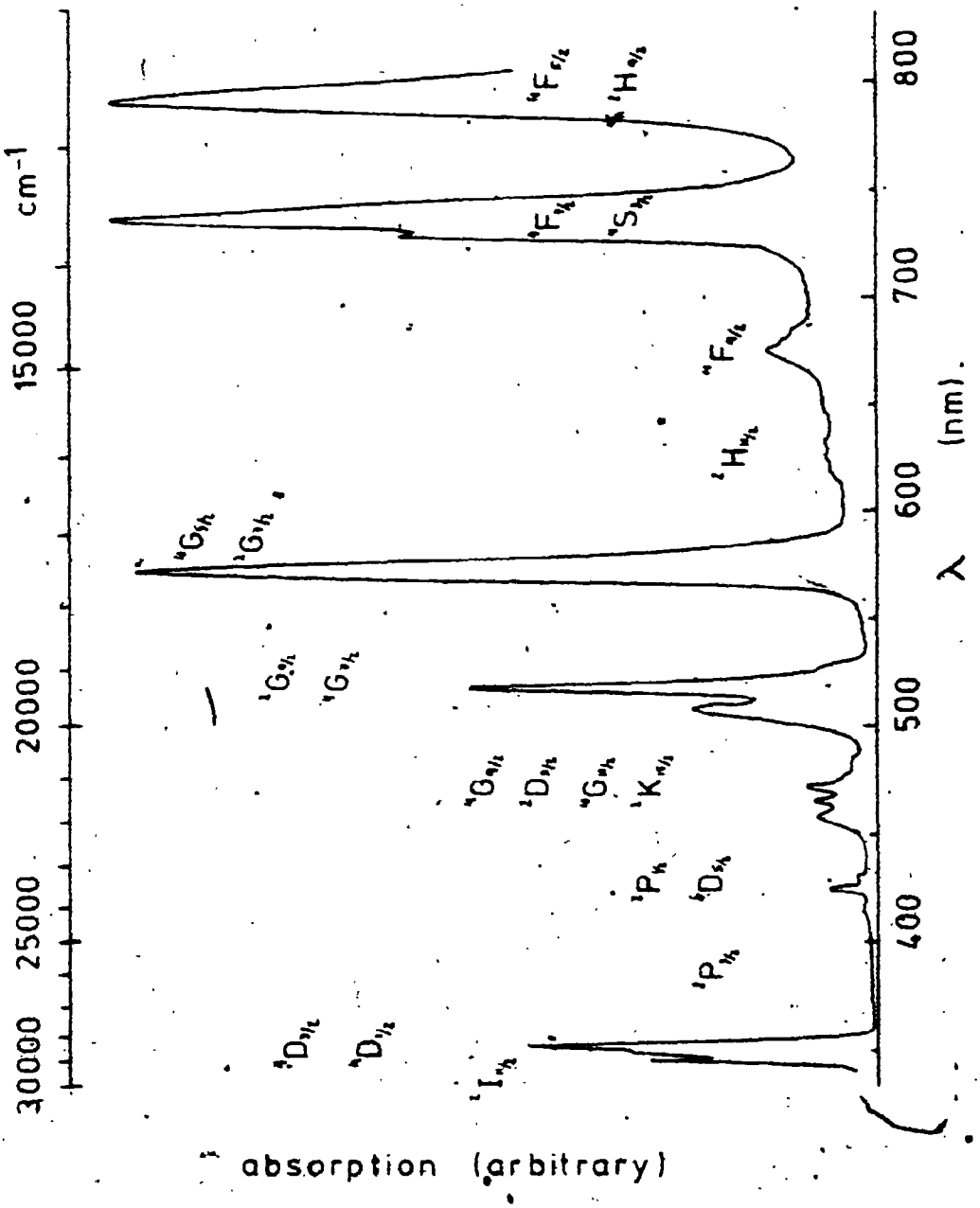

of 0.05 M $NdCl_3$, 0.05 M KH_2PO_4 and 0.32 M HNO_3. Transitions were assigned by comparison of the spectra with published spectra obtained for Nd^{3+} doped into $LaCl_3$ (7,12,13).

Table 4.1 lists some major peaks and extinction coefficients for several standards used in this study. Table 4.2 lists some spectral data for $NdCl_3.6H_2O$ in various solvents. Note that though the variation in extinction coefficient is not large, it is large enough to show that extinction coefficients of REE ions cannot be used indiscriminately. For this reason, standards were generally prepared with chemical matrices similar to those of the solutions to be analyzed.

Minor variations in the chemical composition of the matrix generally do not show up in the spectra. Figure 4.2 shows the spectra of Ho^{3+} in 2M HNO_3 for various H_3PO_4 concentrations. Figure 4.3 shows the effects of varying the total Ho^{3+} concentration. The only observable effect here is the increased signal to noise ratio for the more concentrated solutions. However, in figure 4.4 one can see clear evidence of Er^{3+} complexation with H_3PO_4.

In other words, the chemical effects observed in the spectra are subtle, and variable among REE. As a result, a further precaution was taken in analyzing spectra. Spectra were normally obtained over a range of wavelengths, selected to include at least two characteristic

Table 4-1 Extinction coefficients of major absorption peaks of some REE^{3+} ions in solutions of given composition.

ion	solution composition	λ (nm)		ε ($M^{-1}cm^{-1}$)	
Nd^{3+}	$NdCl_3$= 0.05 M	790	±2	6.0	±0.1
	HNO_3= 0.32 M	735		6.0	
	KH_2PO_4= 0.05 M	727		3.6	
		571*		6.3	
		518		3.5	
		508		1.5	
		352		3.1	
		346		2.0	
Nd^{3+} †	$NdCl_3$= 0.10 M	790		5.8	
	NH_4Cl= 1.0 M	735		6.3	
		727		3.4	
		572*		6.4	
		520		3.7	
		510		1.5	
		354		3.2	
		346		2.1	
Sm^{3+}	$SmCl_3$= 0.0945 M	401*		3.12	
Ho^{3+}	$HoCl_3$= 0.050 M	650		2.0	
		637		3.3	
		534*		4.9	
		484		1.8	
		449		4.2	
		415		2.6	
Er^{3+}	$ErCl_3$= 0.0432 M	647		1.85	
	HNO_3= 1.6 M	519		2.89	
	KH_2PO_4= 0.0450 M	484		1.62	
		376*		5.00	
		362		1.27	

* Principal peaks used in routine chemical analysis.

† Nd^{3+} peak intensities for chloride-dominated media are listed for comparison.

Table 4.2 Major peak positions and molar extinction coefficients of spectra of solutions of $NdCl_3 \cdot 6H_2O$ for various solvents.

DMSO		Et_3PO_4		DMFA		$(PhO)_3P$		H_2O	
λ	ϵ	λ	ϵ	λ	ϵ	λ	ϵ	λ	ϵ
---	---	795	4.3	796	8.2	800	4.0	---	---
743	7.7	740	4.7	742	8.4	744	3.8	738	5.5
578	10.4	581	7.4	581	11.1	583	9.4	573	7.0
521	3.0	522	1.5	523	3.4	525	1.7	520	4.3
510	1.9	510	1.1	511	2.1	514	1.0	510	1.8
355	4.3	354	2.8	356	4.7	358	2.0	354	3.5
349	4.0	348	3.4	351	4.2	352	2.4	---	---

Error in wavelength $\pm$ 2 nm; error in ϵ $\pm$ 0.2 $M^{-1}cm^{-1}$.
DMSO = dimethyl sulfoxide.
Et_3PO_4 = triethyl phosphate.
DMFA = dimethyl formamide.
$(PhO)_3P$ = triphenyl phosphite; may contain $(PhO)_2PhP=O$.

Figure 4.2 Optical absorption spectra of 0.01 M $HoCl_3$ in 2 M HNO_3, with variable H_3PO_4.

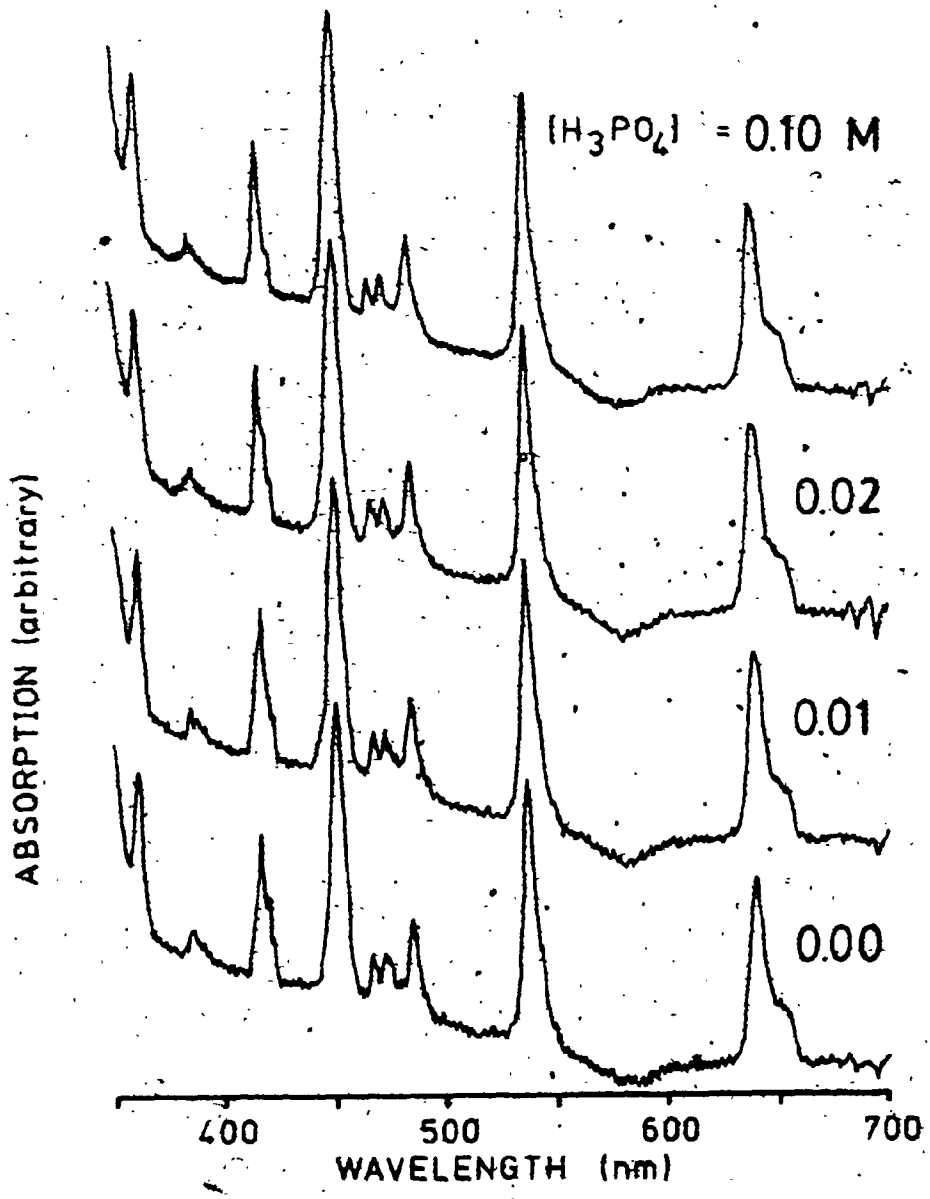

Figure 4.3 Absorption spectra of $HoCl_3$ at three different concentrations, selected to match three absorption scales.

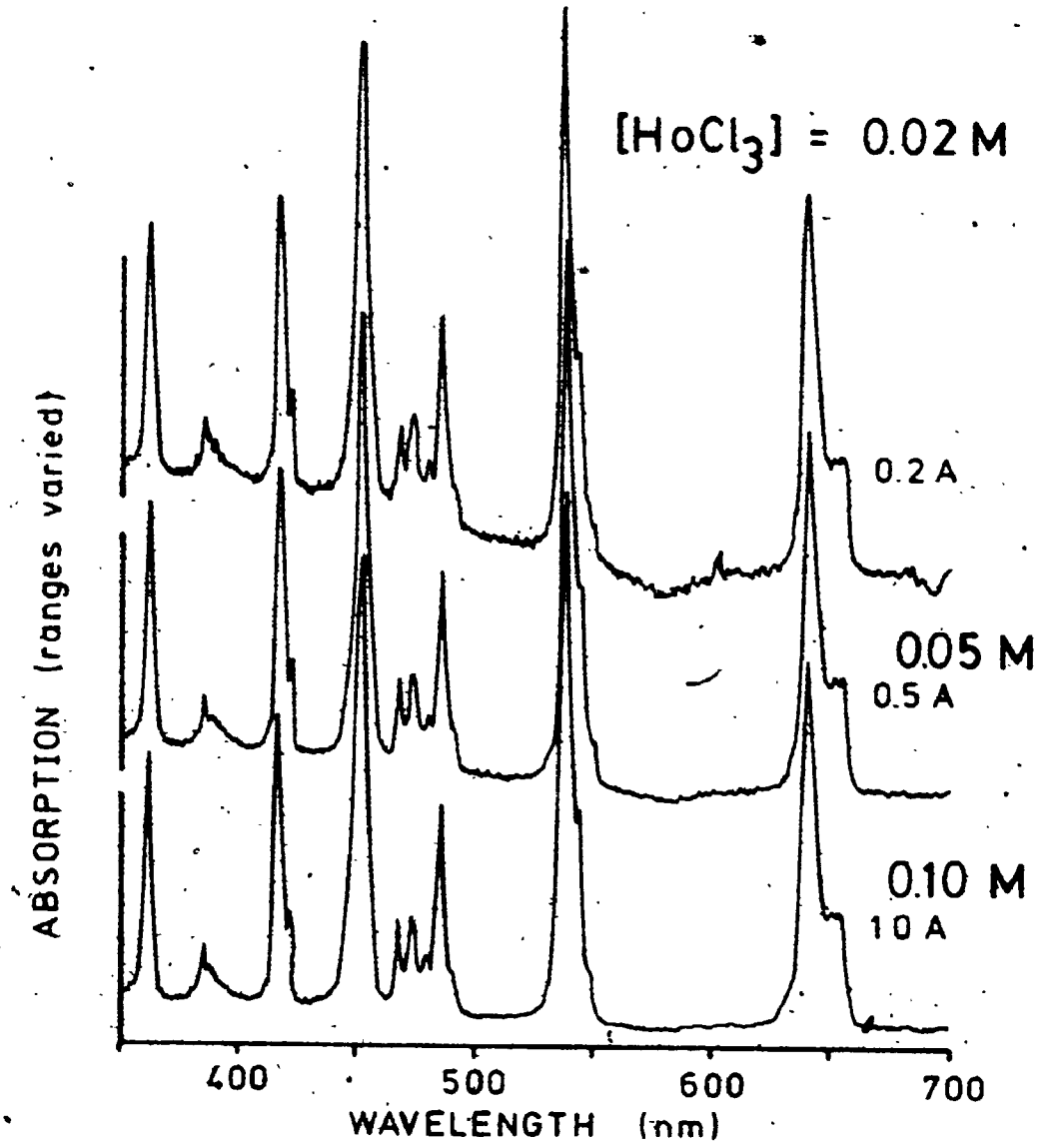

Figure 4.4 Evidence of a 1:1 H_3PO_4/Er complex.
0.09 M ($xErCl_3$ + $(1-x)H_2KPO_4$) in 1.6 M HNO_3 at 25° C.

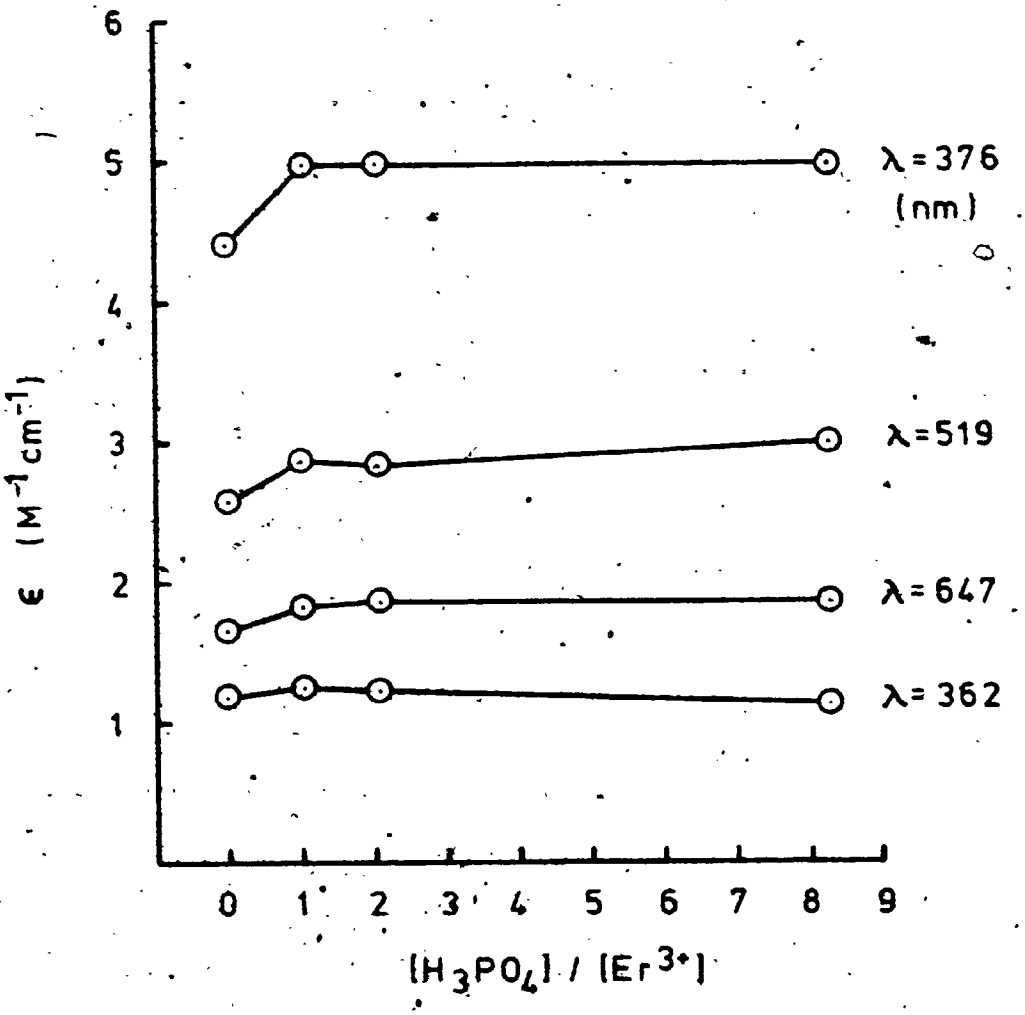

absorption peaks. In this way, the shape of the peaks could be checked for variations, and the presence of colored interferences would show up as an altered base line.

A representative calibration curve is shown in figure 4.5. Normally, only one standard was run during the analysis of a set of samples. The good obedience of the Beer-Lambert law was considered reasonable justification for this procedure.

All spectra were obtained on a Varian CARY 118 spectrophotometer, run in the auto-slit mode and with a gain of 0.45. So long as the gain was maintained at a value of 0.45, spectra were readily reproducible.

Figure 4.5 Calibration curve for Nd^{3+} in dilute HNO_3 using the 575 nm absorption line; $[H_3PO_4] = [Nd]$.

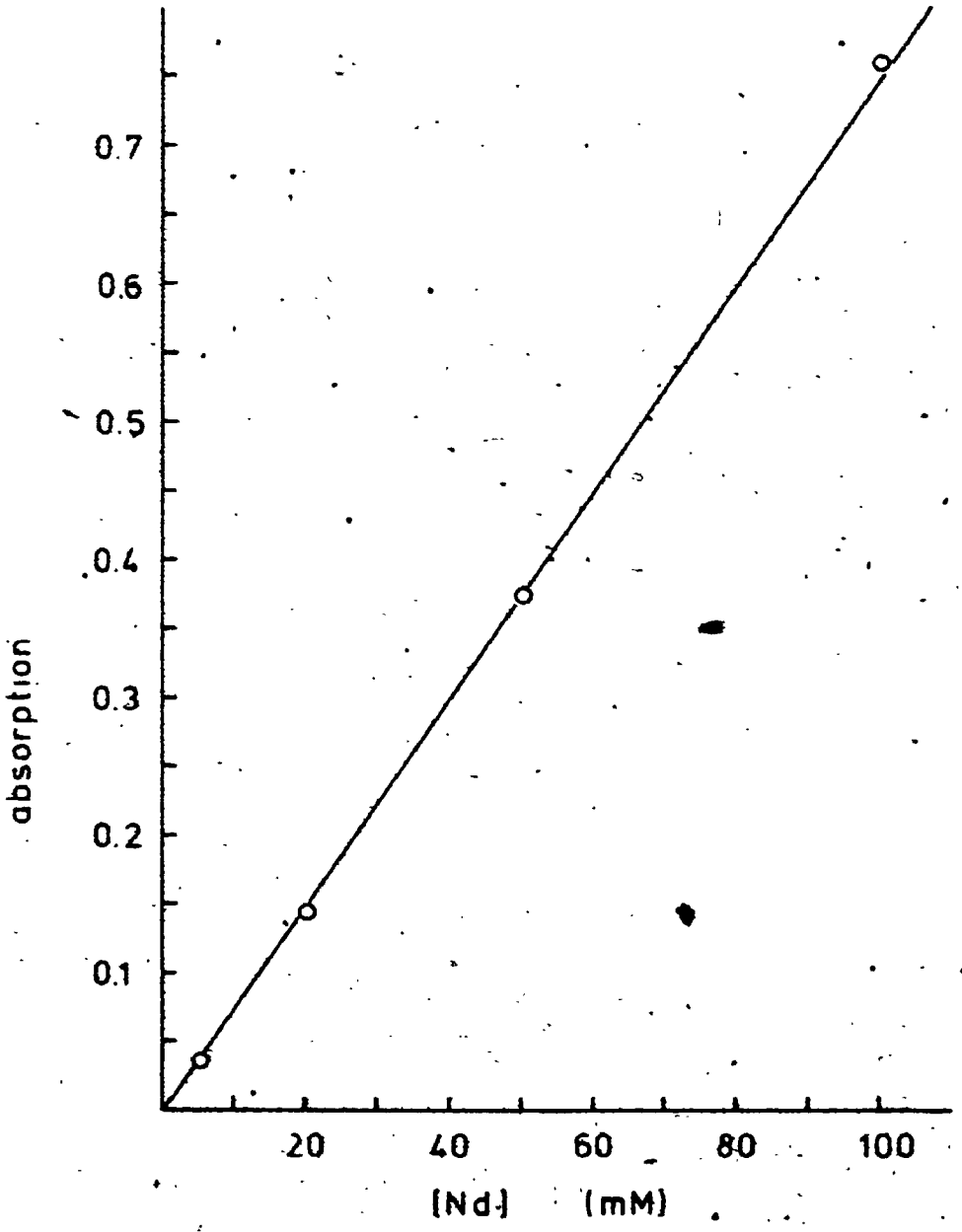

4.2 Activity Coefficients

Some difficulty was encountered in trying to make activity corrections to the solubility data, presented in the next section. This was because some of the data was collected for solutions with ionic strengths greater than 0.1 M, the accepted limit of applicability of the Debye-Hückel equation. Some of the solutions had ionic strengths greater than 0.5 M, the limit of the Davies equation[14]. Beyond this ionic strength, there is no totally acceptable way of dealing with activity coefficients. It was decided therefore that at least the procedure for obtaining single-ion activity coefficients for REE ions should be methodical, and somehow relate to experimentally determined mean activity coefficients for REE salts.

Experimentally determined mean activity coefficients for $LaCl_3$ and $La(NO_3)_3$ were obtained from the literature, (15,16,17). The values are plotted against the molal concentrations of the respective salts in figure 4.6. Because the activity coefficients are given in molal units, and the solubility calculations done in molar units, a conversion was required. It could be assumed that the molal and molar concentrations were numerically equal for a given solution, if the concentrations were less than about 1 M. But this had to be tested.

The molalities corresponding to the literature mean activity coefficients were first converted to mole-fractions

Figure 4.6 Measured mean activity coefficients for $LaCl_3$ (o) and $La(NO_3)_3$ (x) versus the square root of ionic strength, (molality units).

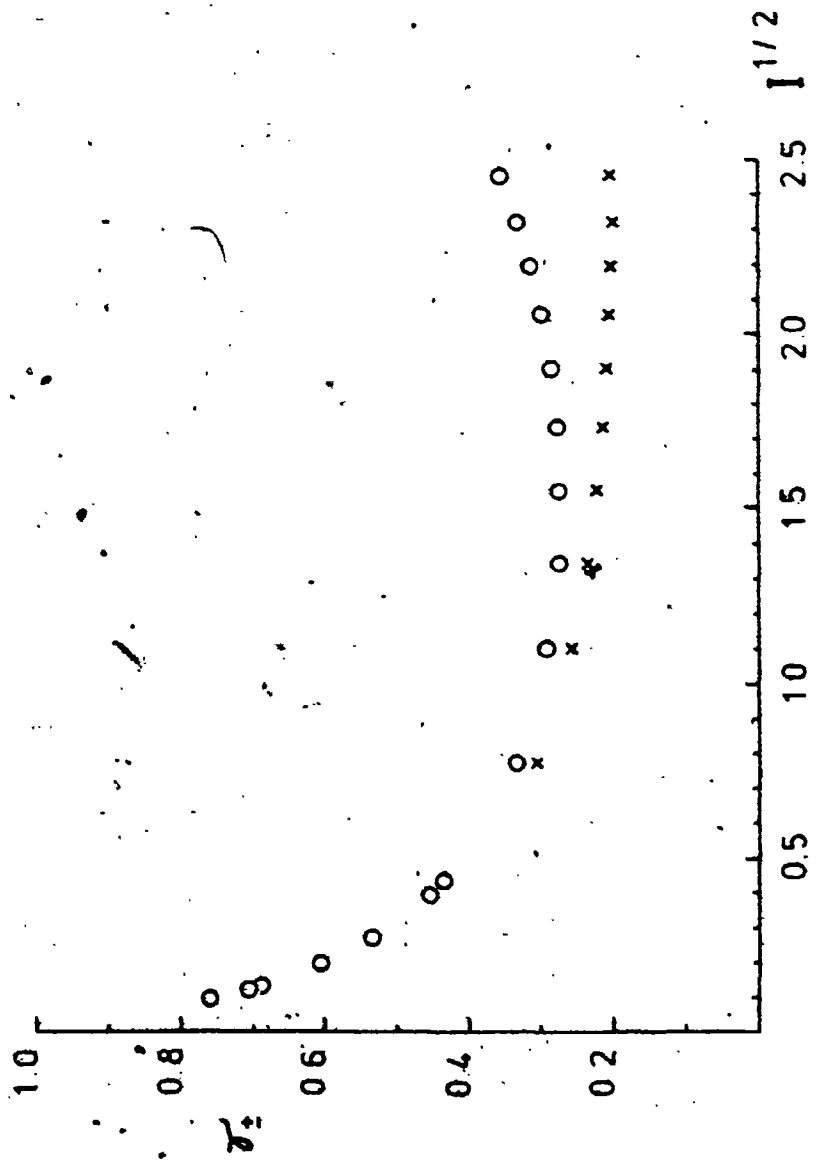

using the relation,

$$x_2 = m/(m + (1000/MW_1)) \qquad (4.3)$$

where x_2 is the mole-fraction of the REE salt, and MW_1 is the molecular weight of water. Next, the mole-fraction data were converted to molarity/density ratios, via

$$M/\rho = 1000\ x_2/(MW_1 + x_2(MW_2 - MW_1)) \qquad (4.4)$$

where ρ is the relative density of the solution, and MW_2 is the molecular weight of the respective REE salt. The relative density of $LaCl_3$ is listed as a function of the molar concentration of $LaCl_3$ in, among other sources, the CRC Handbook of Chemistry and Physics[18]. Next, the molarities had to be guessed in order to estimate the corresponding density values in order to calculate the molarities. The initial values for the iteration were calculated by taking the average of the m and M/ρ values. Because ρ is greater than one, the true M has to lie between m and M/ρ. By interpolation, M values were calculated which differed by less than 1% from the corresponding m values. The iteration converges quickly because the density-concentration curve is fairly flat. Thus the approximation that m and M values are numerically equal for REE salt concentrations less than 1 M is proved valid.

Having obtained mean activity coefficients as a function of molarity, the ionic strength could be calculated for each γ_i.

The ionic strength of a solution is given by

$$I = \tfrac{1}{2}\Sigma C_i z_i \qquad (4.5)$$

where C_i is the concentration of ion ,i, and z_i is the charge on ion ,i. For the LaX_3 salts, this relation is simply,

$$I = 6\ C_{La} \ . \qquad (4.6)$$

This set of I-values was used to calculate single-ion activity coefficients for singly-charged ions using the Davies equation[14],

$$\log \gamma = -Az^2((I^{\frac{1}{2}}/(1 + I^{\frac{1}{2}})) - 0.3\ I) \qquad (4.7)$$

where A = 0.508 at room temperature. The rationale here is that deviations from ideality are proportional to the ionic charge, for a given ionic strength. By using the Davies equation to calculate only singly-charged single ion activity coefficients for ionic strengths greater than 0.5 M, the error is minimized. These single-ion activity coefficients could then be used to calculate La single ion activity coefficients using the relation,

$$\log \gamma_3 = 4\log \gamma_2 - 3\log \gamma_1 \ . \qquad (4.8)$$

The results are plotted in figure 4.7. It was found that for a given molality, the mean activity coefficients for various REE chloride solutions did not vary significantly. Therefore, La activity coefficients were used in calculations

Figure 4.7 Single-ion activity coefficients for La^{3+} in a Cl^- (⊖) matrix and NO_3^- (×) matrix. Solid lines refer to values from the Davies equation. The vertical arrow indicates the ionic strength of seawater, I= 0.7 M.

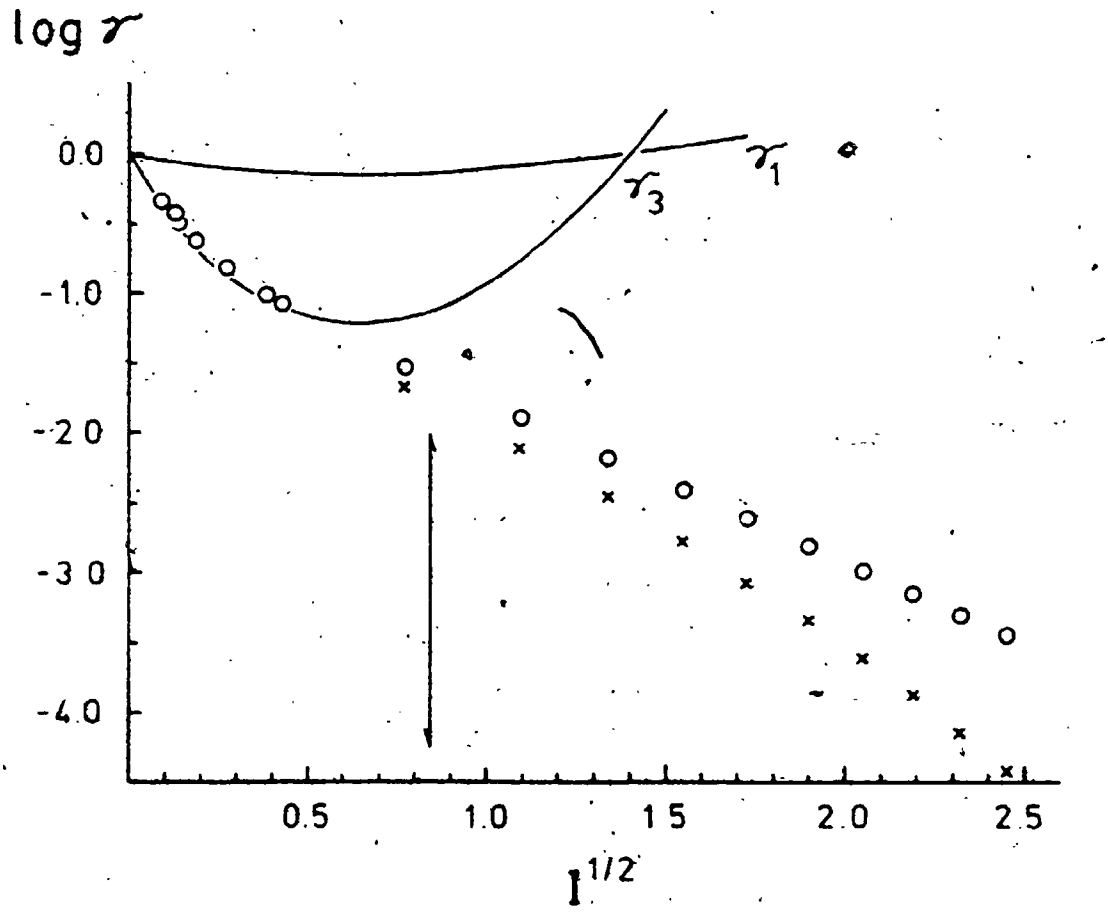

involving other REE.

The further advantage of using this approach is that any ion-pair formation between La and NO_3^- or Cl^- would be included in the activity coefficient values. (Most of the solubility experiments involved solutions dominated by NO_3^-).

Unfortunately, activity coefficient data for REE nitrate solutions at elevated temperatures were not available. Additional discussion of activity coefficients is provided by Harned and Owen[19] and Robinson and Stokes[20].

4.3 Determination of Solubility Products of $REEPO_4 \cdot XH_2O$

4.3.1 Experimental

The synthesis of starting materials is described in sections 2.3 and 2.4. In some cases, the mother liquors were analyzed for REE concentration and pH in order to calculate solubility products. In these particular syntheses, a known slight excess of phosphate was added (as pyrophosphate) initially in order to make the REE ion the limiting reagent. When the reaction was considered complete, normally after 1 to 2 months, the reaction mixtures were filtered through 0.45 μm Millipore filters. Colored [illegible] were measured spectrophotometrically, (section 4.1). Where necessary, the solutions were partially evaporated to known volumes in order to bring the REE concentrations into the analytical range.

Lanthanum was measured by completely evaporating the solution in plastic vials, and submitting the vials for instrumental neutron activation analysis (INAA). The analyses were done by Nuclear Activation Services, Hamilton, Ontario. Standards were run which gave a straight calibration curve passing through zero.

In those experiments where the $REEPO_4$ was dissolved, new nitric acid was used. In some cases, the REE concentration was measured as a function of time, in order to ensure that equilibrium had been reached. (The kinetics of dissolution

will be discussed in a subsequent section.) Equilibrium was typically reached after 4 to 5 weeks.

The pH-meter was calibrated using an HCl solution whose concentration was obtained by titrimetry to be 0.100 M. As long as the solutions to be measured had ionic strenghts similar to that of the HCl solution, the pH reading would be in concentration units. In this way, the measured hydrogen ion concentration could be compared directly with those calculated from a mass balance equation for the solution of interest.

The hydrogen ion concentrations were then converted to activity units using the same single-ion activity coefficients used to obtain REE single-ion values. In this way the solubility calculations would at least be consistent.

4.3.2 Calculation of Solubility Products

The equilibrium studies were carried out at pH values less than three, so that the dominant species in solution are H_3PO_4, $H_2PO_4^-$, H^+ and RE^{3+}. Species of lesser importance include $RE(H_2PO_4)^{2+}$ and $RE(NO_3)^{2+}$. If as an approximation, one ignores these latter two species, then the total phosphate concentration, P, is given by

$$P = [H_2PO_4^-] + [H_3PO_4] \qquad (4.9)$$

which can also be expressed as

$$P = [PO_4^{3-}]\left\{(\gamma_{PO_4}/\gamma_{H_2PO_4})K_2K_3(H^+)^2 + (\gamma_{PO_4}/\gamma_{H_3PO_4})K_1K_2K_3(H^+)^3\right\}, \qquad (4.10)$$

where (H^+) is the hydrogen ion activity, γ_i are single-ion activity coefficients and K_i are <u>association</u> constants of phosphoric acid at zero ionic strength. Values for these K_i are listed in table 4.3 . The convention adopted in this report takes square brackets concentrations, and round brackets activities.

If, as has been assumed, the RE^{3+} ion is not complexed, then the RE concentration is equal to the total, analytical concentration of RE, so that,

$$\log K^o_{sp} = \log\gamma_{RE} + \log[RE] + \log P - \log\left\{(K_2K_3(H^+)^2/\gamma_{H_2PO_4}) + (K_1K_2K_3(H^+)^3/\gamma_{H_3PO_4})\right\}, \qquad (4.11)$$

Table 4.3 Association constants used in the solubility product calculations, for H_3PO_4 at zero ionic strength and 25° and 100°C.

T(°C)	$\log K_1$	$\log K_2$	$\log K_3$
25	2.152	7.204	12.38
	± 0.001	0.003	0.?
100	2.618	7.332	11.125
	± 0.004	0.018	0.4

Data are from Mesmer and Baes, (21) and Marshall and Frank (22).

where K^{o}_{sp} is the thermodynamic solubility product of $REEPO_4 \cdot xH_2O$. Note that because one is dealing with a hydrated salt, corrections to the solubility product would have to be made for solutions in which the activity of water is significantly different from one. The activity coefficient of H_3PO_4 was taken as unity. The results of the calculation are given in table 4.4.

As indicated earlier, the $REE^{3+}/H_2PO_4^-$ complex was ignored in the calculations. In fact, the formation constant of this complex was measured by Rao et al.[23] to be about 40 at an ionic strength of 0.5 M. At the pH values used in the solubility studies reported here, the fully protonated form of H_3PO_4 dominates in solution, so that ignoring the solution complex in the calculations was acceptable.

In the section on spectrophotometry (4.1), it was reported that there is some evidence for a complex between Er^{3+} and H_3PO_4. One might suspect that other REE complex with H_3PO_4 as well. Unfortunately, the extent of this complexation is not known. Attempts were made by the author to measure the degree of complexation between La and H_3PO_4 using ^{31}P NMR. The ^{31}P chemical shift does depend on the La/H_3PO_4 ratio, but not in a manner which would lead to convincing stability constants. (The data are available from the author upon request).

4.3.3 Results

The calculated solubility products for a selection of hydrous REE phosphates are presented along with relevant data in table 4.4 . The $\log K_{sp}$ are valid at zero ionic strength.

The determinations of logK for the La derivative vary from -24 to -25.1. The mean value for the twelve determinations is -24.5, with a standard deviation of 0.32. The estimated errors are listed in table 4.5. Selection of different dissociation constants of phosphoric acid from the literature is estimated to give rise to a variation in solubility products of about 0.6 log units.

The solubility of $LaPO_4$ (freshly precipitated), given by Tananaev and Vasil'eva[24] at an ionic strength of 0.5 is pK_{sp} = 22.4. Activity coefficient corrections yield a pK_{sp} value of 25.1 compared with the mean value given above of 24.5.

The range of pK values for the Nd derivative is 24.5 to 26.2. The two values at room temperature appear to be about an order of magnitude less than the three values at 100°C, (i.e., ten times more soluble). This difference is close to the estimated error in pK, however, and may not be significant. Ideally, the solubilities should be measured for several temperatures between the freezing point of the solutions and the boiling point.

Table 4.4 Solution data and solubility products of some $REEPO_4 \cdot xH_2O$ solids

#	C	RE^{3+}	I	pH_m	pH_c	pH_c^a	γ_1	γ_3	$\log K^o_{sp}$	T(°C)
La01	3.29 E-4	3.29 E-4	0.05	1.7	1.7	1.8	0.823	0.197	-24.16	25
02	2.72 E-4	2.72 E-4	0.05	1.7	1.7	1.8	0.823	0.197	-24.32	
03	2.62 E-4	2.62 E-4	0.03	1.7	1.7	1.8	0.851	0.257	-24.24	
04	3.02 E-4	3.02 E-4	0.05	1.7	1.7	1.8	0.823	0.197	-24.23	
05	1.13 E-4	1.13 E-4	0.04	2.0	2.0	2.1	0.835	0.224	-24.26	
06	1.22 E-4	1.22 E-4	0.01	2.0	2.0	2.0	0.903	0.412	-24.16	
07	0.65 E-4	0.65 E-4	0.01	2.0	2.0	2.0	0.903	0.412	-24.71	
08	0.59 E-4	0.59 E-4	0.04	2.0	2.0	2.0	0.835	0.224	-24.82	
09	0.18 E-4	0.18 E-4	0.03	2.4	2.4	2.5	0.851	0.257	-24.84	
10	0.19 E-4	0.19 E-4	0.03	2.4	2.4	2.5	0.851	0.257	-24.79	
11	0.14 E-4	0.14 E-4	0.01	2.4	2.4	2.4	0.903	0.412	-25.07	
12	0.22 E-4	0.22 E-4	0.03	2.4	2.4	2.5	0.851	0.257	-24.67	
Pr01	3.89 E-4	3.89 E-4	0.16	0.8	0.8	0.9	0.758	0.093	-26.23	100
02	2.65 E-3	2.10 E-4	0.35	0.2	0.5	0.6	0.733	0.049	-26.84	
03	2.9 E-3	1.4 E-3	0.19	0.7	0.8	0.9	0.751	0.081	-24.87	
Sm01	1.02 E-3	1.02 E-3	0.22	1.0	1.0	1.1	0.748	0.069	-25.6	25
02	5.53 E-3	5.53 E-3	0.32	0.5	0.5	0.6	0.736	0.056	-25.7	20

C= total phosphate; RE^{3+} = measured [RE], M; pH_m = -log[H^+], measured; pH_c = -log[H^+], calculated; pH_m^a = -log(H^+), calculated; γ_i is the activity coefficient of an ion with charge i.

(Table continued next page).

Table 4.4 (continued).

#	C	RE^{3+}	I	pH_m	pH_c	pH_c^a	γ_1	γ_3	$\log K^o_{sp}$	T(°C)
Nd01	1.74 E-3	1.04 E-3	0.18	0.8	0.8	0.9	0.753	0.085	-25.20	100
02	1.75 E-2	7.99 E-3	0.87	0.03	0.08	0.2	0.773	0.013	-26.22	
03	4.15 E-3	4.15 E-3	0.29	0.5	0.5	0.6	0.736	0.059	-25.91	
04	3.43 E-3	3.43 E-3	0.22	1.0	1.0	1.1	0.748	0.069	-24.5	25
05	1.58 E-2	1.58 E-2	0.32	0.5	0.5	0.6	0.736	0.056	-24.8	20
Er01	7.89 E-4	1.97 E-4	0.10	0.9	1.0	1.1	0.783	0.129	-25.48	100
02	1.73 E-3	1.73 E-3	0.07	1.1	1.2	1.3	0.803	0.162	-24.18	25
03	4.0 E-4	4.0 E-4	0.22	1.0	1.0	1.1	0.748	0.069	-26.4	25
Ho01	3.0 E-3	3.0 E-3	0.22	1.0	1.0	1.1	0.748	0.069	-24.6	25

C= total phosphate; RE^{3+}= measured $[RE^{3+}]$, M; $pH_m = -\log[H^+]$, measured; $pH_c = -\log[H^+]$, calculated; $pH_c^a = -\log(H^+)$, calculated; γ_i is the activity coefficient of an ion with charge i.

Table 4.5 Estimated errors for solubility products of $REEPO_4 \cdot xH_2O$.

parameter	error (log units)
calculated pH	0.05
measured pH	0.10
concentration of RE^{3+}	0.02
concentration total PO_4^{3-}	0.04
activity coefficient RE^{3+}	0.05
pK_{sp} (calculated)	0.21
pK_{sp}*	0.32
pK_1	0.02
pK_2	0.05
pK_3	0.5
total error in H_3PO_4	0.6

* Standard deviation of 12 $LaPO_4$ pK_{sp} determinations.

The temperature dependence of the solubility product can be estimated in an approximate way from a knowledge of the enthalpy change involved with dissolution via

$$d\ln K/dT = \Delta H/RT^2 \qquad (4.12)$$

where the symbols have their usual meanings. If ΔH for the reaction

$$REPO_4 = RE^{3+} + PO_4^{3-} \qquad (4.13)$$

is positive, the reaction is endothermic and will be favoured by increasing the temperature. This is the case for most dissolution reactions. In the case of $REPO_4$ dissolution, the free energy of dissolution can be obtained from the solubility product. In the absence of entropy data, data for other compounds can be used by writing reactions of the sort

$$MPO_4 + LaX_3 = LaPO_4 + MX_3 \qquad (4.14)$$

where the entropy of $LaPO_4$ is the only unknown. Such reactions yield an average entropy of 125 J/K-mole. The entropy change for the reaction

$$LaPO_4 = La^{3+} + PO_4^{3-} \qquad (4.15)$$

is then -508. J/K-mole. Substitution into the equation

$$-RT\ln K_{sp} = \Delta H - T\Delta S \qquad (4.16)$$

where K_{sp} is about 10^{-24} yields an enthalpy of dissolution of about -13 KJ/mole. Thus the dissolution of anhydrous $LaPO_4$ is exothermic, so that the solubility decreases with increasing temperature, at least until the approximations made in the calculation no longer hold.

These results are consistent with the observed trend for Nd-RHABDOPHANE dissolution. They are reversed for the trend observed for $ErPO_4 \cdot xH_2O$, although examination of the solubility data in table 4.4 will reveal that the data are not unequivocal.

4.4 Dissolution Kinetics

Several kinetics of dissolution experiments were carried out in order to ensure that equilibrium had been reached in the solubility studies. (Equilibrium data from the kinetics studies are included in the solubility section). Also, some knowledge of the rate law governing the dissolution was desired. This knowledge would be of some value in interpreting results from other surface reaction studies.

Figure 4.8 shows the dissolution of Nd-RHABDOPHANE in dilute HNO_3 (pH=0.5), at 25°C. It was found that the data could be fit by a first order rate law for reversible reactions[25],

$$dC/dt = k(C_{eq}-C) \qquad (4.17)$$

where C_{eq} is the concentration of either Nd or total phosphate at equilibrium. This rate law can be integrated to give

$$(C_{eq}-C)/C_{eq} = \exp(-kt) \qquad (4.18)$$

where C=0 for t=0. The rate constant can be easily obtained from a linear plot of $-\ln(C_{eq}-C)/C_{eq}$ versus time. The value of C_{eq} was obtained by selecting a reasonable initial value for C_{eq} and iterating the relation for C_{eq} and k until a straight line was obtained with an acceptable correlation coefficient.

Figure 4.8 Dissolution kinetics of Ni-RHABDOPHANE in dilute HNO_3 (pH = 3.5) at 25° C.

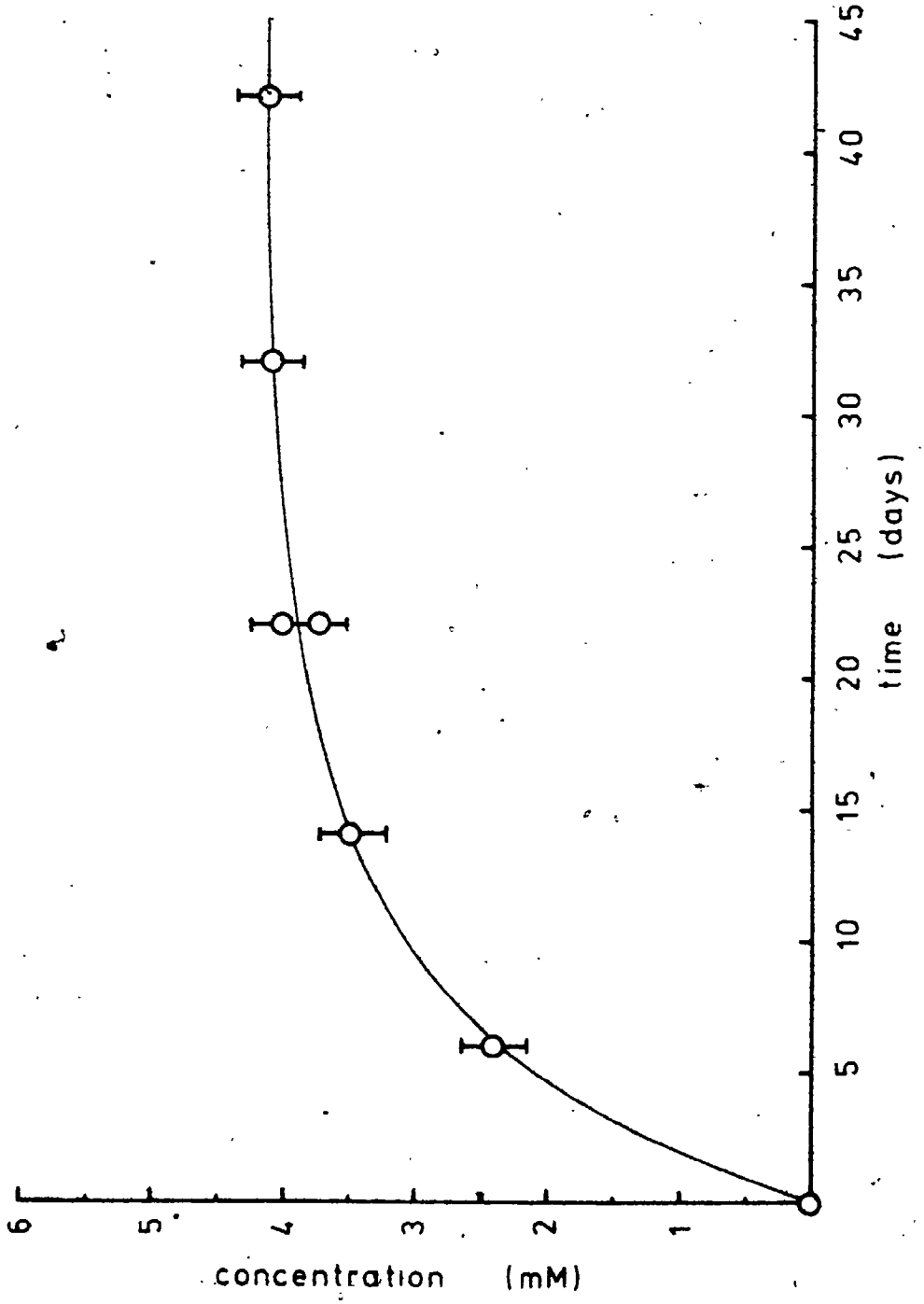

Figure 4.9 Integrated rate law for the dissolution of Nd-RHABDOPHANE.

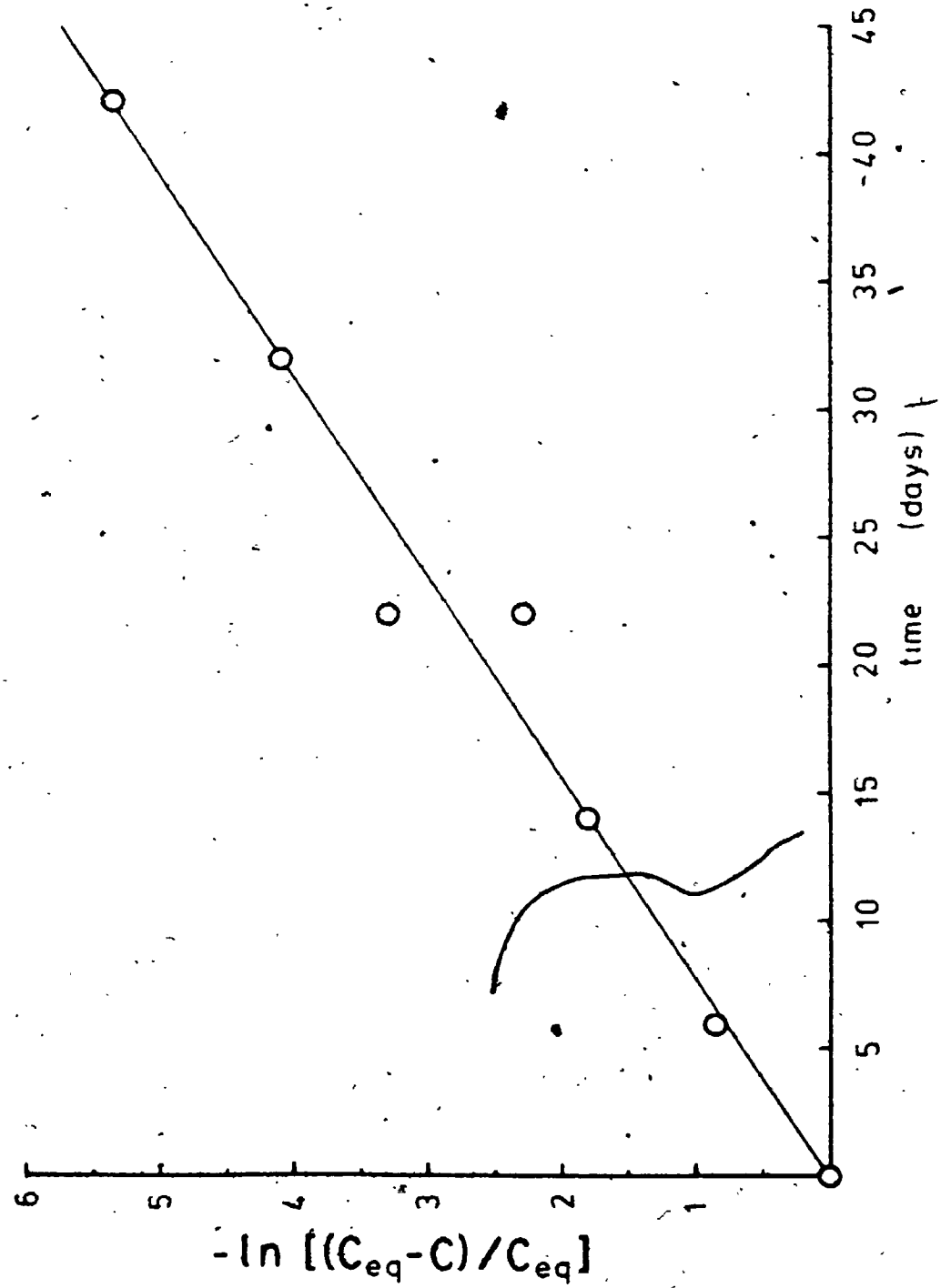

interferences. The peaks observed are definitely those of Ce^{3+}, however, as can be seen by comparison with those in figure 4.15, which shows the UV spectrum of aqueous $CeCl_3$. As the SIMS and INAA results of monazite analysis show, Ce is the dominant REE in natural monazite, followed by Nd. A visible spectrum of the leachate solution used for the latest Ce-determination showed no trace of Nd, (i.e., the Nd concentration is less than background). Thus monazite dissolves much more slowly than, for example, Nd-RHABDOPHANE, even though the acid concentration used for monazite dissolution was ten times that used for Nd-RHABDOPHANE dissolution.

In a related experiment, single crystals of anhydrous REE phosphate were placed in 20 mL of 1 M HCl for five months. Not one of the crystals of Nd-, Sm-, Er- or Ho-phosphate showed signs of dissolving. These results are consistent with those obtained for the New Mexico monazite.

4.4.2 Comparison with Other Studies

In 1985, Tole[28] investigated the dissolution of natural and amorphous zircon ($ZrSiO_4$) samples at a pH of 5.0. Only the amorphous zircon was observed to dissolve. Further, the reaction was observed to be reversible. The kinetics were found to be first order in silica. Zirconium presumably reprecipitated immediately upon

Figure 4.10 Changes in REE concentration with time after effective equilibrium. Samples of the respective hydrous REE phosphate were reacted with a solution of 0.118 M $HClO_4$ + 0.10 $NaClO_4$ (pH 0.9) at room temp.

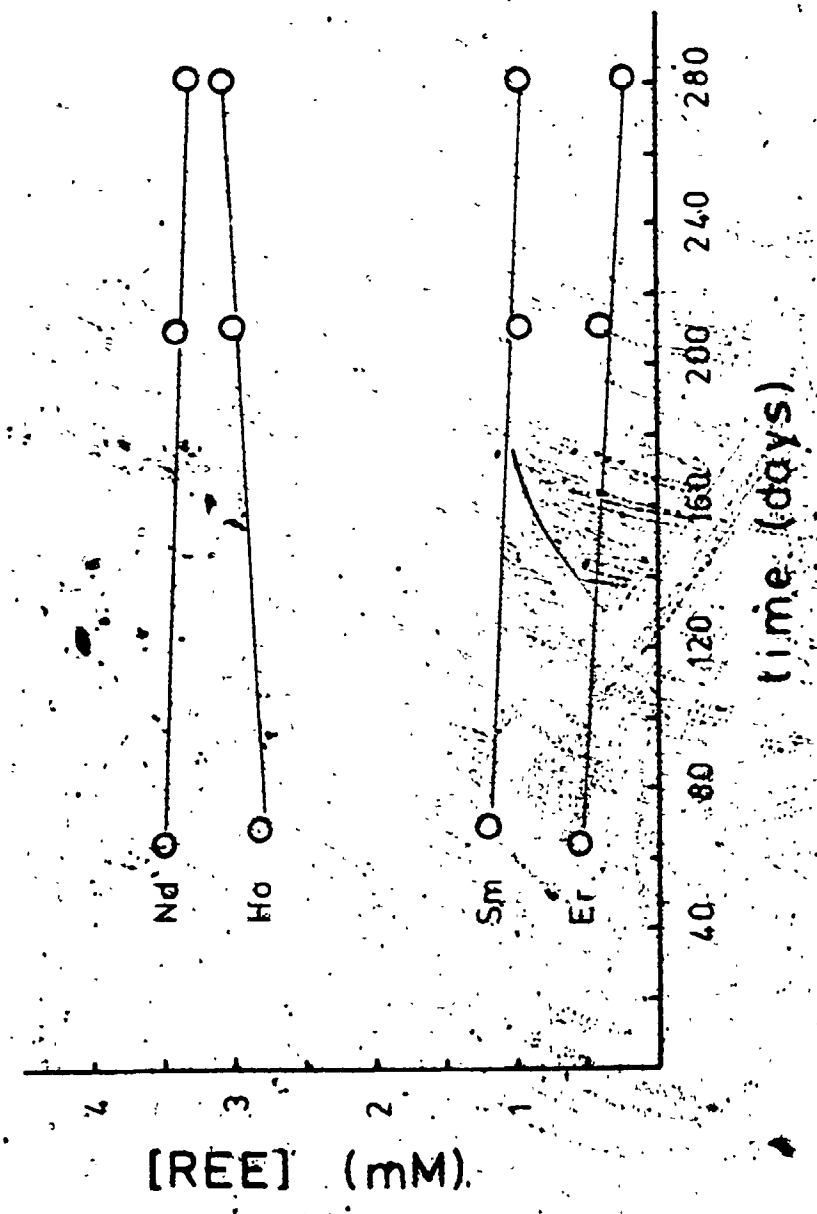

Figure 4.11 Dissolution kinetics of hydrous phosphates of Nd, Sm and Er at a pH of 0.5 and a temperature of 20° C.

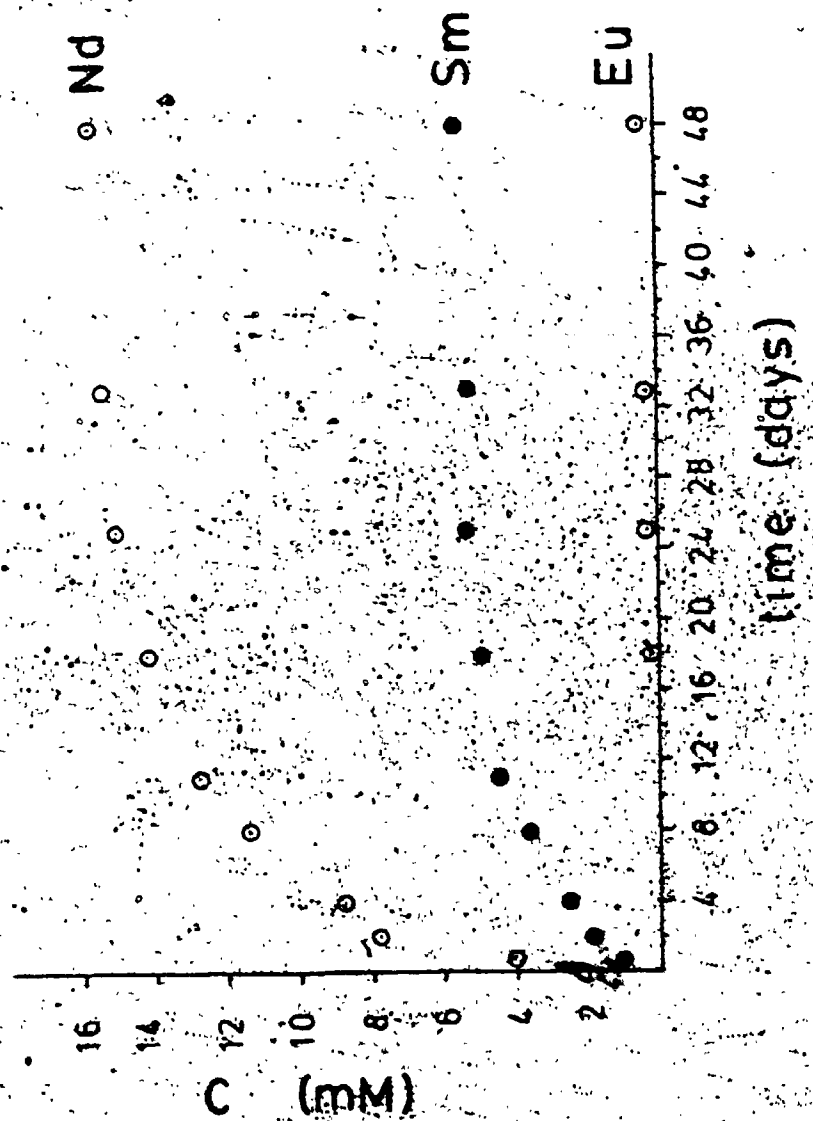

Figure 4.12 Integrated rate law for the dissolution of the second sample of Nd-RHABDOPHANE. Note that the first two points at t=0.0 and t=0.7 days were not included in the linear regression. The correlation coefficient is 0.999; k= 0.10 $days^{-1}$; the effective C_{eq} = 15.775 mM.

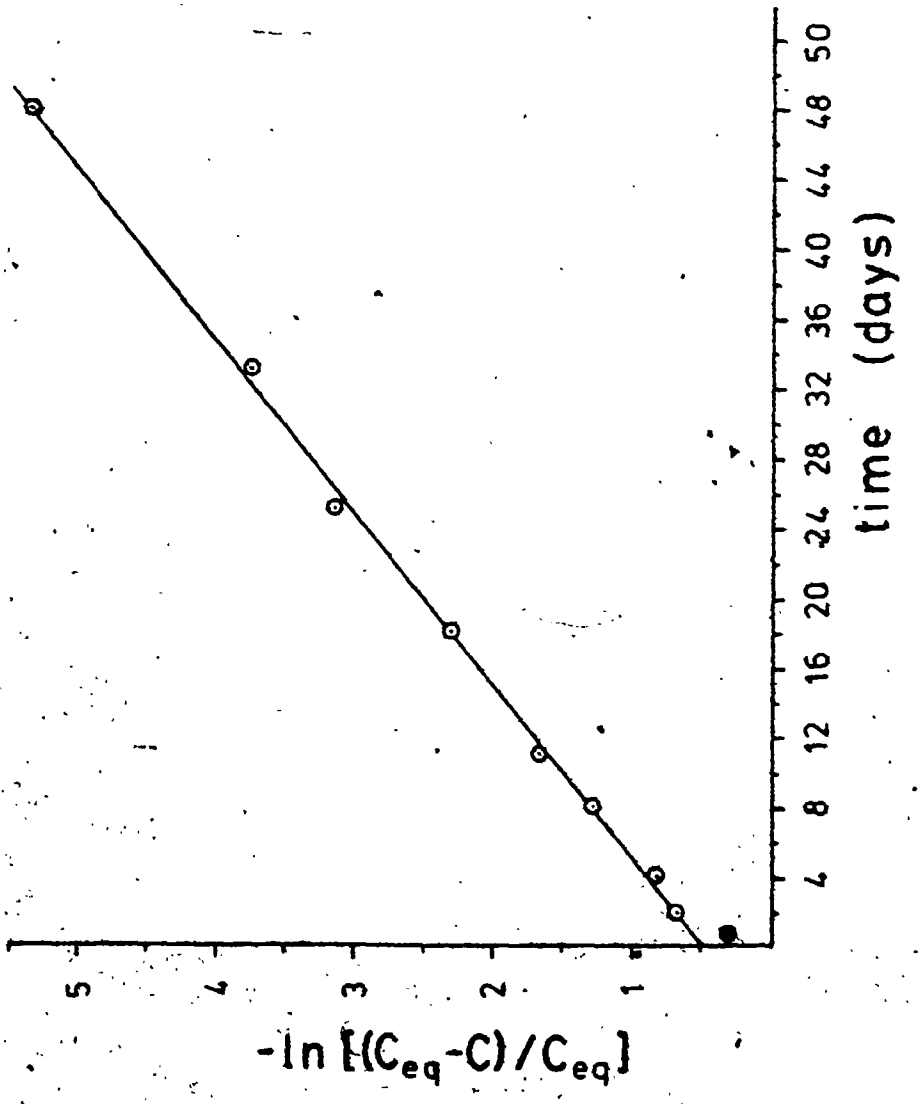

Figure 4.13 Integrated rate law for the dissolution of Sm-RHABDOPHANE. Note that the points at t=0.0 and t=33 days were not included in the linear regression. The correlation coefficient is 0.999; $k = 0.11$ days^{-1}; the effective $C_{eq} = 5.53$ mM.

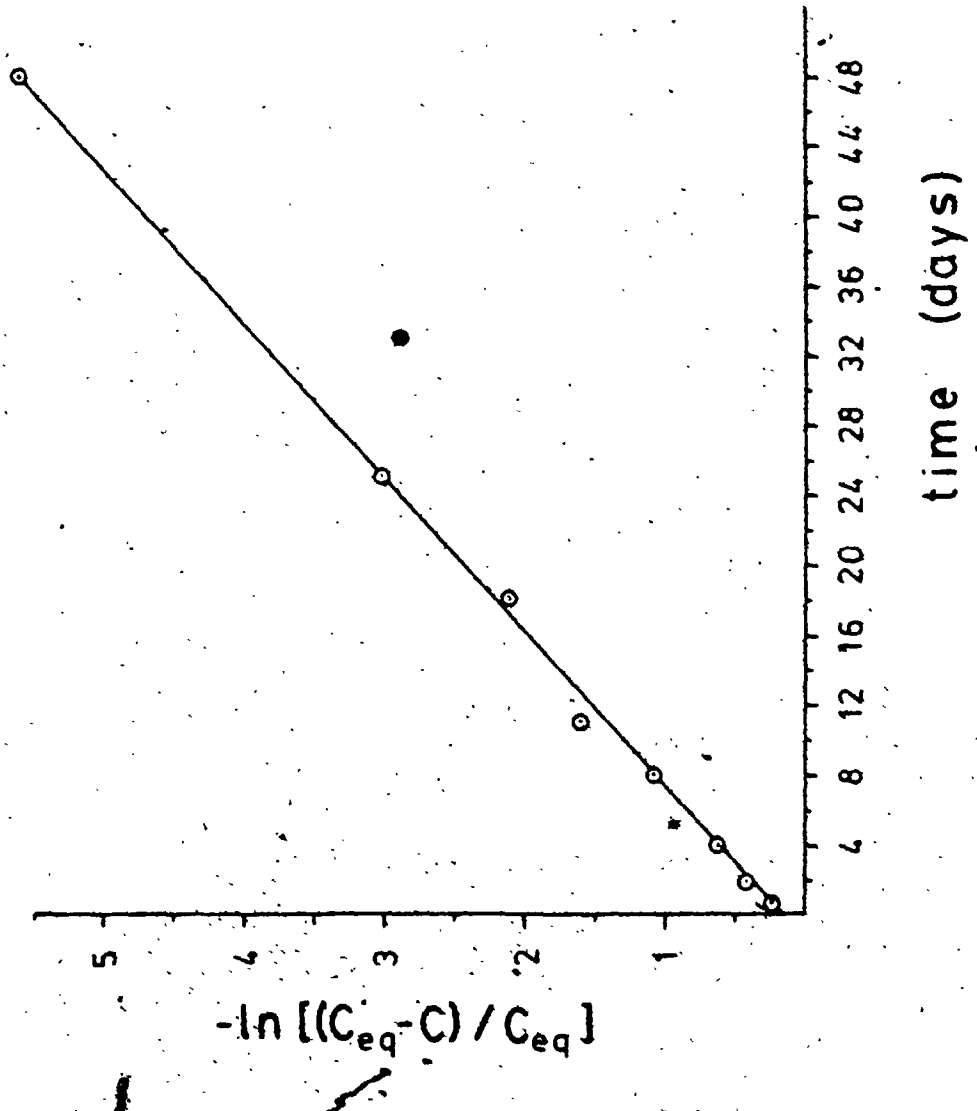

reactive Nd, which resulted in the anomalously rapid rise in concentration initially. This was corrected by ignoring the first data point, (solid circle), and allowing the line to pass through an intercept not equal to zero. This interpretation is not without precedent. The initial, anomalous rise in concentration has been observed in mineral dissolution studies, particularly when the mineral sample was previously crushed, with the result that a significant amount of highly reactive particles was created,[26,27].

The dissolution behavior of Sm-RHABDOPHANE depicted in figures 4.11 and 4.13 is similar to that of the Nd-RHABDOPHANE. Note that the rate constants are similar for all three examples.

The dissolution of $ErPO_4 \cdot xH_2O$ is too insignificant under these conditions to allow rate constants to be obtained from the data.

4.4.1 The Anhydrous Phosphates

In figure 4.14 the UV spectra of leachates from dissolution experiments involving natural monazite are shown. It was found that nitrate absorbs strongly in the UV region of the spectrum, so that the experiments were carried out with 1M H_2SO_4. The entire spectra are plotted as a function of time since the cerium concentration could not be measured in view of the large background

Figure 4.14 Absorption spectra of monazite leachates as a function of time. Spectral range 200-400 nm. Leachate is 1 M H_2SO_4; temperature 20° C. Observed peaks correspond to those of Ce^{3+}.

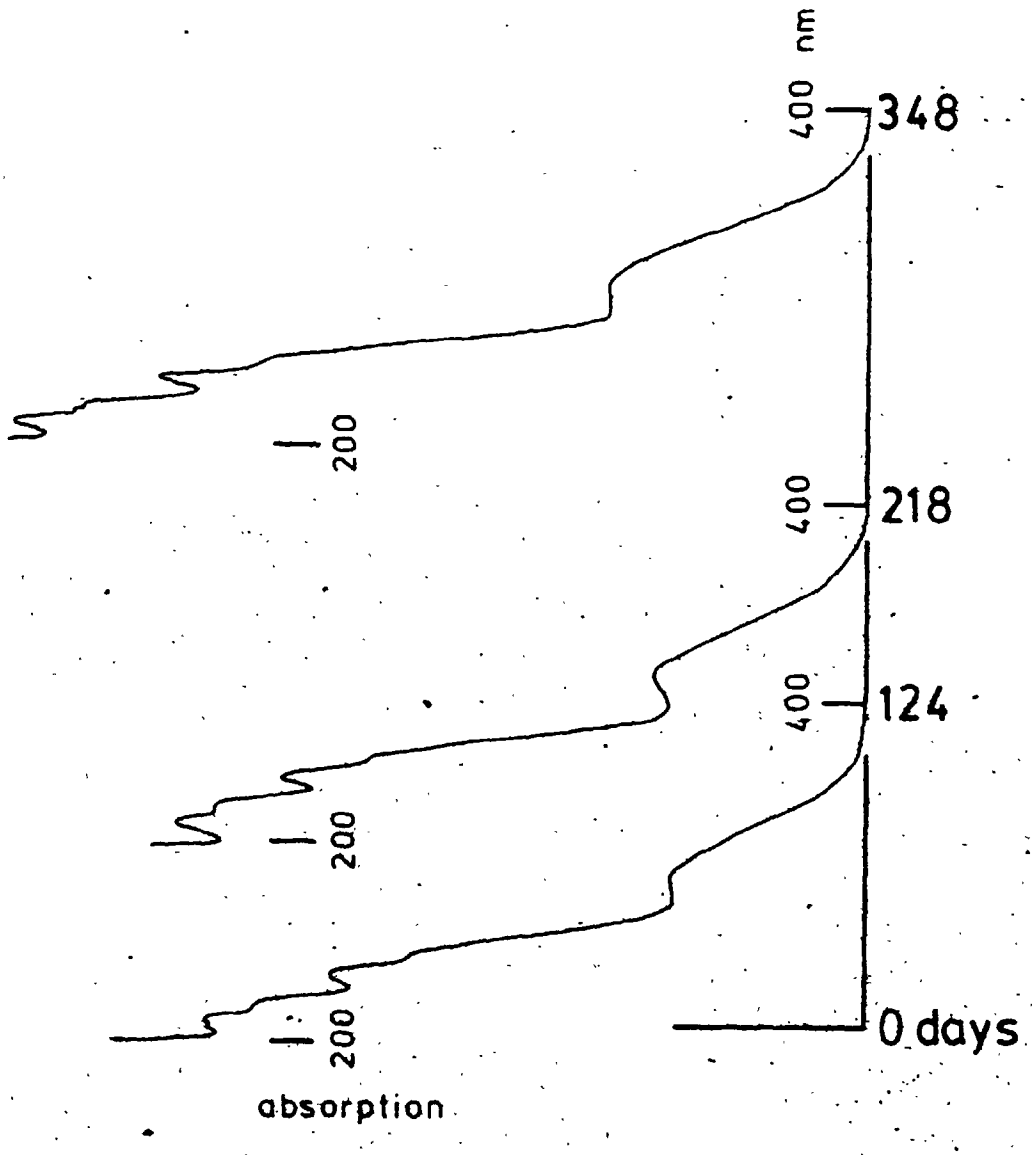

Figure 4.15 UV absorption spectrum of $CeCl_3$ (aq); [Ce] = 1.72 mM. Note that it becomes increasingly difficult to assign a baseline as the wavelength decreases.

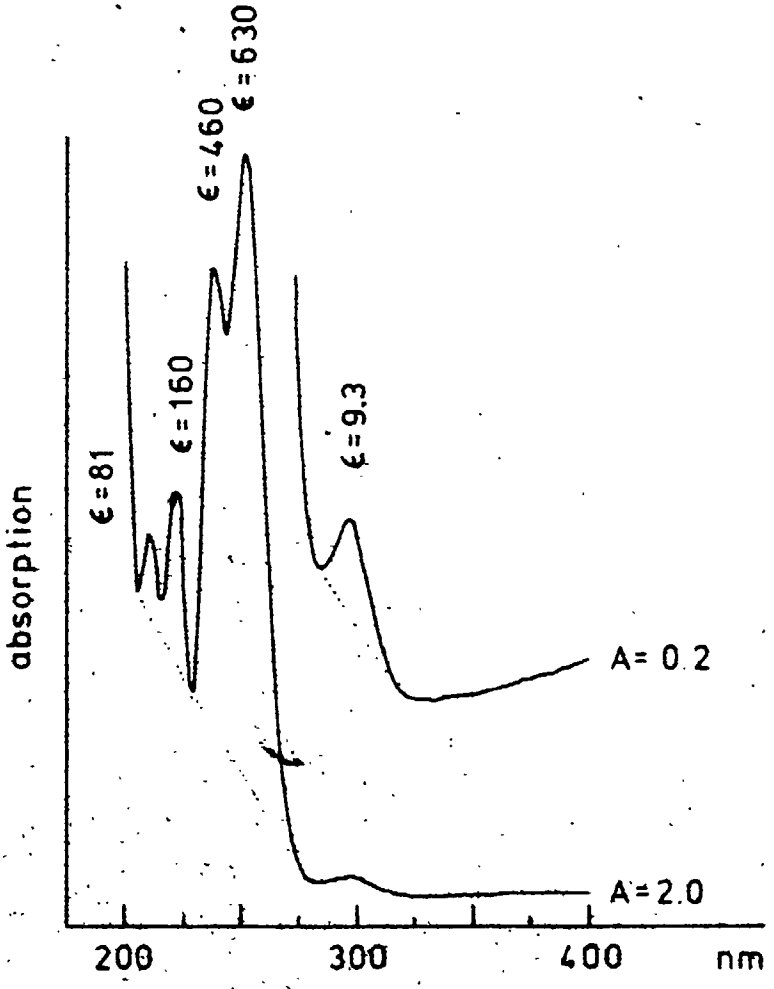

interferences. The peaks observed are definitely those of Ce^{3+}, however, as can be seen by comparison with those in figure 4.15, which shows the UV spectrum of aqueous $CeCl_3$. As the SIMS and INAA results of monazite analysis show, Ce is the dominant REE in natural monazite, followed by Nd. A visible spectrum of the leachate solution used for the latest Ce-determination showed no trace of Nd, (i.e., the Nd concentration is less than background). Thus monazite dissolves much more slowly than, for example, Nd-RHABDOPHANE, even though the acid concentration used for monazite dissolution was ten times that used for Nd-RHABDOPHANE dissolution.

In a related experiment, single crystals of anhydrous REE phosphate were placed in 20 mL of 1 M HCl for five months. Not one of the crystals of Nd-, Sm-, Er- or Ho-phosphate showed signs of dissolving. These results are consistent with those obtained for the New Mexico monazite.

4.4.2 Comparison with Other Studies

In 1985, Tole[28] investigated the dissolution of natural and amorphous zircon ($ZrSiO_4$) samples at a pH of 5.0. Only the amorphous zircon was observed to dissolve. Further, the reaction was observed to be reversible. The kinetics were found to be first order in silica. Zirconium presumably reprecipitated immediately upon

dissolution, since the concentration of Zr was at all times below the detection limit. The dissolution kinetics could be modelled using the rate law for first order reversible kinetics. Newly formed zircon crystals were observed under certain circumstances.

These results are similar to those obtained for the dissolution of REE phosphates. Both experiments show reversible, first order kinetics. The dissolution of well crystallized samples was observed to be much slower than that of finer-grained, or less well crystallized materials. Finally, the poorly crystallized materials tend to recrystallize.

4.5 Seawater REE Concentrations

4.5.1 Introduction

The REE concentrations in seawater are very low. For example, Hoyle etal.[29] measured the concentrations of La, Ce, and Nd in coastal water to be 44, 63 and 46 pmol/kg, respectively. DeBaar etal.[30] found La-concentrations from 16 pmol/kg near the surface of the ocean to 80 pmol/kg near the bottom, at 4.5 km. Other REE were found to have concentrations of about an order of magnitude less.

It is likely that one or more REE phosphate phases control the REE concentrations, since these phases are so insoluble. In figures 4.16 and 4.17 are shown the pH-stability diagrams of $Eu_2(CO_3)_2$ and Nd-RHABDOPHANE, respectively. Note that the concentration of Eu is at no pH value low enough to explain the seawater concentration of Eu. The Nd phosphate diagram, on the other hand, does predict a Nd concentration consistent with measured values.

The association of REE with marine phosphorites has been known for some time[31,32]. Elderfield et al[33] and Li[34] have demonstrated an association between phosphate and REE in ferromanganese nodules and associated sediments. Turner and Whitfield[35] suggested that as a first step in the immobilization process the REE are adsorbed onto various mineral phases. Then as diagenetic reactions occur, the REE are incorporated into various

Figure 4.16 Stability diagram for europium carbonate. Solid lines are for concentrations of Eu^{3+} and the indicated carbonate species; dashed lines are for the carbonate ion only.

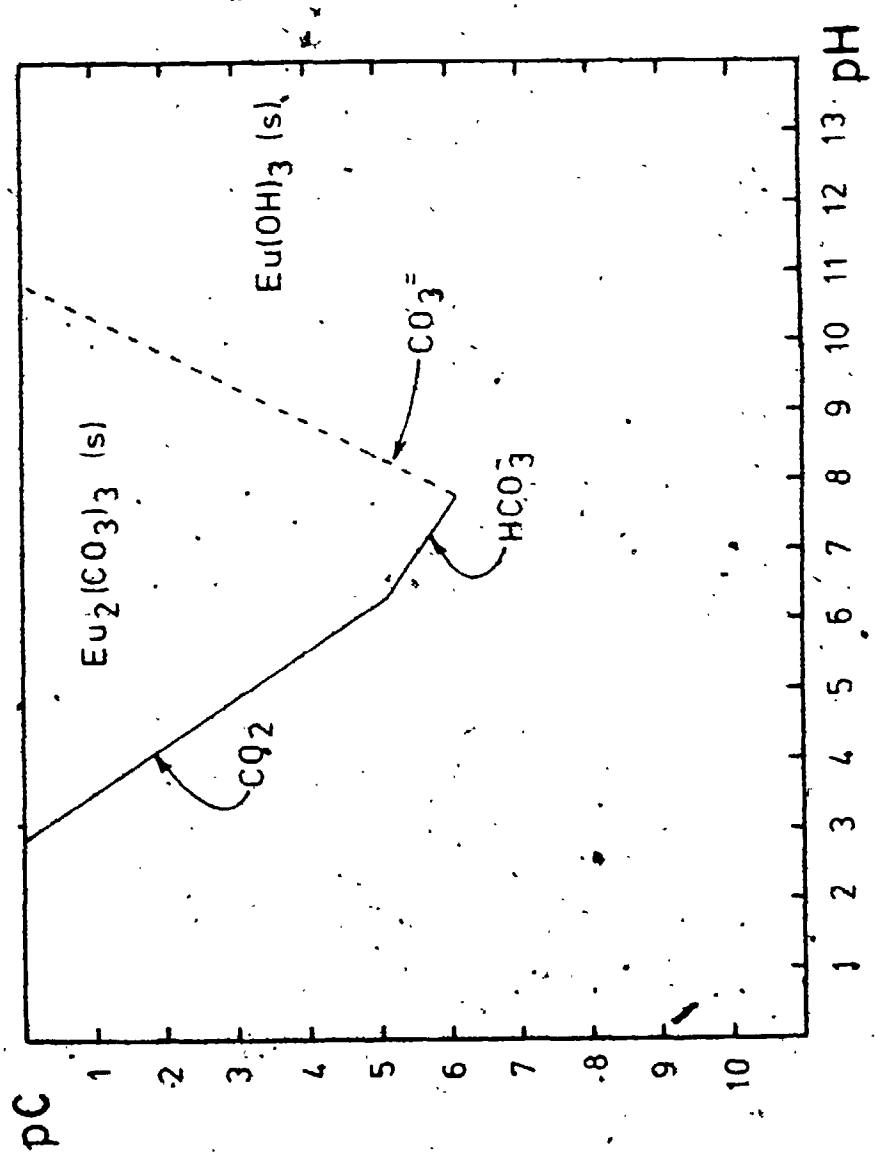

Figure 4.7 Stability diagram for $NdPO_4.xH_2O$ with a solubility product of $10^{-26.2}$. Note the importance of $Nd(OH)_3$ at pH's above 11. The solid line refers to total-phosphate concentration; the dotted line refers to total Nd^{3+} concentration, where it differs from that of total phosphate.

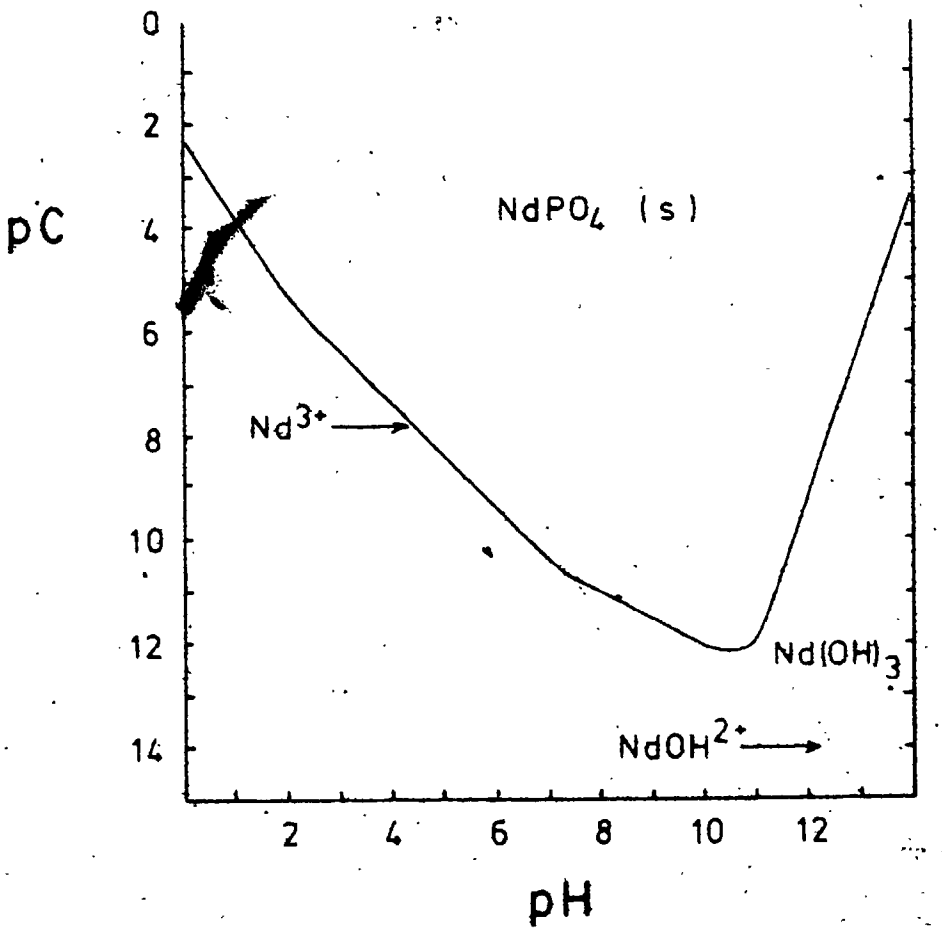

authigenic mineral lattices. Elderfield et. al.[33] also concluded that initially the REE are immobilized by surface reactions. In ferromanganese nodules the REE are bound initially by two sites: a phosphatic phase and a surface layer of phosphate which had previously been adsorbed onto hydrous iron oxides. Upon diagenesis the REE may be incorporated into recrystallized biogenic apatite. It is known the REE concentrations in marine apatite increase with the age of the sediment[36].

4.5.2 Calculations of REE Concentrations

The total dissolved phosphate concentration in recent marine sediments ranges from $1x10^6$ to $1x10^8$ pM[37,38]. From these values one should be able to predict the REE concentrations in interstitial water in sediments. If the reactions in sediments control seawater REE concentrations, then the sediment pore water concentrations are a useful guide to seawater concentrations. In calculating the La concentration, the ionic strength was taken as 0.7 M[39]. The activity coefficient of HPO_4^{2-} was calculated as in section 4.2 by the Davies equation. The La activity coefficient was interpolated from figure 4.7. Assuming for the sake of argument that ion-pair formation between La and HPO_4^{2-} is negligible, and that the concentration of HPO_4^{2-} is $1x10^7$ pM, then the predicted La concentration

is given by,

$$\log[La] = \log K^{o}_{sp} - \log K_3 - \log[HPO_4^{2-}] - \log \gamma_{HPO_4^{2-}} + \log(H^+) - \log \gamma_{La} \qquad (4.19)$$

where K_3 is the third dissociation constant of phosphoric acid. Substitution of values gives,

$$\log[La] = -24.5 + 12.35 + 7 + 0.49 - 8 + 1.62$$
$$= 9.0 \text{ pM}. \qquad (4.20)$$

The range in La concentration corresponding to the range in phosphate concentration is therefore 0.90 to 90 pM.

If ion-pair formation between Ca^{2+} and Mg^{2+} and HPO_4^{2-} is considered in the calculation, the free phosphate concentration will be reduced, and the calculated La concentration increased. Also, if complexation between La and other ligands is considered, the total La concentration will also be higher.

One way around the difficulty in estimating the free phosphate concentration is to write a reaction between La^{3+} and apatite[40],

$$3La^{3+} + Ca_5(PO_4)_3OH = 3LaPO_4 + 5Ca^{2+} + OH^- . \qquad (4.21)$$

The corresponding equilibrium constant for the reaction is given by,

$$\log K^{o}_{ap} - 3\log K^{o}_{rh} = 5\log(Ca) + \log(OH) - 3\log(La) \quad (4.22)$$

where $\log K^{o}_{ap} = -58.5$ is the log of the solubility product of apatite[41]., K^{o}_{rh} is the solubility product of La-RHABDOPHANE (table 4.4), the activity of Ca^{2+} in seawater is 0.0021 M[39] and the activity of the hydrogen ion is 1×10^{-8} M. Taking the activity coefficient of La^{3+} as 0.024, as was done previously, the calculated La concentration is 140 pM. The range in La concentrations corresponding to the range of pK^{o}_{rh} values, (i.e., plus or minus one standard deviation), is 68 to 300 pM. Estimates of several other REE concentrations are also listed in table 4.6. These are compared with values measured in open seawater by other workers. Note that these concentrations were calculated assuming no solution complexes with the REE ion. Also important was the use of solubility products valid at room temperature. Because the solubilities of hydrous REE phosphates increase with decreasing temperature, the estimates of REE concentrations given in table 4.6 are probably on the low side.

Table 4.6 Predicted and measured concentrations of La, Nd, Sm, Ho and Er in seawater.

REE	1 pM	2 pmol/kg	3 pmol/kg
La	68-300	44	15-82
Nd	5.6	----	3.0-10.7
Sm	9	----	2.8-7.9
Ho	110	----	1.2-2.7
Er	2: 300	9.9	----

1. This work.
2. Hoyle et al. (29).
3. DeBaar et al. (30).

4.5.3 Discussion

It is common practice in geochemical discussions to normalize the REE patterns obtained for a given geochemical system to either chondrite or average shale values. The chondrite values are taken to represent cosmic REE abundances, while the shale values are taken to represent crustal abundances[42,43]. Any chemical differentiation that has taken place in the system of interest can thus be separated from global abundance variations among REE due to nucleosynthesis effects. One such effect is the Oddo-Harkins rule[43] which basically states that even-numbered elements have a greater cosmic abundance than odd-numbered elements. This zig-zag pattern for which the normalization is intented to correct, is not expected to depend in any way on the crystal-chemical or thermodynamic properties of the REE. In other words, if the REE are saturated in seawater, and if they are in dynamic equilibrium with the sediments, then the non-normalized REE pattern for seawater is not expected to show the familiar zig-zag pattern. Seawater concentration data from Hoyle et al.[29], DeBaar et al.[30] and Elderfield et al.[33] all suggest a zig-zag pattern in seawater REE concentrations.

The conclusion to be drawn is that the REE are in fact undersaturated in seawater with respect to the less stable REE-containing phases. The concentration data given in

table 4.6 suggests that seawater is undersaturated in REE even with respect to the hydrous REE phosphates, to the extent that the calculations are reliable. It is not inconceivable that the monazite form of REE phosphates is less soluble than the rhabdophane form.

In any case, if a steady-state exists in seawater such that the rate of dissolution of metastable REE-phases is equal to the rate of precipitation of stable REE-phases such as monazite then the seawater concentration of a particular REE will reflect the abundance of that REE in the dissolving host phases. The more abundant a REE is in a dissolving phase, the more rapid will be its relative transfer to the solution phase, and consequently the higher the steady-state concentration of that REE will be.

Calculations of residence times of the REE, based on the assumption of steady-state kinetics, have been made. Goldberg et al.[31] found that the elements La to Gd, except Ce, have residence times of about 300 years. The elements Ho to Lu have residence times of about 500 years. (The residence time is the concentration of a chemical species in a system divided by its rate of removal or rate of introduction).

A further complication is the fact that the dissolved REE are enriched in the heavy fraction[43]. This may be due to the fact that the HREE phosphates are more soluble

than the LREE phosphates. The solubility data obtained in this study does not support this hypothesis, however. An alternative hypothesis is that the HREE form complexes with dissolved organic matter which are more stable than those of the LREE. The REE/EDTA complexation data presented in chapter 1 does support this hypothesis if EDTA is a good model for dissolved marine organic matter. LuEDTA is 5 orders of magnitude more stable than LaEDTA. The longer residence times of the HREE also support the hypothesis.

Additional evidence for the partial control of seawater REE concentrations by REE phosphates is the fact that the dissolved REE concentrations in seawater increase with depth.[30] It was shown in section 4.3 that the solubilities of REE phosphates should increase with a decrease in temperature. Though there are local fluctuations in temperature in the oceans, in general, the temperature decreases with increasing depth. Thus the increase in REE concentration with depth in seawater is explained by postulating the existence of a REE-containing phase with a positive enthalpy of formation in seawater, (such as a REE phosphate).

Thus the hydrous and/or anhydrous REE phosphates are important in helping to understand the REE concentrations in seawater. However, the connection between the hydrous and anhydrous forms is not yet clear. The synthesis studies carried out in this study suggest that in acid solution

at room temperature, the hydrous REE phosphates are usually formed. Monazite can form at somewhat higher temperatures. It is not clear whether the rhabdophane/ monazite boundary is affected by other variables such as pH. The pH of seawater is somewhat higher than that used in the syntheses. Many examples exist in marine geochemistry of phase relations complicated by kinetic factors. A good example is the relation between opal and quartz. Biogenic and inorganically precipitated opal are much more common in marine sediments, as well as subaerial soils, than is authigenic quartz, though quartz is clearly the more stable phase. Indeed, many natural waters are supersaturated with respect to quartz.

The problem could be resolved by obtaining solubility products for the anhydrous REE phosphates. Unfortunately, these data could not be obtained by the methods employed in this study. Also of interest, but much more difficult to obtain, would be data of rhabdophane : monazite ratios in marine sediments as a function of time.

REFERENCES FOR CHAPTER 4

1. Woyski M.M. and R.E. Harris (1963) IN Treatise on Analytical Chemistry, Part II, Vol. 8, Eds. I.M. Kolthoff, P.J. Elving and E.B. Sandell. Interscience.
2. Carnall W.T. (1979) IN Handbook on the Physics and Chemistry of Rare Earths, Vol. 24. Eds. K.A. Gschneidner Jr. and L. Eyring. North-Holland Publ.
3. Hessler J.P. and W.T. Carnall (1980) IN ACS Symposium Series 131: Lanthanide and Actinide Chemistry and Spectroscopy. Ed. N.M. Edelstein. Amer. Chem. Soc.
4. Piriou B. and D.-R. Svoronos (1985) J. Less-Comm. Met. 112, 275-285.
5. Judd B.R. (1962) Phys. Rev. 127, 750-761.
6. Ofelt G.S. (1962) J. Chem. Phys. 37, 511-520.
7. Morrison C.A. and R.P. Leavitt (1982) IN Handbook on the Physics and Chemistry of Rare Earths, Vol. 46. Eds. K.A. Gschneidner Jr. and L. Eyring. North-Holland Publishers.
8. Hüfner S. (1978) Optical Spectra of Transparent Rare Earth Compounds. Academic Press.
9. Wybourne B.G. (1965) Spectroscopic Properties of Rare Earths. Interscience Publishers.
10. Caro P., O.K. Moune, E. Antic-Fidancev and M. Lemaitre-Blaise (1985) J. Less-Comm. Met. 112, 153-173.
11. Seminara A. and A. Musemeci (1984) Inorg. Chim. Acta 95, 291-307.

12. Carlson E.H. and G.H. Dieke (1961) J. Chem. Phys. 34, 1602-1609.

13. Crosswhite H.M., H. Crosswhite, F.W. Kaseta and R. Sarup (1976) J. Chem. Phys. 64, 1981-1985.

14. Davies C.W. (1962) Ion Association. Butterworths.

15. Rard J.A., D.C. Miller and F.H. Spedding (1979) J. Chem. Eng. Data 24, 348-354.

16. Spedding F.H., H.O. Weber, V.W. Saeger, H.H. Petheram J.A. Rard and A. Habenschuss (1976) J. Chem. Eng. Data 21, 341-360.

17. Spedding F.H., P.E. Porter and J.M. Wright (1952) J. Amer. Chem. Soc. 74, 2781-2783.

18. Weast R.C. (Ed.) (1983) CRC Handbook of Chemistry and Physics. 64th Ed. CRC Press, Inc.

19. Harned H.S. and B.B. Owen (1958) The Physical Chemistry of Electrolyte Solutions. 3rd Ed.

20. Robinson R.A. and R.H. Stokes (1958) Electrolyte Solutions. 2nd Ed. Butterworths.

21. Mesmer R.E. and C.F. Baes Jr. (1974) J. Solution Chem. 3, 307-322.

22. Marshall W.L. and E.U. Frank (1981) J. Phys. Chem. Ref. Data 10, 295-304.

23. Rao V.K., C.J. Shahani and C.L.Rao (1970) Radiochim. Acta 14, 31-34.

24. Tananaev I.V. and V.P. Vasil'eva (1963) Russ. J. Inorg. Chem. 8, 555-558.

25. Lasaga A.C.(1981) IN Reviews in Mineralogy Vol. 8: Kinetics of Geochemical Processes Eds. A.C. Lasaga and R.J. Kirkpatrick. Mineralogical Society of America.

26. Petrovich R. (1981) Geochim. Cosmochim. Acta 45, 1665-1674.

27. Petrovich R. (1981) Geochim. Cosmochim. Acta 45, 1675-1686.

28. Tole M.P. (1985) Geochim. Cosmochim. Acta 49, 453-458.

29. Hoyle J., H. Elderfield, A. Gledhill and M. Greaves (1984) Geochim. Cosmochim. Acta 48, 143-149.

30. DeBaar H.J.W., M.P. Bacon and P.G. Brewer (1983) Nature 301, 324-327.

31. Goldberg E.D., M. Koide, R.A. Schmitt and R.H. Smith (1963) J. Geophys. Res. 68, 4209-4217.

32. Schofield A. and L. Haskin (1964) Geochim. Cosmochim. Acta 28, 437-446.

33. Elderfield H., C.J. Hawkesworth, M.J. Greaves and S.E. Calvert (1981) Geochim. Cosmochim. Acta 45, 513-528.

34. Li Y. (1982) Geochim. Cosmochim. Acta 46, 1053-1060.

35. Turner D.R. and M. whitfield (1979) Nature 281, 468-469.

36. McArthur J.M., J.N. Walsh (1984/1985) Chem. Geol. 47, 191-220.

37. Sayles F.L., F.T. Manheim and L.S. Waterman (1973) Interstitial water studies on small core samples, Leg 15. IN Initial Reports of the Deep Sea Drilling Project 20 U.S. Government Printing Office, Washington, D.C.

38. Gieskes J.M. (1974) Interstitial water studies, Leg 25 IN Initial Reports of the Deep Sea Drilling Project 25, U.S. Government Printing Office, Washington, D.C.

39. Stumm W. and J.J. Morgan (1981) Aquatic Chemistry 2nd Ed. John Wiley and Sons.

40. Jonasson R.G. and H.W. Nesbitt (1983) Lanthanide and actinide solubilities in natural systems. Atomic Energy of Canada Limited, #TR-216, 215-220. (This is an unrestricted, unpublished report available from SDDO, CRNL-AECL).

41. McDowell H., T.M. Gregory and W.E. Brown (1977) J. Res. N.B.S. -A. Physics and Chemistry 81A, 273-281.

42. Gromet L.P., R.F. Dymek, L.A. Haskin and R.L. Korotev (1984) Geochim. Cosmochim. Acta 48, 2469-2482.

43. Piper D.Z. (1974) Chem. Geol. 14, 285-304.

5. SURFACE REACTIONS

5.1 Adsorption and Related Processes

In section 1.4, a definition of adsorption was given. In this section this definition will be further discussed in terms of processes which might be confused for adsorption. In particular, processes must be distinguished which result in irreversible immobilization of solution species, since such processes must be treated differently in geochemical models of waste transport, for example. The distinction between true adsorption and other surface reactions has been discussed previously[1-4], so the following discussion will be fairly gene[illegible].

Examples of surface reactions which might be confused for adsorption include:

1) liquid/liquid phase separation,
2) ion-exchange in substances with a permanent intrinsic electric charge, (i.e., sorption),
3) precipitation of new phases onto inert substrates,
4) precipitation onto soluble substrates, (herein called "incipient mineral replacement").
5) reaction of solution species with one or more components of the substrate to form new phases. The new phase could conceivably be isostructural with the substrate, in which case the new phase may not be distinguishable from the substrate by such techniques as XRD.

Many criteria exist for distinguishing such surface reactions.

SPECTRAL CHANGES ON ADSORPTION: Changes in the vibrational and electronic spectra of a chemical species are expected to occur upon adsorption, when the adsorption process involves the strong distortion ~~or breaking~~ of bonds.

Good examples of this are provided by the study of gases on metal surfaces. In a review of electron energy loss spectroscopy, (EELS), Avouris and Demuth[25] point out, for example, the large changes in the vibrational spectra of CO when it is adsorbed onto various metal substrates. Interpretation of the spectra yields information about the strength and geometry of surface complexes. CO tends to be strongly bonded, while saturated hydrocarbons, for example, are not. EELS has also been used to study the electronic spectra of molecules on surfaces. Changes in the electronic transitions of aromatic hydrocarbons have been interpreted to suggest different orientations of the benzene ring with respect to the metal surface.

The situation with adsorption from aqueous solutions is not so well advanced. Goldberg et al.,[19] attempted to use IR spectroscopy to distinguish colloidal goethite adsorbed onto quartz, adsorbed onto kaolinite and as free particles. The results were inconclusive.

A familiar example of changes in the optical spectrum of adsorbed species is provided by the use of $CoCl_2$-charged silica-gel as moisture indicators. Unfortunately, the spectra of adsorbed species are rarely so easily observed.

time, but to be continually decreasing as the new layer contined to grow and hinder diffusion of reagents. The tell-tale of such processes is the presence of asyptotic tails in the rate/time curve.

REVERSIBILITY: Every chemistry undergraduate student who has been exposed to ion-exchange chromatography, knows that one does not add silver nitrate solution to a column charged with halide ion. This constitutes a good example of the difference between reversible and irreversible adsorption. Drastic measures are required in the case of precipitate formation, to reverse the "adsorption". The problem in the example is obvious. But it is often not clear in adsorption experiments why the adsorption is not reversible, or only partly reversible. As more and more drastic measures are taken to remove the adsorbate, the greater the chance that the substrate will dissolve first. The natural conclusion is that the "adsorbate" has reacted to form a phase more stable than the substrate.

An example of the use of reversibility in adsorption experiments is provided by Thornton and Renn[7], who measured the kinetics of release of some simple ions from a selection of surfaces, and concluded that the kinetics were too slow to be explained by simple diffusion.

A non-reversible adsorption of phosphate on iron oxides has been observed by Madrid and De Arambarra[8]. The fact

that the solubilities of ferric phosphates such as strengite ($FePO_4 \cdot 2H_2O$), are very low, ($pK_{sp} = 26.5$)[9] suggests that one might be dealing with similar crystalline phases on the iron oxide surfaces. Indeed, a very simple experiment involves the soaking of ordinary iron-rust in a solution of a phosphate such as KH_2PO_4 for several days. The pale yellow-brown coating that forms is identical in appearance to the material one gets on reacting ferric nitrate with aq. KH_2PO_4. (see section 2.3).

EXCHANGE CAPACITIES: If the measured surface area of a substrate turns out to be much less than that calculated on the basis of the amount of material lost from solution, then either multilayer adsorption or crystal growth of a new phase are likely explanations. Misra and Bowen[10] showed that in the reaction of zinc ions with hydroxyapatite the first layer of substrate should have reacted in the first few minutes. In fact, the solution concentration of zinc continued to decrease for more than ten days. (Powder x-ray diffraction showed that two new Zn-phosphate phases were in fact forming.)

In a study of the adsorption of various cations onto mica surfaces, Claesson et al.[11] found that whereas the adsorption of Na^+, Cs^+ and Ca^{2+} obeyed a simple site binding model, H_3O^+ did not. It seems likely to this author that excess H_3O^+ is being consumed during a dissolution reaction involving the mica substrate:

COMPETITION: If an adsorption model is designed to be general, as simple ion-exchange is, then the strength of adsorption will be a smooth function of some physical property of the ion, such as charge/radius ratio. The competition between ions for binding sites will depend only on the relative binding strengths and relative concentrations of the ions in question. If the exchange experiment shows that some ions are anomalously well adsorbed, that is beyond that indicated by their charge/radius ratio, then some additional adsorption process is occurring.

Alternatively, if a substrate seems to have an exceptional preference for certain ions, then another process must be assumed. For example, upon exposing crystals of aragonite, (orthorhombic $CaCO_3$), calcite (rhombohedral $CaCO_3$), dolomite (rhombohedral $CaMg(CO_3)_2$) and magnesite (rhombic $MgCO_3$) to synthetic seawater, Mucci and Morse[12] found that the surface Mg/Ca ratio depended very much on the nature of the substrate: Mg/Ca was smaller on aragonite than on calcite; the ratio was about 3 for dolomite, and about 120 for magnesite. These results suggest that the substrate is more than passively involved with the adsorption of Ca^{2+} and Mg^{2+}. The experiments imply a dynamic equilibrium between the surface and solution, in which crystal-packing forces favour appropriate substitutions of cations in the surface layer. In support of this interpretation, Möller and Sastri[13] showed using Ca-^{45}Ca

isotope exchange, that the equilibrium reaction involved no more than one layer of substrate. Interestingly, $SO_4^=$ and Cl^- ions had no appreciable effect on the exchange process,[14] which is consistent with a crystal growth mechanism.

SURFACE CHARGE MODIFICATION: One important method for studying the surfaces of particles is electrophoresis. The movement of suspended particles in an electric field is a function of the sign and magnitude of the effective surface charge of the particles. Changes in the surface charge as a function of pH are not surprising, in view of the fact that the adsorbates, H_3O^+ and OH^-, are charged species. Further, each mineral substance seems to possess a characteristic zero-point-of-charge. (The zero-point-of-charge is that pH for which the speed of the suspended particles is zero in the presence of an electric field). Such values have been tabulated for many substances[3]. Just as the pH of the solution is expected to change the surface charge, so is the presence of adsorbable ions. Thus the surface charge has been used as an important parameter in adsorption models[15-18].

The nature of the surface charge has been used in an explanation of the differences in the adsorption of colloidal goethite (α-FeOOH), onto quartz and kaolinite[19]. The fact that kaolinite has a permanent charge means that it can adsorb charged materials via coulombic forces over

a wider pH range than can quartz, whose surface charge is entirely pH-dependent.

INHIBITION OF SUBSTRATE CRYSTAL GROWTH: The fact that substances in solution can variously affect the growth of crystals is well known. The fact that this occurs by the formation of an adsorbed layer on the growing crystal faces, rather than by the formation of solution complexes with the reagent can also be shown. For example, Tomažič and Nancollas[20] studied the kinetics of precipitation of three hydrates of calcium oxalate, namely the mon-, di- and tri-hydrates. It was found that polyphosphate inhibited the formation of only the monohydrate phase, and not of the others. Somehow the surface geometry of the calcium oxalate monohydrate favoured the adsorption of the polyphosphate species.

The use of polyphosphonate and polyacrylate compounds as scale inhibitors in industry is routine. Such compounds can reduce the rates of formation of $CaSO_4 \cdot \frac{1}{2}H_2O$ and $CaSO_4$ at concentrations as low as 10^{-7} mol/L [21].

The ability of Mg^{2+} ions to markedly reduce the rates of precipitation of hydroxyapatite and fluoroapatite was interpreted in terms of the blocking of surface sites by Mg^{2+} [22].

HETEROGENEOUS CATALYSIS: There are many examples of redox reactions which are catalyzed by the presence of certain solid substances. For example, Keeney-Kennicutt and Morse[23] studied the reactions of PuO_2^+ on various substrates. On MnO_2 the plutonium was oxidized to Pu(VI); on goethite, a disproportionation occurred to form Pu(IV) and Pu(VI). Though the reactions seemed to depend on the nature of the substrate, it was noted that the reaction was faster in the light than in the dark. On carbonate minerals no redox reactions were observed. It is difficult to decide on the basis of the experimental data whether the reactions observed were truly catalytic, or whether the substrate was consumed in the redox reactions.

In a study of the adsorption of technetium, as TcO_4^-, on various minerals, Vandergraaf et al.,[24] found that immobilization of the technetium only occurred under reducing conditions in the presence of certain types of ferrous-iron containing minerals. Studies with iron metal were used as control experiments. The implication in this study was that the substrates favoring Tc immobilization were consumed in the redox reactions.

A reaction in which the substrate could truly be shown to act as a catalyst would be good evidence for adsorption processes involving the formation of inner-sphere complexes on the surface.

SPECTRAL CHANGES ON ADSORPTION: Changes in the vibrational and electronic spectra of a chemical species are expected to occur upon adsorption, when the adsorption process involves the strong distortion ~~or breaking~~ of bonds.

Good examples of this are provided by the study of gases on metal surfaces. In a review of electron energy loss spectroscopy, (EELS), Avouris and Demuth[25] point out, for example, the large changes in the vibrational spectra of CO when it is adsorbed onto various metal substrates. Interpretation of the spectra yields information about the strength and geometry of surface complexes. CO tends to be strongly bonded, while saturated hydrocarbons, for example, are not. EELS has also been used to study the electronic spectra of molecules on surfaces. Changes in the electronic transitions of aromatic hydrocarbons have been interpreted to suggest different orientations of the benzene ring with respect to the metal surface.

The situation with adsorption from aqueous solutions is not so well advanced. Goldberg et al.,[19] attempted to use IR spectroscopy to distinguish colloidal goethite adsorbed onto quartz, adsorbed onto kaolinite and as free particles. The results were inconclusive.

A familiar example of changes in the optical spectrum of adsorbed species is provided by the use of $CoCl_2$-charged silica-gel as moisture indicators. Unfortunately, the spectra of adsorbed species are rarely so easily observed.

Electron paramagnetic resonance (EPR) has recently been used to study the adsorption of Cu(II)/glycine complexes on gibbsite ($Al(OH)_3$) and boehmite (AlOOH). McBride[26] obtained ESR parameters for adsorbed Cu that were similar to those of free $Cu(gly)^+$. For the case of gibbsite, there was some evidence for a Cu-O-Al bond. On boehmite, the ESR spectrum was more similar to $Cu(gly)_2$. Excess glycine was found to desorb the Cu.

Motschi[27] studied the adsorption of Cu(II) aquo complexes on Al_2O_3, SiO_2 and TiO_2. He found the ESR spectrum for Cu on the various oxide surfaces to be considerably different from that of frozen $Cu(H_2O)_4^{2+}$. He pointed out however, that EPR on its own is insufficient for establishing an unequivocal assignment of the structure of the surface complex. The use of model compounds was found to be very important in the interpretation of the spectra.

Other forms of spectroscopy are potentially useful for studying the adsorption surface. X-ray photoelectron spectroscopy, (XPS), has been used in this regard[28] and in particular on mineral surfaces[29]. The chemical shifts obtained from XPS are large enough to yield clues of the oxidation state of a particular adsorbate [30]. They are not generally large enough to yield detailed bonding information.

NEW PHASES: The convincing evidence of surface reaction, as opposed to surface complexation, is the formation of new phases at or near the solid/solution interface. Scanning electron microscopy (SEM), might show up new crystallites[30] or amorphous agglomerations on the surface. Where the reaction has proceeded far enough, powder x-ray diffraction might indicate the presence of new crystalline phases. Misra and Bowen[10] showed that the products of reaction between hydroxyapatite and Zn^{2+} ions are hopeite ($Zn_3(PO_4)_2 \cdot 4H_2O$) and Zn-libethenite ($Zn_2(OH)PO_4$).

Clarke et al.,[31] found that Fe(II) salts react with calcite in oxidizing aqueous environments to produce crystalline Fe(III) oxides, (lepidocrocite). These results should not be surprising.

In those cases where insufficient material has accumulated, information about the surface distribution of new phases can give clues about the adsorption process. Ion-imaging by secondary ion mass spectrometry (SIMS) can yield surface element distributions on surfaces[32] when the sample is of sufficient size and shape, (i.e., flat) and the adsorbate concentration is high enough that it can be detected before it is etched away by the primary beam.)

Autoradiography is useful when dealing with low surface concentrations of radioactive elements. Knowledge of the components and their distribution in rock samples for example, can be used to rationalize the distribution

of radionuclides[33,34]. Adsorption was found to be greatest on mafic minerals, for the radionuclides ^{75}Se, ^{90}Sr, ^{137}Cs, ^{147}Pm and ^{241}Am. Adsorption was minimal on K- and plagioclase felspars, and negligible on quartz[34]. There was some evidence for precipitation of Am and Pm.

EXTRAPOLATION FROM SOLUTION CHEMISTRY: Because the surface layers in an adsorption experiment are so difficult to see and characterize, a great deal about the nature of the adsorption process must be inferred from other known reactions in solution.

Beall and Allard[33] and Stryker and Matijević[35] interpreted the adsorption of Am(III), Pu(IV) and Np(V), and Hf(IV), respectively, in terms of metal hydrolysis. The adsorption was measured as a function of pH, and then compared with the known hydrolysis behaviour of the metal ion in question. But whereas Beall and Allard interpreted the adsorption as essentially a precipitation reaction, (where other adsorption processes could be ruled out), Stryker and Matijević interpreted the results in terms of the adsorption of mononuclear $Hf(OH)_4$.

The other reactions referred to by Beall and Allard involved the reaction of metal ions with phosphate and carbonate minerals occurring in the substrate, to form insoluble precipitates. Knowledge of the insolubility of the various actinide salts lead to this interpretation of the radiography results.

5.2 Rationale for the Surface Reaction Experiments

The first objective in the following experiments was to discover whether adsorption-like reactions occur at all in the case of REE phosphates. The second objective was to discover the time scale for these reactions, so that detailed kinetics experiments could be planned at a later date. The third objective was to discover the process or processes involved with the adsorption reactions. A parallel objective, mentioned in chapter 1 was to evaluate surface analytical techniques, such as SIMS and XPS, for their ability to yield information about surface reactions.

As the introduction to this chapter shows, there are many processes which might be going on, and many ways of studying these processes. It was suspected that in the case of REE phosphates, dissolution might be important in determining or modifying the adsorption reactions. It was suspected that although the compounds were quite insoluble, the surfaces of the REE phosphate crystals would be, or tend to be, in dynamic equilibrium with the surrounding solution. This suggested that the adsorption process might take the form of an exchange reaction. Because mineral replacement reactions are common in nature, (indeed, some of the synthesis methods in this thesis work are replacement reactions), examples must also exist of <u>incipient</u> replacement reactions.

5.3 Introduction to SIMS Depth-Profiling

One of the surface analytical techniques evaluated for adsorption studies was SIMS depth-profiling. Section 3.1 of the thesis outlined the SIMS technique. In this section an introduction to depth-profiling will be given. Because SIMS is an inherently destructive technique, the sampling region changes with time, depending on the primary beam current, the nature of the sample, and the area sampled. Rastering reduces the rate at which the third dimension in the sample is analyzed. In any case by sampling a portion of the mass spectrum at regular intervals as the primary beam etches away at the sample, a record of the abundance of that particular isotope with depth is obtained.

There are experimental difficulties which limit the quality of information which can be gained, however. If the primary beam is not rastered across an area of the sample, the crater formed tends to be steep and narrow, allowing for a simultaneous sampling of the specimen all the way down the crater walls. Even if the beam is rastered, the primary beam tends to collide with atoms in the sample, knocking these atoms deeper into the sample, only to be sampled by the mass spectrometer at a later time in the analysis. Both these effects result in an averaging of the composition of the sample over the depth of the analysis.

The effects of "knock-on" are demonstrated in figure 5.1. Here the beam was rastered over an area of 250 by 250 μm. This sample happened to be gold-coated, and is therefore particularly good for demonstrating this effect. The carbon is an ubiquitous surface contaminant. Initially the signals due to Ho and C are seen to rise as the Au coating is penetrated. Thereafter, the signals due to C and Au continue to remain significantly above background, long after the Ho signal has stabilized. It would be difficult to estimate the thickness of the gold layer from this depth profile.

Another experimental problem is due to fluctuations in primary beam current. Figure 5.2 shows a record of the primary beam current for five minutes, obtained on the same day as was the depth profile. This day the beam current was fairly stable. A less stable beam can lead to severe artifacts in the depth profile.

An unfortunate aspect of the depth profiling procedure used in this study is that there is a considerable "dead" time when the profiling starts. Mass numbers must be sampled sequentially, which means that the material closest to the surface is etched away before its composition can be fully measured.

Surface roughness of the sample can also lead to problems. Fortunately, the crystals used in the subsequent studies had fairly flat crystal faces naturally.

Further information can be found in references 35 and 36.

Figure 5.1 Depth profile of $HoPO_4$ single crystal, showing the ability of the primary beam to knock Au and C from the surface layers into the bulk of the crystal. This effect severely limits the ability to estimate layer-thicknesses in SIMS.

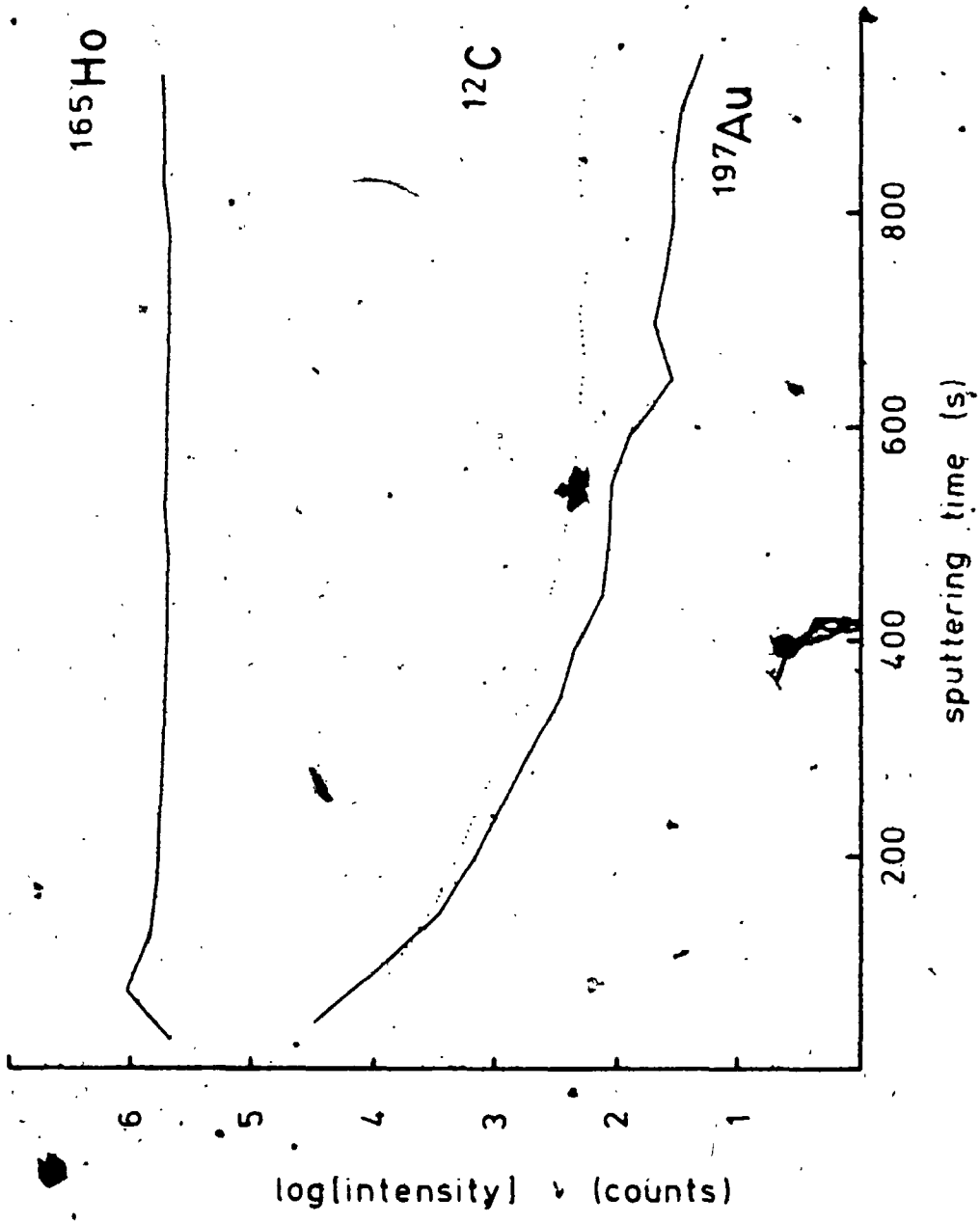

Figure 5.2 Record of primary beam stability for a beam of O^- ions. Maximum value: 90.16 nA; minimum: [illegible]; mean: 88.47. $\frac{\text{Max.} - \text{Min.}}{\text{Mean}} \times 100 = 1.081\ \%$.

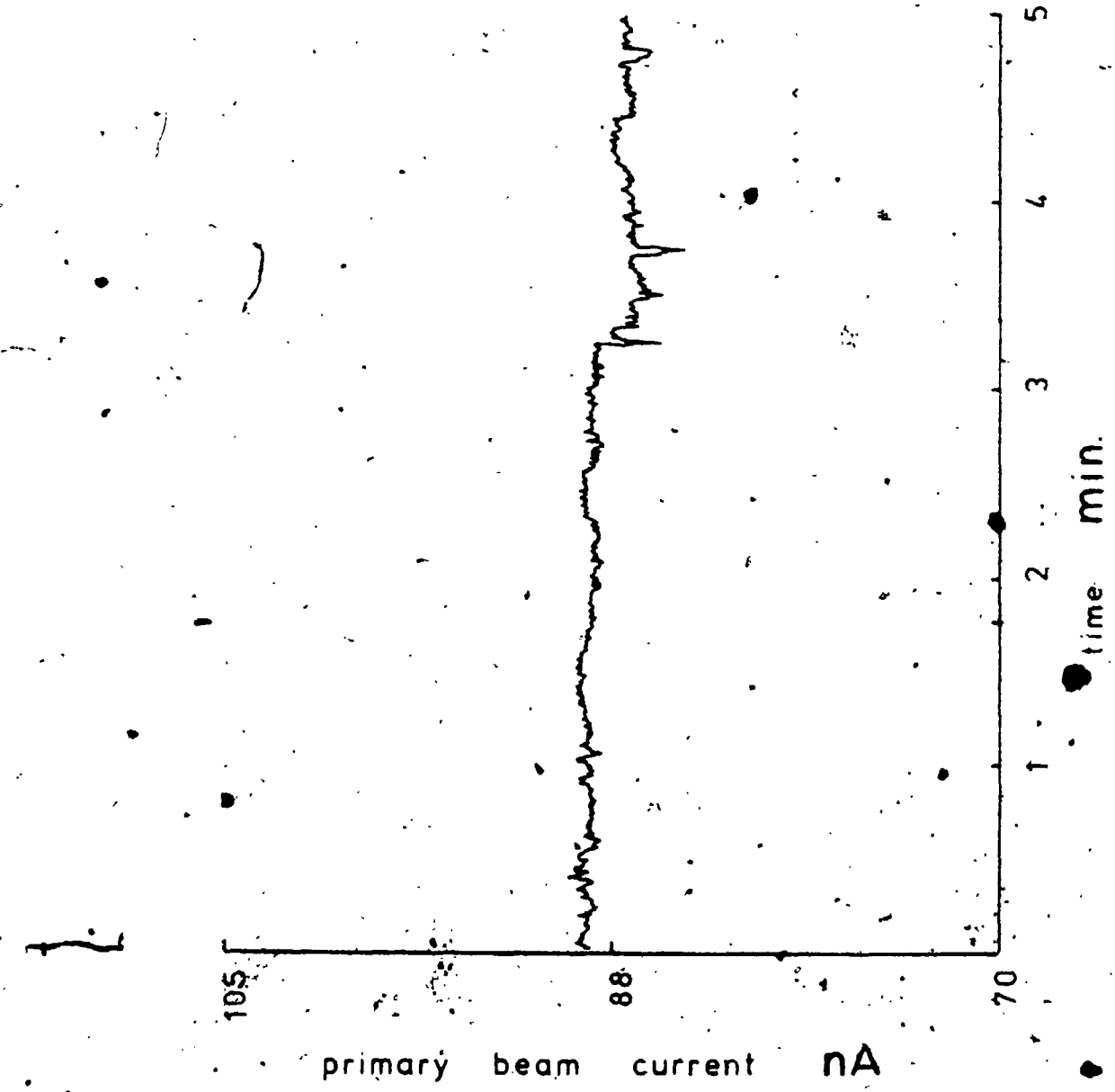

Table 3.3 Results of DTA, TGA (100° min⁻¹) and isochronal (1hr) heating for hydrated phosphates, $REEPO_4 \cdot xH_2O$.

REE	T_p(°C)	I	T_1	x	T_2	T_3	F
La	100	M	100,230	0.7	(a)	---	M
	25	R	100,230	1.6	(a)	500	M
Ce	100	M+R	80,200	0.6	700w	600	M
	60	R	100,250	1.0	715vw	600	M
Pr	100	R	120,250	0.7	(a)	700	M
Nd	100	R	100,230	0.7	790vw	700	M
	100	R	110,230	0.7	680vw	700	M
Sm	100	R	80,220	1.0	800m	700	M
Gd	100	R	210	0.8	815s	800	M
Dy	60	X+R	80,180	1.0	950w	900	X*
Ho	100	X	110	1.4	---	---	X
Er	100	X	110	0.8	---	---	X
Yb	100	X	65	1.1	---	---	X
Nat.	?	R+M	120,230	1.7	(a)	(b)	M

T_p = preparation temperature.
I = initial phase, (by powder XRD).
T_1 = endothermic peak temperature, ± 5°C.
T_2 = exothermic peak temperature, ± 50°C.
T_3 = isochronal heating experiments, ± 50°C.
F = final phase.
M = monazite; R = rhabdophane; X = xenotime
(a) = absent; (b) = not determined; vw = very weak;
w = weak; m = medium; s = strong.
X* = unique transformation: R to M to X at temperatures above 900°C.

5.4 X-Ray Photoelectron Spectroscopy, (XPS)

In XPS a beam of photons at a particular x-ray energy, (in this case Al K radiation was used), is interacted with a portion of the surface of a solid, and the energy distribution of the photoelectrons measured. Assuming no other processes occur during the photoelectric interaction, the difference between the energy of the incident photon and the kinetic energy of the emitted electron is the binding energy of the electron in a particular atomic orbital of a particular atom in the solid, (Koopmann's theorem). Molecular orbitals are generally more efficiently studied using UV-energy photons. Auger electrons are also seen in the energy spectrum, but can usually be quickly identified by their energy and the fact that Auger electron peaks are often much broader than photoelectron peaks.

Normally the valence electrons are not seen using XPS, but the 4f electrons of the REE are an exception. This effect is greatest for the later REE, since the cross-section for photoelectron emission increases sharply as the 4f shell is filled,[37]. This fact has allowed the valence shell in REE oxides to be modelled on the basis of XPS spectra,[38,39].

The strength of XPS lies in its ability to measure binding energies of core-level orbitals of atoms, however. This allows XPS to be used as an analytical tool for detecting major elements on surfaces, and for

estimating their concentrations through the use of known orbital cross-sections,[40]. Further, the core-level binding energies are not entirely insensitve to the chemical environment of the respective atom. Thus chemical shift data can yield information about the oxidation state of that atom. A problem with measuring chemical shifts is that non-conducting samples tend to become electrically charged during analysis, which tends to shift photoelectron peaks. Most of the XPS spectra obtained in this study were obtained using an electron flood-gun to help neutralize the charge. Further, because carbon is always present on the surface, other peaks in the spectrum can be related to the C 1s peak.

In this study, the principal use of XPS will be to identify elements on the specimen surface, and to gain a rough estimate of the element's concentration in the upper few atomic layers of the specimen. All XPS spectra reported here were obtained on a Surface Science Laboratories SSX-100 ESCA Specrometer.

5.5 Reaction of $PrCl_3$ with Apatite, $Ca_5(PO_4)_3(F,OH)$

In chapter 4 reactions were written between dissolved REE ions and apatite in order to estimate seawater REE concentrations. In order to test whether in fact such a reaction proceeds, a sample of clear green fluoro-apatite was reacted with a solution of 0.05 M $PrCl_3$ at 100° C for two weeks. The apatite block was then removed, washed with deionized water and dried at 80° C for four days. Figure 5.3 shows a broadscan XPS spectrum of the apatite surface after exposure. Peaks with binding energies characteristic of F, P, O and Pr were all found, but those of Ca were all lower than the background signal. The spectrum of unreacted apatite was also run for control. The results suggest that the surface layer is at least the thickness corresponding to the sampling depth of the instrument, (5-10 atomic layers), in the case of reacted apatite. The results are also consistent with those of the Zn/apatite experiments mentioned in section 5.1.

The exact nature of the surface layer of Pr/apatite is not clear from this experiment, however. A subsequent reaction was therefore carried out between a REE salt solution and commercial bone meal, (fine-grained hydroxy-apatite).

Figure 5.3 Broadscan XPS spectrum of the surface of apatite, $Ca_5(PO_4)_3(F,OH)$ which had been reacted with an aqueous solution of 0.05 M $PrCl_3$ at 100° C for two weeks. The expected position of a Ca peak is indicated.

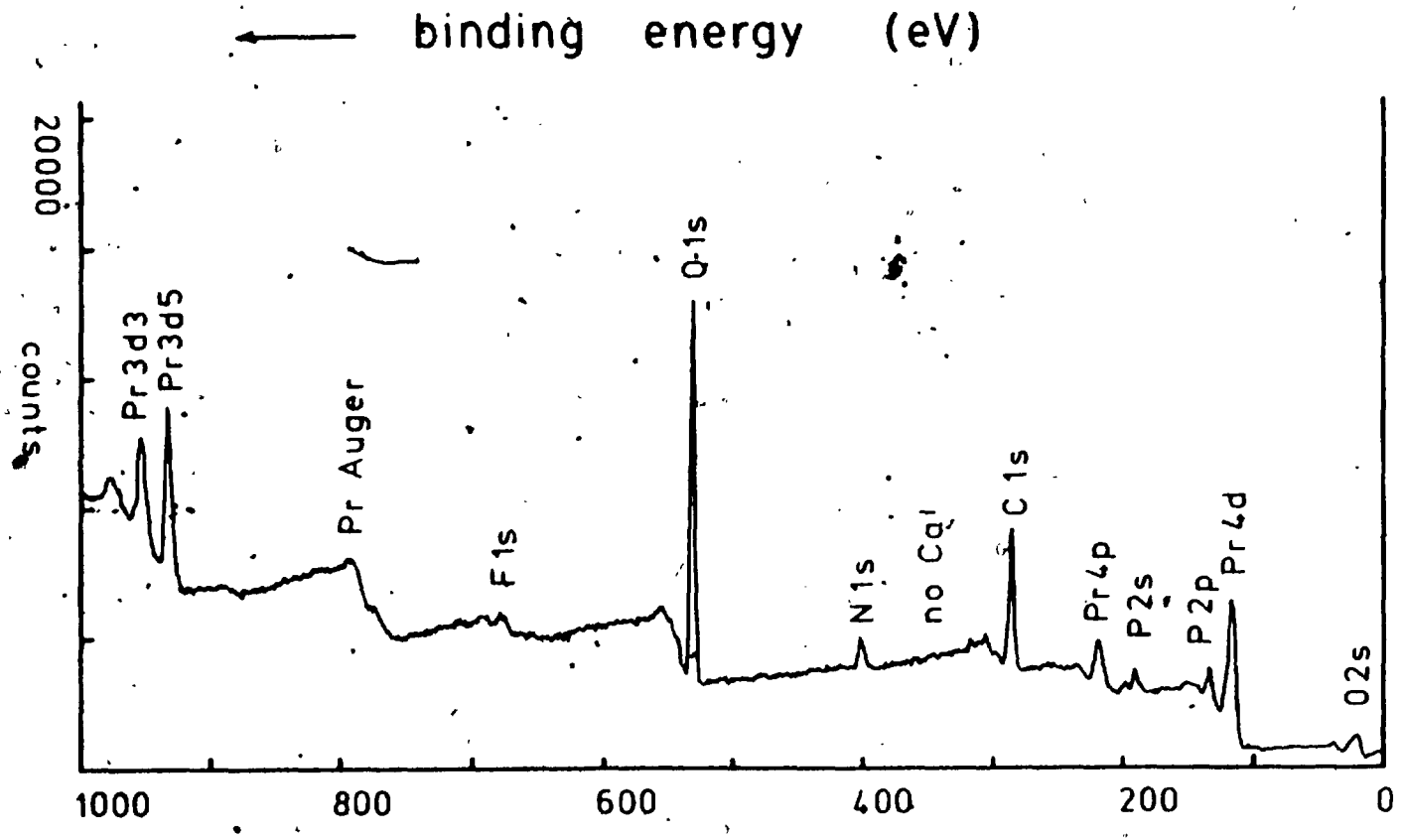

5.6 Reaction of $NdCl_3$ Solution with Bone Meal

The commercial bone meal was shown by XRD to consist largely of poorly crystallized apatite. A suspension of the bone meal was prepared by mixing 1 g of the material with 60 mL of a solution of 0.1 M $NdCl_3$ and 1.0 M NH_4Cl. The bone meal was wetted initially with a few drops of methanol. The NH_4Cl was added to control the pH. The solution was sampled from time to time and analyzed by spectrophotometry for the Nd concentration after filtration through 0.45 μm Millipore filters. After analysis the solution was returned to the reaction flask to maintain a constant solid/solution ratio. The Nd concentration dropped to 0.08 M after three days, and remained at that value for the duration of the experiment. The pH of the solution dropped from 4.8 to 4.5 during this period. After 130 days the solution was filtered and the residue washed with deionized water. The dried powder was analyzed by powder XRD, and shown to contain significant amounts of poorly crystallized rhabdophane.

These results supplement the previous surface reaction results in that they show the dissolved REE ions react with apatite to form new phases.

5.7 The $Nd^{3+}/HoPO_4 \cdot xH_2O$ and $Ho^{3+}/NdPO_4 \cdot xH_2O$ Exchange Reaction Experiments

In this experiment, two solutions were made up consisting of 0.15 M NH_4Cl + 0.025 M $NdCl_3$ and 0.15 M NH_4Cl + 0.025 M $HoCl_3$ which were then allowed to react with Ho-XENOTIME and Nd-RHABDOPHANE, respectively. The NH_4Cl was added to keep the pH around 4.2. It was intended that the pH of each solution would be the same. It later turned out that the pH of the $Nd^{3+}/HoPO_4 \cdot xH_2O$ system was 2.3. For this reason the experiments are not directly comparable. But the results are non-the-less interesting.

The solution composition was monitored by visible spectrophotometry for close to two years. For seven months, no evidence that the REE in the solid phase was dissolving, in either experiment, was found. After 13½ months, the Ho^{3+} concentration in the first system had increased from below the detection limit to 0.002 M. The use of ESCA showed the presence of Nd in the $HoPO_4$ solid.

In the complimentary system, no trace of Nd^{3+} could be found in the solution phase, and no trace of Ho could be seen in the ESCA spectrum of the $NdPO_4$ solid.

After 18 months, the Ho^{3+} concentration in the first solution was still 0.002 M; the Nd^{3+} concentration in the second solution was still below the detection limit.

After 19 months the powders were again filtered off, washed and analyzed by powder x-ray diffraction. The diffraction pattern of the first powder contained peaks characteristic of rhabdophane, in addition to those of the expected xenotime. The diffraction pattern of the second powder was entirely that of rhabdophane, suggesting that only the original Nd-RHABDOPHANE was present.

In the absence of powder diffraction data, one might have concluded from the ESCA data and solution data that adsorption of Nd^{3+} onto $HoPO_4 \cdot xH_2O$ had occurred, and that some of the substrate had dissolved. The presence of diffraction peaks characteristic of rhabdophane in the diffraction pattern of $HoPO_4 \cdot xH_2O$ proves that the substrate had reacted with Nd^{3+} to form a new phase.

Unfortunately, because the pH's of the two solutions were different, one cannot conclude from these experiments that Nd-RHABDOPHANE is less soluble than Ho-XENOTIME. However, the experiment done more carefully would provide a more reliable ordering of solubility products for pairs of REE phosphates, than the values of the solubility products themselves. (Recall the variation of solubility product values for Nd-RHABDOPHANE for example).

The other conclusion to be drawn from these experiments is that these exchange reactions are quite slow, so that if the experiments had been terminated after a couple of months one would have erroneously concluded that the REE hydrous phosphates are kinetically inert.

Figure 5.9 Depth profile of $LuPO_4$ crystal reacted with 0.005 M $ErCl_3$ for 12 months. (The slightly different appearance of the curves reflects a different data plotting program.)

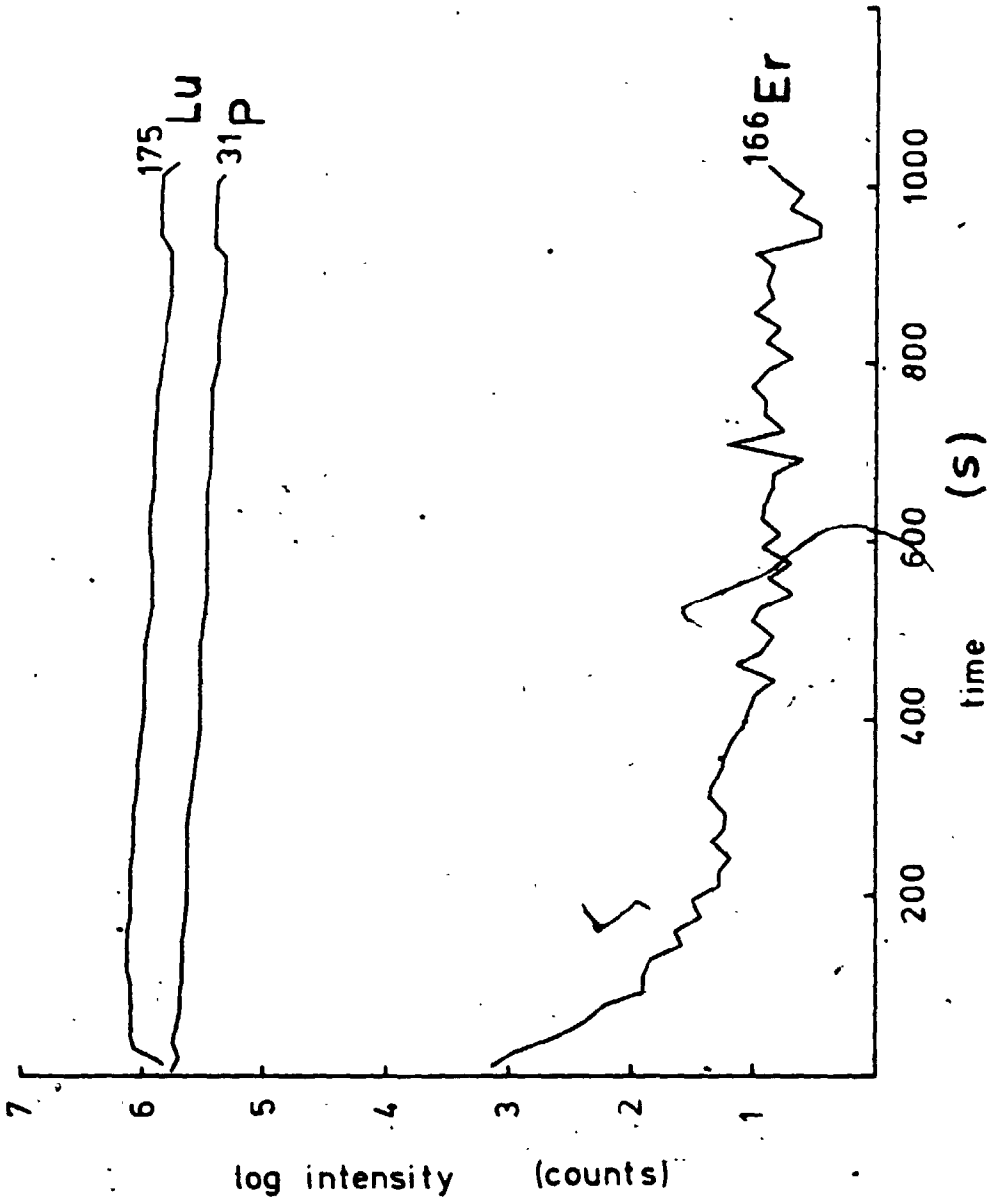

5.8 Exchange Reactions with $LuPO_4$ Single Crystals

The $LuPO_4$ crystals were a convenient substrate for carrying out surface reactions. First a large number were available with smooth, flat crystal faces. Second, the cross-section of 4f electrons in Lu are particularly high, and the peak positions uniquely located at very low binding energies. This allowed the presence of Lu in the spectrum to be easily detected.

In the first two experiments $LuPO_4$ crystals were reacted with 0.0075 M YCl_3 solution at 25° C for 31 months at pH's of 3.2 and 5.5, respectively. The XPS spectra are given in figures 5.5 and 5.6. In both spectra several peaks characteristic of Y are present. The Y:Lu ratios estimated from the two spectra, using known cross-sections for the relevant peaks, are 1:1 and 1:5 for pH's 3.2 and 5.5 respectively. Though the errors associated with the concentration estimates are not small, (10-20%), the ratios are different enough that the difference is significant. Even a visual examination of the relative heights of the P 2p and Y 3d peaks in the two spectra proves a significant relative difference in Y concentration.

These results are at variance with results of other adsorption experiments, which typically show an increase[3] of adsorption with increasing pH. The effect observed in

Figure 5.5 XPS spectrum of Y on $LuPO_4$ (single crystal). Concentration of Y = 0.0075 M; pH = 3.2. Reaction time 31 months; temperature 25° C.

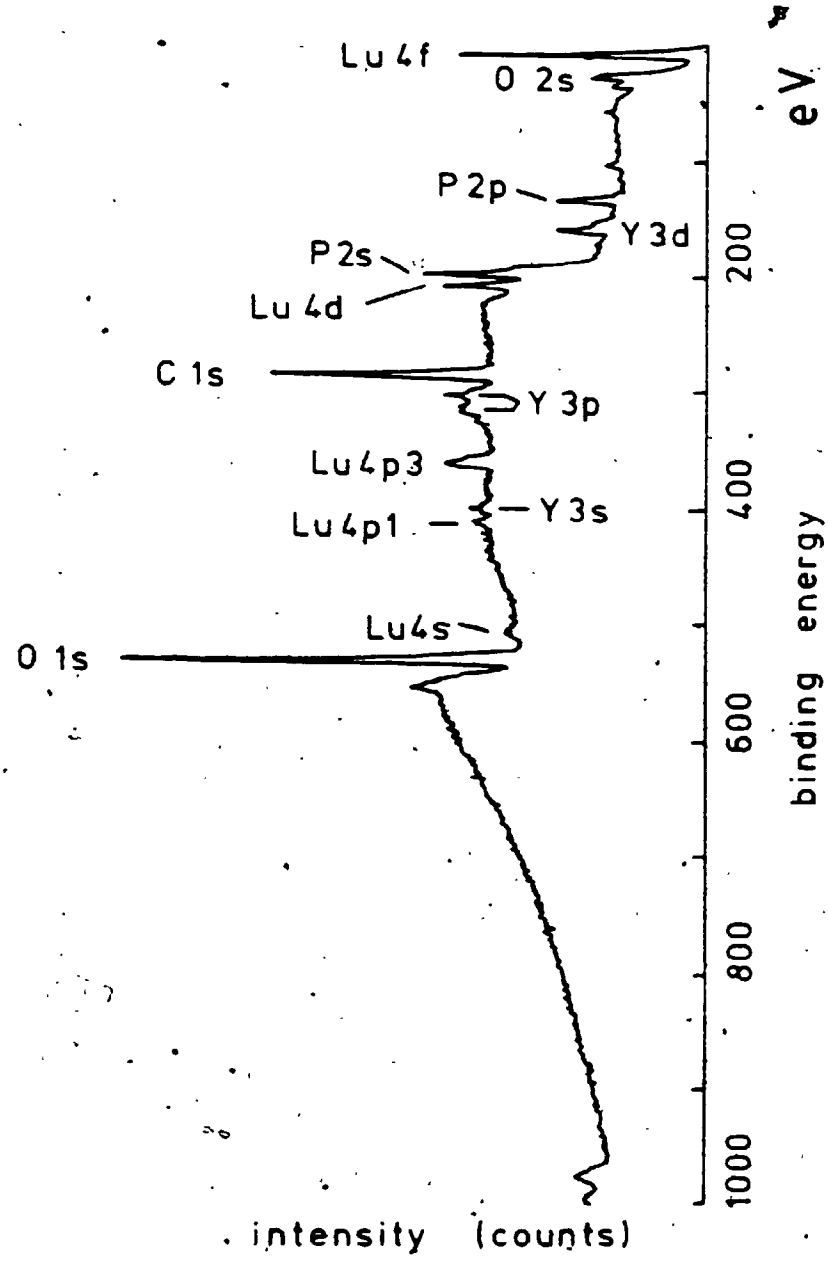

Figure 5.6 XPS spectrum of Y on $LuPO_4$.
Concentration Y = 0.0075 N; pH = 5.5. Reaction time 31 months; temperature 25° C.

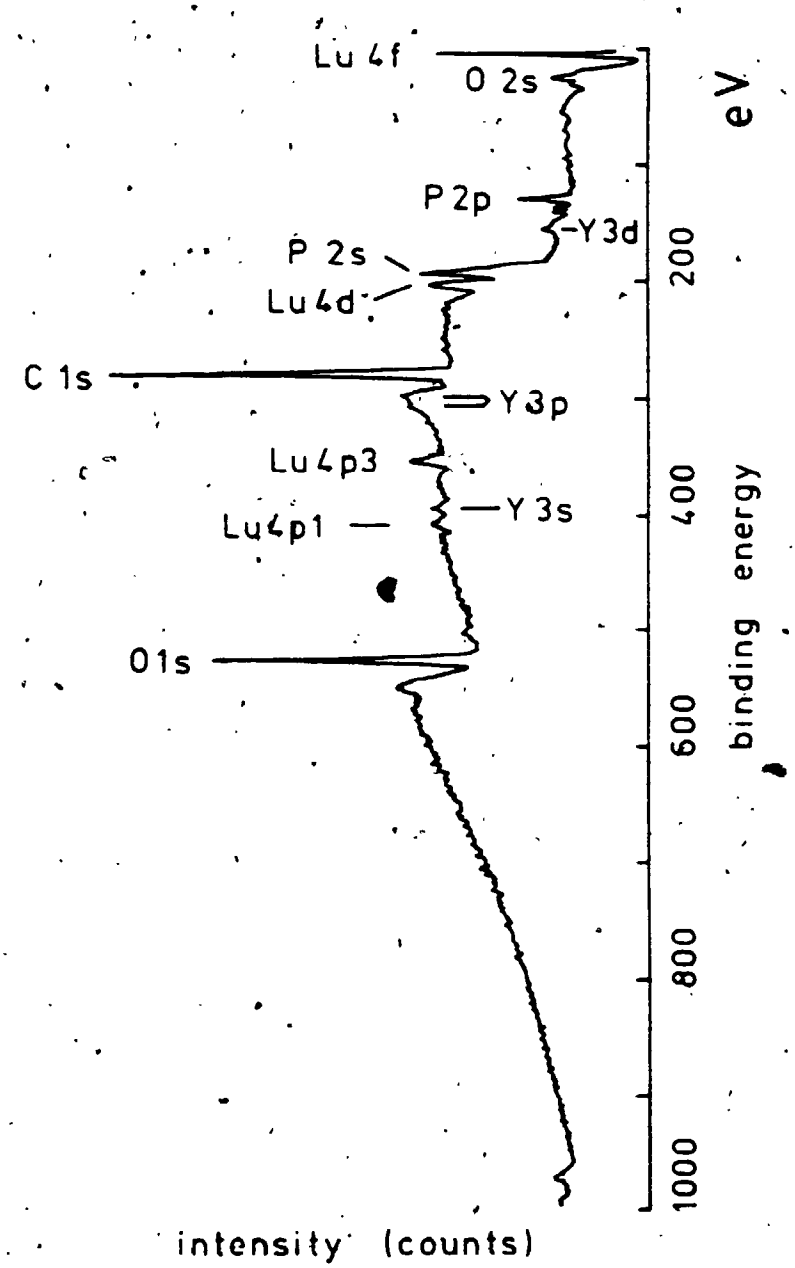

the above two experiments is consistent with a dissolution precipitation or surface-exchange process, in which the extent of exchange at a certain point in the reaction depends on the solubility of the substrate. Since the solubility of REE phosphates increases with decreasing pH, the extent of surface exchange also increases with decreasing pH.

In the next experiment involving $LuPO_4$ crystals, a dozen $LuPO_4$ crystals were placed in a solution of composition 0.01 M HNO_3, 0.1 M KCl and 0.005 M $ErCl_3$. The crystals were allowed to react at room temperature. At certain intervals, one of the crystals would be removed, washed with deionized water, dried and stored for surface analysis. It was hoped that kinetics data could be obtained in this way.

Five crystals were removed over a period of 47 days, and examined by XPS. No evidence of Er on the surface was found. However the fifth crystal was studied by SIMS depth profiling. The results are shown in figure 5.7. It would appear that the surface of the $LuPO_4$ crystal was enriched with Er by as much as two orders of magnitude in concentration, with respect to bulk concentrations. As a control experiment, a depth profile of unreacted $LuPO_4$ was also obtained. This is shown in figure 5.8. The bulk concentrations of Er in the two crystals agree, within error.

Figure 5.7 SIMS depth profile of a $LuPO_4$ crystal soaked in 0.005 M $ErCl_3$ for ~7 days. (Without rastering of primary beam).

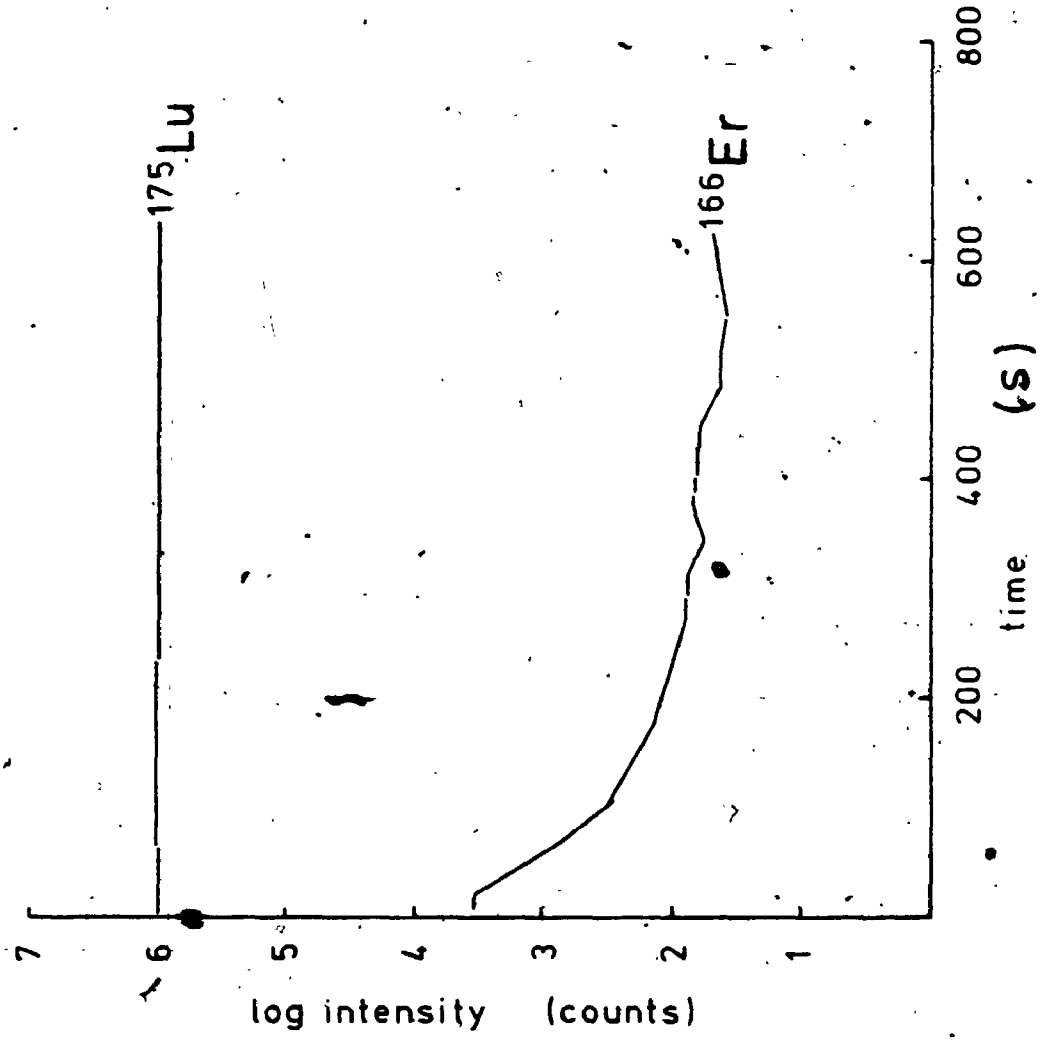

Figure 5.8 SIMS depth profile of unreacted $LuPO_4$ crystal.

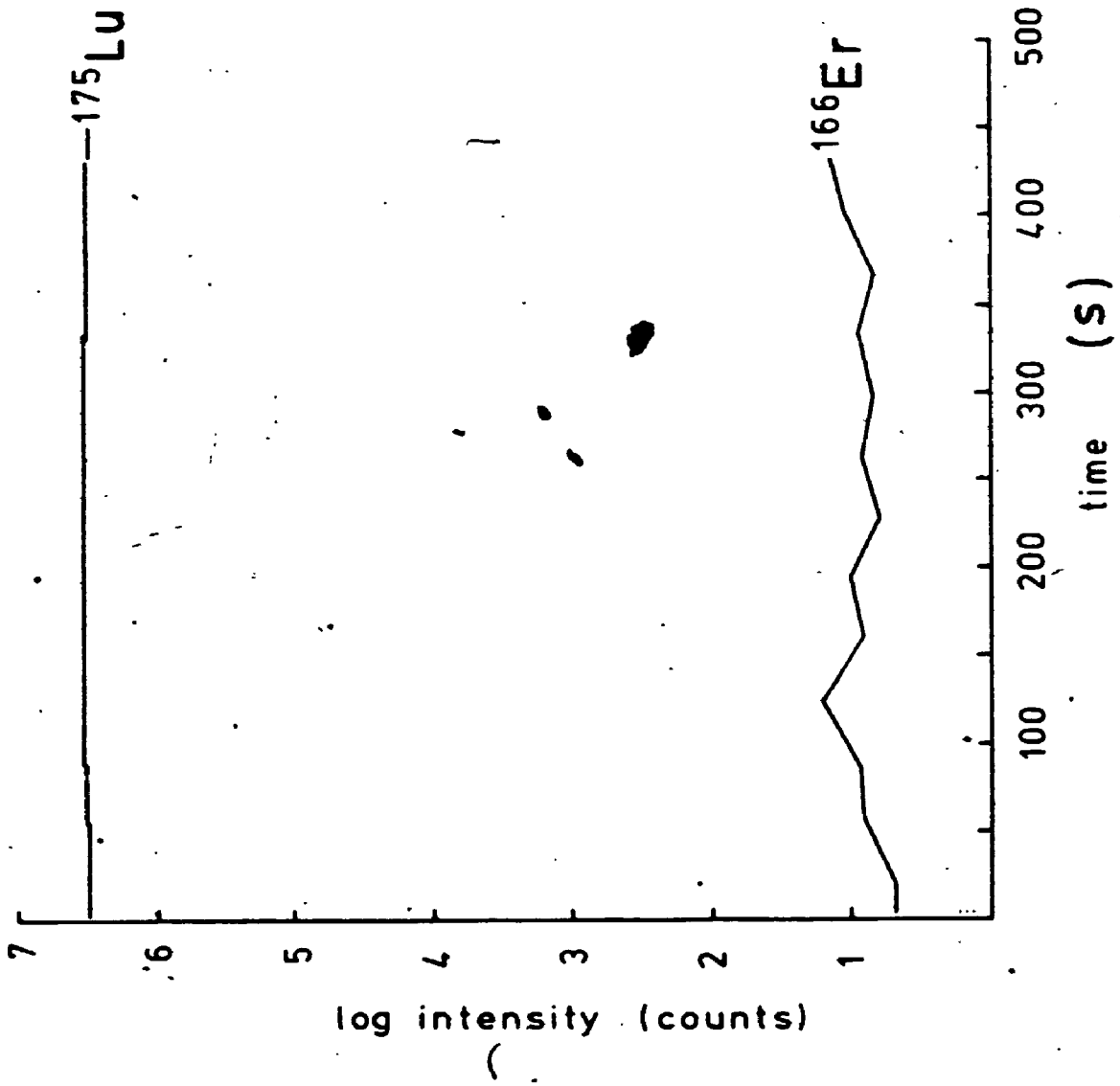

Figure 5.9 Depth profile of $LuPO_4$ crystal reacted with 0.005 M $ErCl_3$ for 12 months. (The slightly different appearance of the curves reflects a different data plotting program.)

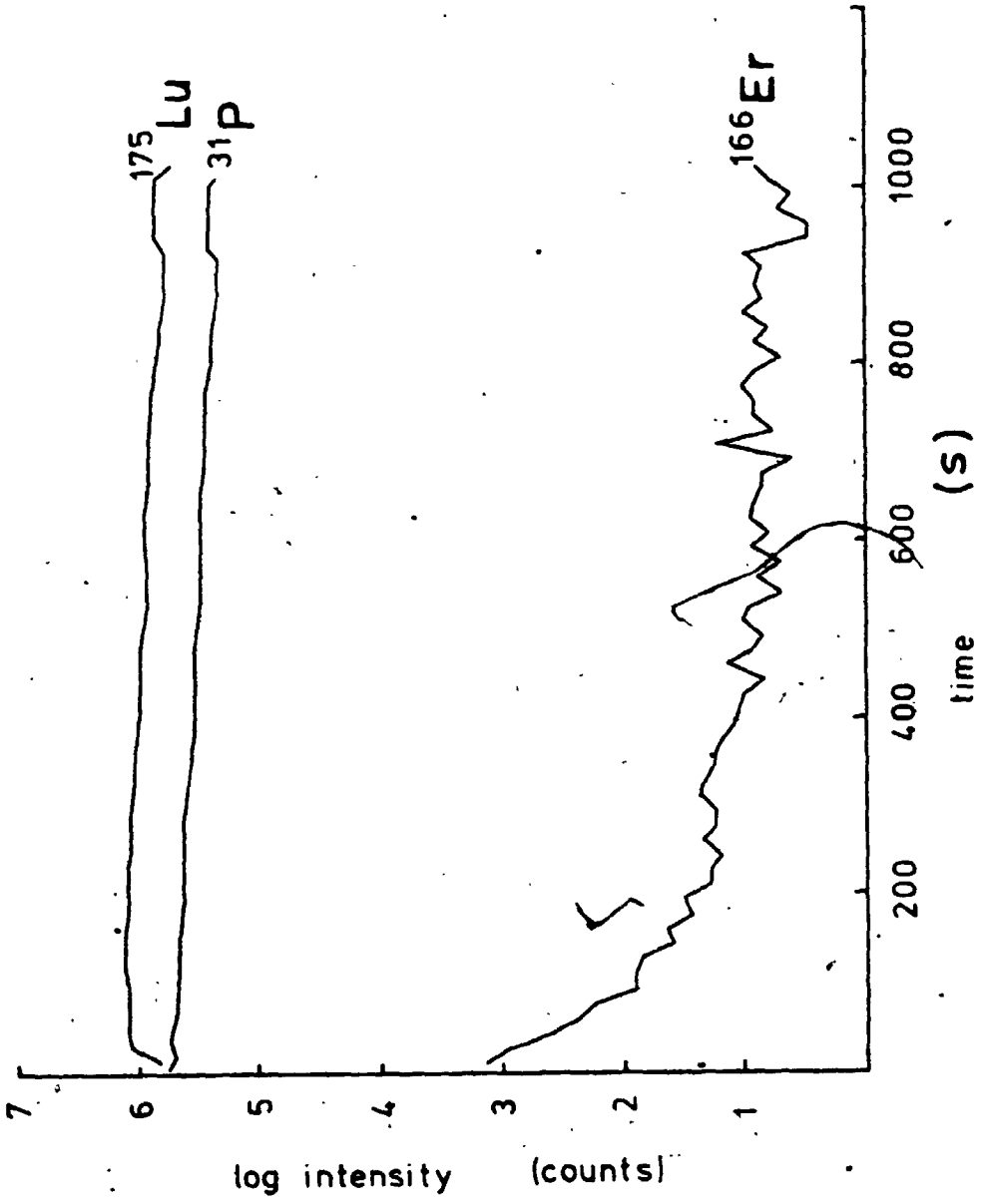

Thus it seemed that SIMS depth profiling would be a more sensitve surface analytical technique than XPS. However, when a crystal was analyzed by SIMS which had been reacted for 12 months, the surface concentration of Er was not higher than that of the previous sample. Comparison of the Er:Lu ratio for figures 5.7 and 5.9 shows that in fact the Eu:Lu ratio for the 12-month crystal is lower than that of the 47-day crystal.

It was difficult to decide whether the difference was real, or an artifact of the SIMS method. Replicate depth profiles obtained for several regions of the same crystal agreed with each other, in terms of the Er:Lu ratio. (Absolute ion-intensities vary from one run to the next).

The SIMS results did explain why XPS failed to detect any Er on the 47-day crystal. The maximum Er:Lu ratio obtained by SIMS was 0.004, or 4 ppt. Because the signal to noise ratio in XPS rarely exceeds 20 for the REE, the Er would have to be present in percent quantities on the surface, even to be detected.

When a 17-month crystal was analyzed by XPS, only a hint of Er was detected: the intensities in the energy regions characteristic of Er were no more than twice background.

The principal objective of the experiment was not realized, namely to obtain quantitative kinetics data. The reason was, of course, that the surface analytical

tools, namely XPS and SIMS, were being evualuated at the same time as they were being used to obtain analytical results on surfaces.

Lesser objectives were realized, however. Er was shown to adsorb on or react with $LuPO_4$ surfaces, but at a slow rate. SIMS depth profiling is a sensitve tool for surface studies, but needs much optimization and further study before quantitative results can be obtained, at least in the case of REE phosphates. XPS can yield semi-quantitative results, if the surface species are present in percent quantities.

5.9 Single Crystal Mutual Exchange Studies

The previous experiments had supported the hypothesis that adsorption reactions involving REE and phosphate at reduced pH's, involve surface reactions in which the substrate dissolves to some degree, allowing foreign species to get caught up in the dissolution/precipitation reactions at the surface. The next step was therefore to demonstrate that these reactions are driven by thermodynamic forces. Specifically, it had to be shown that given two experiments, one involving the reaction of REE "a" with a phosphate of REE "b", the other involving REE "b" and the phosphate of REE "a", that the extent of reaction would be greatest after a certain reaction time for that reaction with the greatest free energy change. If $REE(b)PO_4$ was less soluble than $REE(a)PO_4$, the former should react more slowly, if at all, than the latter, given reversible kinetics.

Two experiments were carried out. In both cases the pH of the solutions was controlled by 1 M NH_4Cl. The reactions were carried out at 65° C for five days. The respective solution concentrations of $REECl_3$ were set initially at 0.05 M.

In the first experiment, a crystal of $SmPO_4$ was placed in a solution of $NdPO_4$, and a crystal of $NdPO_4$ was placed in a similar solution containing $SmCl_3$.

After the five days had passed, the crystals were removed, washed and dried before analysis was done by SIMS depth profiling and XPS. The SIMS data were corrected for isotopic abundances and replotted in figure 5.10. The filled circles refer to the experiment with $NdPO_4$, while open circles refer to the experiment with $SmPO_4$. The results suggest that the Sm had reacted more extensively with the $NdPO_4$, than the Nd had reacted with $SmPO_4$.

The XPS data are presented in figures 5.11 and 5.12. The peak areas were measured, corrected for the appropriate cross sections and tabulated in table 5.1. The results suggest that the Nd had reacted more extensively with the $SmPO_4$ than the Sm had reacted with the $NdPO_4$; the reverse of what the SIMS data showed! Again, the SIMS depth profile data seems difficult to interpret directly.

The solubility products obtained in section 4.3 for the hydrous phosphates of Nd and Sm at 25° C are Nd: pK= 24.5 and 24.8 and Sm: pK= 25.6 and 25.7 +/- 0.2. The $SmPO_4 \cdot xH_2O$ is about an order of magnitude less soluble than the Nd analog. If this is also true for the anhydrous phosphates then thermodynamics would predict that the Sm would react more extensively with $NdPO_4$ than vice-versa. This is opposite to what was actually observed by XPS. Because of this result, further exchange experiments were planned.

Figure 5.10 In this graph, the depth profile intensities were corrected for isotopic abundance and ratioed such that the intensity for the incoming REE was divided by that of the REE in the substrate. The filled circles refer to data from the experiment of the reaction of Sm^{3+} with $NdPO_4$.

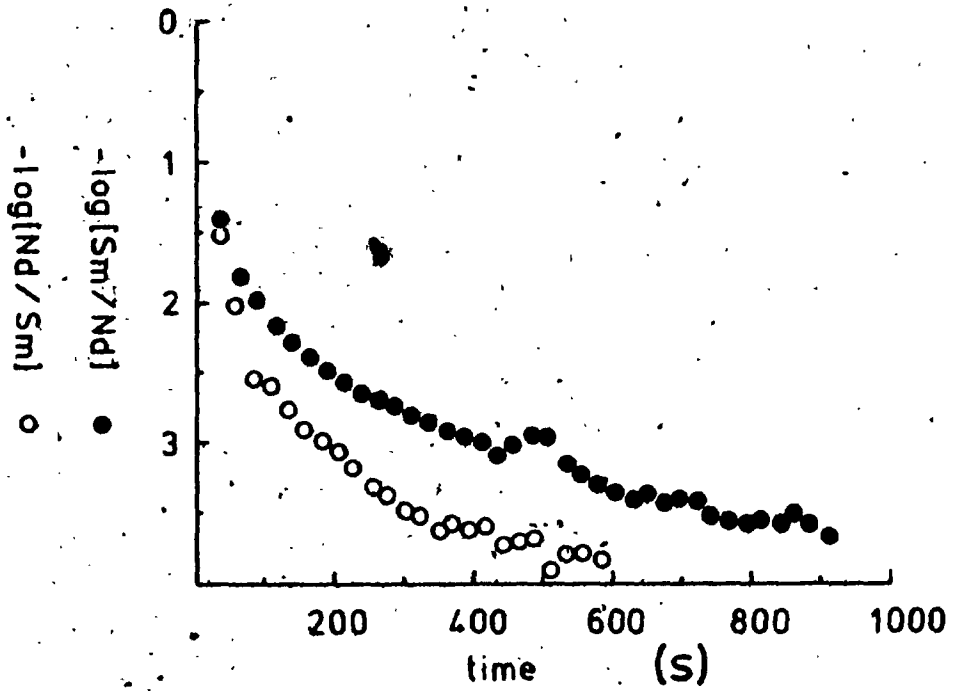

Figure 5.11 Narrow scan XPS spectra for two positions on the surface of $SmPO_4$ crystal soaked in Nd^{3+} solution. The peak areas were measured and corrected for cross-sections; see table 5.1

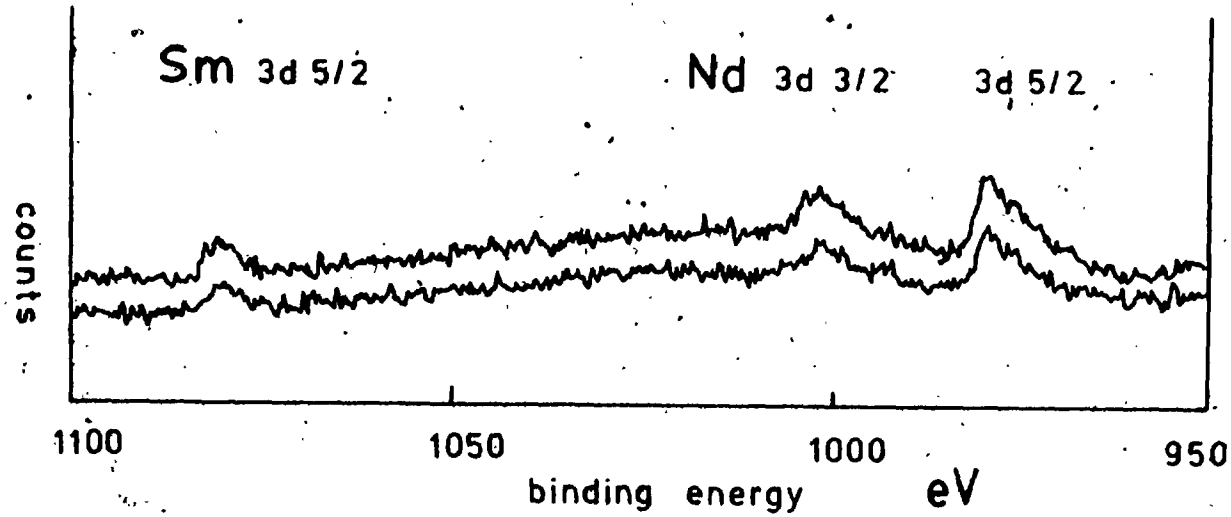

Figure 5.12 Narrow scan XPS spectra for two positions on the surface of a $NdPO_4$ crystal soaked in Sm^{3+} solution.

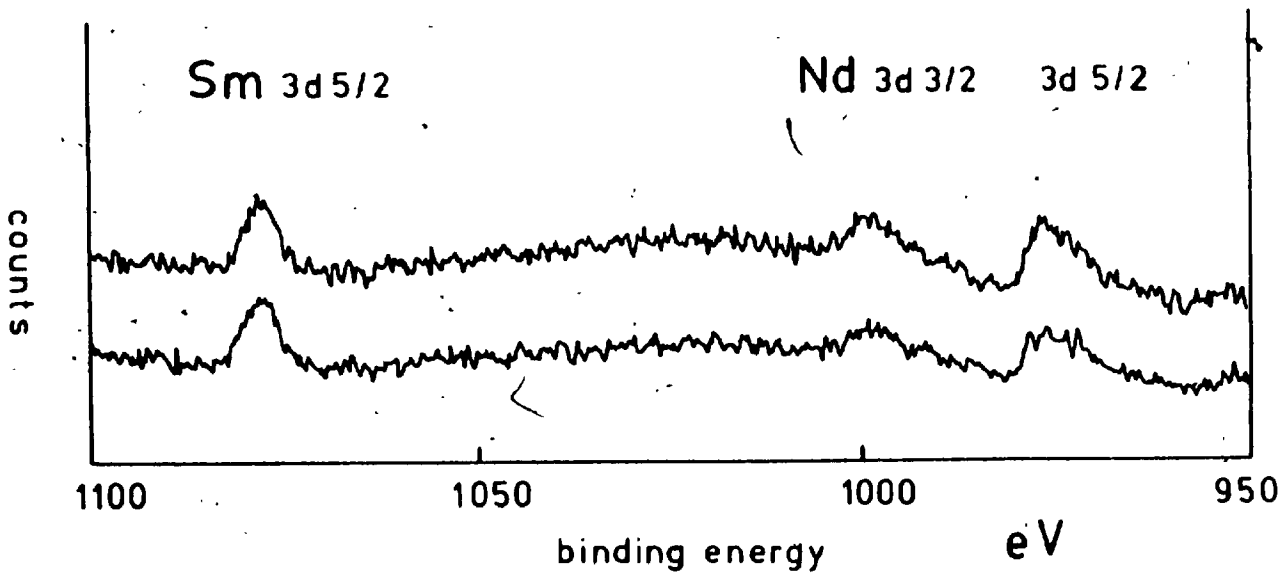

Table 5.1 Quantitative XPS data obtained for the surfaces of $SmPO_4$ reacted with Nd^{3+} and $NdPO_4$ reacted with Sm^{3+}. One of the Sm peaks and two of Nd were used for the analysis. Cross-sections, σ, are for AlK_α radiation.

case	peak area/cross-section			ratios		best
Nd:$SmPO_4$	Sm3d5/2 σ=40.4	Nd3d3/2 σ=24.3	Nd3d5/2 σ=35.3	Nd/Sm	Nd/Sm	
region 1	0.25	0.74	0.74	3.0	3.0	3
2	0.17	0.45	0.54	2.6	3.2	
Sm:$NdPO_4$				Sm/Nd	Sm/Nd	
region 1	0.37	0.41	0.45	0.90	0.82	1
2	0.45	0.29	0.48	1.6	0.94	

Peak areas were measured by counting squares under each peak.

In the second single crystal mutual exchange experiment Ho was reacted with $ErPO_4$ and Er was recated with $HoPO_4$ in separate test tubes. Again, the reaction was carried out at 65° and for five days.

The SIMS data were again corrected for Isotopic abundances, and ratioed in terms of adsorbing-REE over substrate-REE. The results are presented in figure 5.13. It would appear from the SIMS results that the Ho had reacted more extensively with $ErPO_4$ than vice-versa.

The XPS results for the Ho-on-$ErPO_4$ reaction showed evidence for the presence of Ho on the surface. But since the peak intensities for both REE were low, atomic ratios could not be calculated. (Unfortunately, the peaks with the highest cross sections of Ho and Er lie beyond the energy range of the instrument). The XPS results for the Er-on-$HoPO_4$ reaction were even less informative.

The solubility data from section 4.3 suggest that $ErPO_4$ is less soluble than $HoPO_4$. The resulting prediction for the surface exchange reaction is therefore opposite to that observed by SIMS.

In both these experiments, no clear support for the hypothesis of thermodynamic control of surface reactions was obtained.

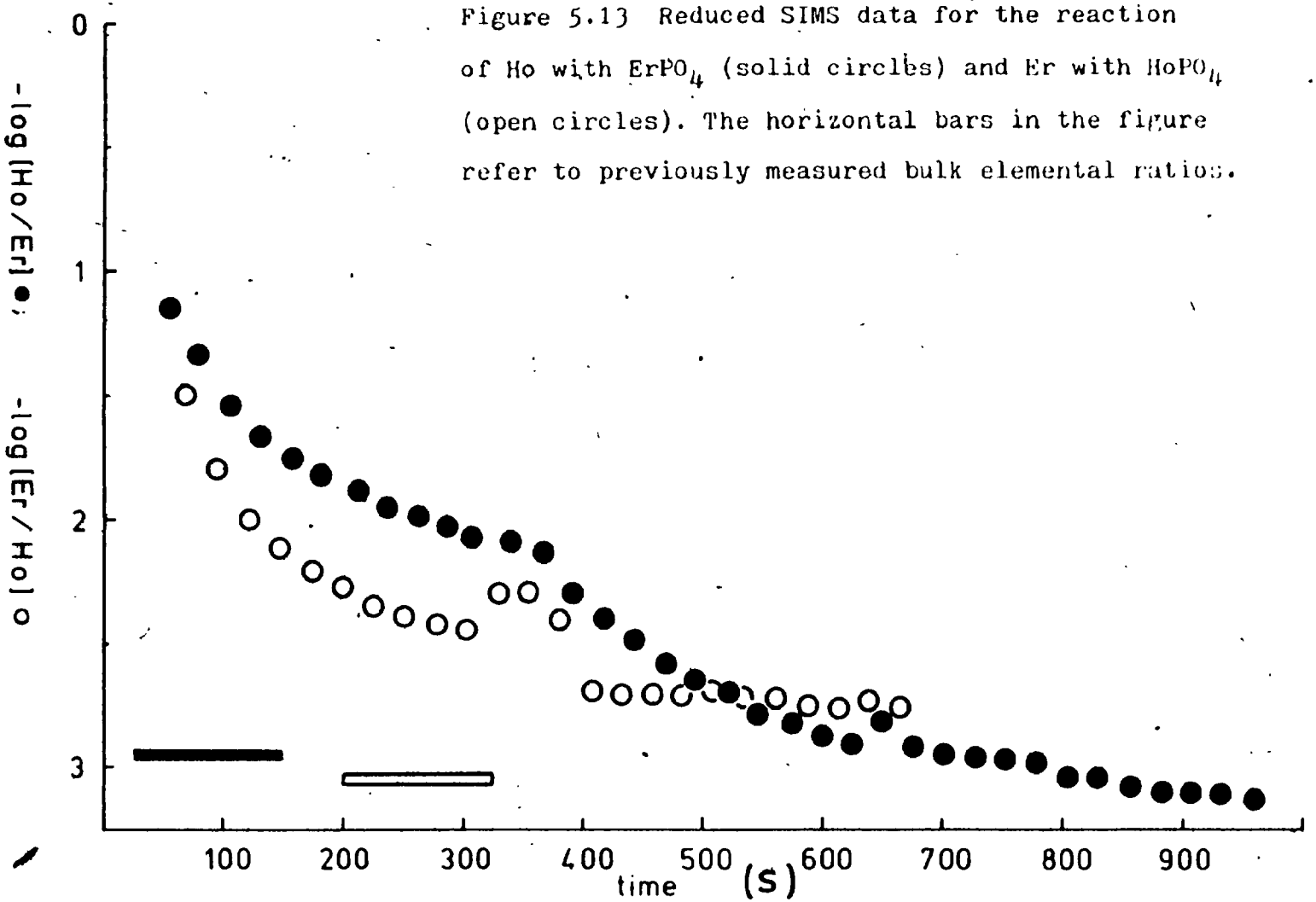

Figure 5.13 Reduced SIMS data for the reaction of Ho with $ErPO_4$ (solid circles) and Er with $HoPO_4$ (open circles). The horizontal bars in the figure refer to previously measured bulk elemental ratios.

5.10 Conclusions

The surface exchange reactions could not be quantified at this stage because of difficulties inherent in the surface analytical techniques used to measure surface concentrations. Though the XPS technique is reasonably quantitative, it is not sufficiently sensitive to allow study of the early stages in a surface reaction. Though SIMS in the depth profiling mode does have considerable sensitivity, it does not readily give quantitative results.

Several surface reaction experiments were carried out, but the detailed processes involved with the surface reactions could not be identified in a manner outlined in section 5.1. However, several lines of evidence point to a process in which the surface exchange or adsorption depends on the dissolution of the substrate. Bone meal reacted with dissolved Nd to form rhabdophane. Apatite surfaces reacted with Pr to form multilayer coatings depleted in Ca. Xenotime reacted with Nd to form rhabdophane. The exchange reactions involving REE phosphates were very slow. The kinetics for exchange and dissolution were found to be of the same order of magnitude.

These results are all consistent with those observed for the reaction of apatite with Zn ions[10] mentioned in section 5.1. Because these "adsorption" reactions result in the formation of new phases, they are important for immobilizing ions, such as those of the REE, for

considerable lengths of time in nature. For example, McArthur and Walsh[41] found that the abundances of the REE increase in marine phosphorites with the geological age of the phosphorite, that is with increasing time of exposure to REE-bearing solutions, such as seawater and sediment pore-water.

It is well to point out that these studies were carried out at pH's less than 7 or 8. Above these pH values other reactions become important. This is illustrated by a recent study of the movements of various radionuclides in shallow seepage trenches at Oak Ridge National Laboratory[42]. Intermediate radioactive liquid waste dumped into these trenches was kept at a high pH to ensure the precipitation of Sr. The phosphate concentration in the initial waste was 150 ppm. The bedrock consisted of shale and mudstone cemented with calcite. Cesium was quickly immobilized by irreversible exchange with illite. Curium, however, which would be expected to resemble the REE, was found to be very mobile; more mobile than Pu, for example. The authors suggested that low molecular weight complexes of Cm with organic and inorganic ligands were probably responsible for the mobility of Cm.

This study also brings up a point about adsorption made in section 5.1, namely that different processes of adsorption can result in entirely different geochemical behaviours of chemical species. Cesium is quickly and

irreversibly immobilized by ion-exchange with illite. Other chemical species are eventually mobilized by rain and groundwater, even though they are also expected to be involved in adsorption and ion-exchange reactions with the clay minerals present in the ground. Species such as complexed-Cm and TcO_4^- are mobilized very rapidly; Sr is immobile as long as the surrounding solutions have a high pH, (that is, as long as $SrCO_3$ is insoluble). Clearly, in order to understand and model the movements of radionuclides in ground waters the processes of adsorption and other surface reactions must be clearly distinguished and understood.

REFERENCES FOR CHAPTER 5

1. Adamson A.W. (1982) Physical Chemistry of Surfaces. 4th Ed. John Wiley and Sons.
2. Wedler G. (1976) Chemisorption: An Experimental Approach. Transl. D.F. Klemperer. Butterworths.
3. Stumm W. and J.J. Morgan (1981) Aquatic Chemistry 2nd Ed. John Wiley and Sons.
4. Sposito G. (1984) The Surface Chemistry of Soils. Oxford University Press.
5. Kummert R. and W. Stumm (1980) J. Colloid Interface Sci. 75, 373-385.
6. De Kanel J. and J.W. Morse (1978) Geochim. Cosmochim. Acta 42, 1335-1340.
7. Thornton E.W. and G. Renn (1985) Adsorption Sci. Technol. 2, 9-22.
8. Madrid L. and P. De Arambarri (1985) J. Soil Sci. 36, 523-530.
9. Nriagu J.O. (1972) Amer. J. Sci. 272, 476-484.
10. Misra D.N. and R.L. Bowen (1981) IN Adsorption from Aqueous Solutions. Ed. P.H. Tewari. Plenum Press.
11. Claesson P.M., P. Herder, P. Stenius, J.C. Eriksson and R.M. Pashly (1986) J. Colloid Interface Sci. 109, 31-39.
12. Mucci A. and J.W. Morse (1985) Amer. J. Sci. 285, 306-317.

13. Möller P. and C.S. Sastri (1974) Z. Phys. Chemie, Neue Folge 89, 80-87.

14. Möller P. and G. Werr (1972) Radiochim. Acta 18, 144-147.

15. Bowden J.W., S. Nagarajah, N.J. Barrow, A.M. Posner and J.P. Quirk (1980) Aust. J. Soil Res. 18, 49-60.

16. Brown N.J., J.W. Bowden, A.M. Posner and J.P. Quirk (1980) Aust. J. Soil Res. 18, 37-47.

17. Westall J. and H. Hohl (1980) Adv. Colloid Interface Sci. 12, 265-294.

18. van Riemsdijk W.H., G.H. Bolt, L.K. Koopal and J. Blaakmeer (1986) J. Colloid Interface Sci. 109, 219-228.

19. Goldberg M.C., E.R. Weiner and P.M. Boymel (1984) J. Chem. Soc. Faraday Trans. 80, 1491-1498.

20. Tomažič B. and G.H. Nancollas (1980) J. Colloid Interface Sci. 75, 149-160.

21. Nancollas G.H. and J.S. Gill (1979) Soc. Petro. Engineers J. Trans. 423-429.

22. Amjad Z., P.G. Koutsoukos and G.H. Nancollas (1984) J. Colloid Interface Sci. 101, 250-256.

23. Keeney-Kennicutt W.L. and J.W. Morse (1985) Geochim. Cosmochim. Acta 49, 2577-2588.

24. Vandergraaf T.T., K.V. Ticknor and I.M. George (1984) IN ACS Symposium Series 246, Geochemical Behaviour of Disposed Radioactive Waste. Eds. G.S. Barney, J.D. Navratil and W.W. Schultz. Amer. Chem. Soc.

25. Avouris P. and J. Demuth (1984) Ann. Rev. Phys. Chem. 35, 49-73.

26. McBride M.B. (1985) Clays & Clay Minerals 33, 397-402.

27. Motschi H. (1985) Adsorption Sci. Technol. 2, 39-54.

28. Riggs W.M. and M.J. Parker (1975) IN Methods of Surface Analysis Vol.1 Ed. A.W. Czanderna. Elsevier.

29. Bancroft G.M., J.R. Brown and W.S. Fyfe (1979) Chem. Geol. 25, 227-243.

30. Jean G.E. and G.M. Bancroft (1985) Geochim. Cosmochim. Acta 49, 979-987.

31. Clarke E.T., R.H. Loeppert and J.M. Ehrman (1985) Clays & Clay Minerals 33, 152-158.

32. Werner H.W. and P.R. Boudewijn (1984) Vacuum 34, 83-101.

33. Beall G.W. and B. Allard (1981) IN Adsorption from Aqueous Solutions Ed. P.H. Tewari. Plenum Press.

34. Vandergraaf T.T., D.R.M. Abry and C.E. Davis (1982) Chem. Geol. 36, 139-154.

35. Zinner E. (1980) Scanning 3, 57-78.

36. Werner H.W. and P.R. Boudewijn (1984) Vacuum 34, 83-101.

37. Kutzler F.W., D.E. Ellis, D.J. Lam, B.W. Veal, A.P. Paulikas, A.T. Aldred and V.A. Gubanov (1984) Phys. Rev. B 29, 1008-1021.

38. Ryzhkov M.V., V.A. Gubanov, Yu A. Teterin and A.S. Baev (1985) Z. Phys. B -Condensed Matter 59, 1-6.

39. ibid. pp 7-14.

40. Carlson T.A. (1975) Photoelectron and Auger Spectroscopy Plenum Press.

41. McArthur J.M. and J.N. Walsh (1984/85) Chem. Geol. 47, 191-220.

42. Olsen C.R., P.D. Lowry, S.Y. Lee, I.L. Larsen and N.H. Cutshall (1986) Geochim. Cosmochim. Acta 50, 593-608.

6. GENERAL DISCUSSION

In terms of applications to nuclear waste disposal, the thesis work has demonstrated that REE ions can be precipitated from acidic, aqueous solutions by the hydrolysis products of pyrophosphoric acid to form easily filtered, highly insoluble phosphates. These solids are refractory to at least 1200° C, and undergo no chemical reactions during heating, aside from water loss and solid state phase changes. Evidence was provided to show that the trivalent actinides would behave similarly, and that the tetrvalent actinides would be caught up in the precipitation.

Though all the radionuclides resulting from nuclear waste treatment deserve careful study and handling, the actinides are of particular concern[1,2,3] both because of their chemical and radio- toxicities, and because several isotopes, namely ^{237}Np, ^{239}Pu and ^{242}Pu have particularly long half-lives. Others decay to daughters with long half-lives.

In terms of geochemistry, a study of the REE phosphates should help to increase the understanding of the environmental behaviours of lanthanides and actinides. Transuranium elements are now routinely introduced into the environment. Windscale alone introduced an average of 1200 Curies per year of plutonium isotopes into the sea

during the period from 1971 to 1978[4]. Recently[5] new limits were placed on the low level discharges into the Irish Sea from Sellafield, (Windscale). No more than 300 000 curies of beta/gamma wastes may be dumped per year. The corresponding limit for alpha wastes is set at 6000 curies per year. The reprocessing plant at Sellafield is only one of several in operation in the world today.

Further, of the many methods proposed for the disposal of spent fuel and reprocessing waste, deposition of sealed containers onto, or into, the sea bed in zones away from continental margins, oceanic trenches and midoceanic ridges, is one of the more promising under consideration[1,2,3]. Clearly, the oceans constitute an important environment for the containment and dispersal of radionuclides, and therefore deserve considerable study.

The calculations done in this thesis on the basis of measured REE phosphate solubility products demonstrate the importance of these phases in limiting, if not controlling, the concentrations of the REE in seawater. Further, because the lanthanides are good geochemical analogues for the trivalent actinides[6], the concentration of these species is not expected to exceed 10 to 100 pmol/L.

Many predictions of equilibrium concentrations of chemical species in the environment are based on thermodynamic data and assumptions. This implies that

that the mineral surfaces controlling the solution concentrations are in dynamic equilibrium with the solution phase. The mineral surfaces are therefore not static, or inert, but rather change with time, and changing chemical conditions in the solution. This naturally leads to the expectation that mineral surfaces are in a state of "incipient mineral replacement". Where the changes in the solutions chemistry are drastic enough, this ultimately leads to complete mineral replacement. The thesis work has demonstrated the importance of these replacement reactions in the case of REE phosphates, for time scales as short as weeks or months. In natural environments, where time scales can be as long as geological time itself, such mineral replacement reactions are at least as important as adsorption processes for retarding and halting the solution transport of chemical species in rocks and sediments.

REFERENCES

1. Marshall W. (Ed.) (1983) Nuclear Power Technology Vol.2. Fuel Cycle. Clarendon Press.
2. Gilmore W.R. (Ed.) (1977) Radioactive Waste Disposal. Noyes Data Corporation.
3. Brookins D.G. (1984) Geochemical Aspects of Radioactive Waste Disposal. Springer-Verlag.
4. Stanners D.A. and S.R. Aston (1984) Chem. Geol. 44, 19-32.
5. Anonym. (1986) Nuclear News 29, 68.
6. Krauskopf K.B. (1986) Chem. Geol. 55, 323-335.

APPENDIX I

Powder diffraction data for three REE pyrophosphates: $PrHP_2O_7 \cdot 1\text{-}2H_2O$; Y-pyrophosphate; $HoHP_2O_7 \cdot 3\text{-}5H_2O$.

Pr		Y		Ho	
d	h/h_o	d	h/h_o	d	h/h_o
9.04	100	9.34	100	9.30	54
----	--	----	--	8.22	15
----	--	6.49	24	6.51	100
5.34	3	4.87	1	5.40	1
4.57	33	4.74	14	4.67	6
4.32	30	4.62	1	4.48	3
3.74	3	3.53	14	3.52	3
3.34	2	3.39	12	3.37	17
3.19	5	3.25	18	3.24	48
3.13	16	3.17	17	----	--
3.06	30	3.04	15	3.03	6
2.95	4	----	--	2.74	3
----	--	2.66	7	2.65	3
2.52	4	2.56	1	2.51	2
2.40	41	2.36	16	2.36	13
2.29	2	----	--	2.30	6
2.26	12	----	--	----	--
2.17	2	2.17	5	2.16	18
----	--	2.14	6	----	--
----	--	2.11	12	2.11	5
2.01	6	----	--	2.04	2
1.93	19	1.91	7	1.90	3
1.87	4	----	--	----	--
1.83	4	----	--	1.83	6
1.77	5	1.78	4	1.78	5

APPENDIX II

Neutron activation analysis of natural monazite.

Analyses by Nuclear Activation Services, Limited.

element	concentration	method
Ag	l.t. 100 ppm	INAA
As	250 ppm	
Au	l.t.1000 ppb	
Ba	interference	
Ca	interference	
Co	l.t. 50 ppm	
Cr	interference	
Cs	l.t. 40 ppm	
Fe	l.t. 2 %	
Hf	l.t. 40 ppm	
Mo	l.t.2000 ppm	
Na	interference	
Ni	l.t.6000 ppm	
P	insufficient sample	
Rb	l.t. 800 ppm	
Sb	l.t. 20 ppm	
Sc	l.t. 15 ppm	
Se	l.t. 160 ppm	
Sr	l.t.5000 ppm	
Ta	l.t. 50 ppm	
Th	150000 ppm	
U	2000 ppm	
W	l.t. 300 ppm	
Y	7700 ppm	DCP
Zn	interference	INAA
La	78000 ppm	
Ce	143000 ppm	
Pr	21000 ppm	DCP
Nd	81000 ppm	INAA
Sm	30000 ppm	
Eu	1400 ppm	
Gd	34000 ppm	DCP
Tb	8000 ppm	INAA
Dy	20000 ppm	
Ho	1400 ppm	DCP
Er	1800 ppm	DCP
Tm	150 ppm	DCP
Yb	600 ppm	INAA
Lu	60 ppm	

l.t. = less than; DCP= Direct Current Plasma.

After 19 months the powders were again filtered off, washed and analyzed by powder x-ray diffraction. The diffraction pattern of the first powder contained peaks characteristic of rhabdophane, in addition to those of the expected xenotime. The diffraction pattern of the second powder was entirely that of rhabdophane, suggesting that only the original Nd-RHABDOPHANE was present.

In the absence of powder diffraction data, one might have concluded from the ESCA data and solution data that adsorption of Nd^{3+} onto $HoPO_4 \cdot xH_2O$ had occurred, and that some of the substrate had dissolved. The presence of diffraction peaks characteristic of rhabdophane in the diffraction pattern of $HoPO_4 \cdot xH_2O$ proves that the substrate had reacted with Nd^{3+} to form a new phase.

Unfortunately, because the pH's of the two solutions were different, one cannot conclude from these experiments that Nd-RHABDOPHANE is less soluble than Ho-XENOTIME. However, the experiment done more carefully would provide a more reliable ordering of solubility products for pairs of REE phosphates, than the values of the solubility products themselves. (Recall the variation of solubility product values for Nd-RHABDOPHANE for example).

The other conclusion to be drawn from these experiments is that these exchange reactions are quite slow, so that if the experiments had been terminated after a couple of months one would have erroneously concluded that the REE hydrous phosphates are kinetically inert.